



저작자표시-비영리-변경금지 2.0 대한민국

이용자는 아래의 조건을 따르는 경우에 한하여 자유롭게

- 이 저작물을 복제, 배포, 전송, 전시, 공연 및 방송할 수 있습니다.

다음과 같은 조건을 따라야 합니다:



저작자표시. 귀하는 원저작자를 표시하여야 합니다.



비영리. 귀하는 이 저작물을 영리 목적으로 이용할 수 없습니다.



변경금지. 귀하는 이 저작물을 개작, 변형 또는 가공할 수 없습니다.

- 귀하는, 이 저작물의 재이용이나 배포의 경우, 이 저작물에 적용된 이용허락조건을 명확하게 나타내어야 합니다.
- 저작권자로부터 별도의 허가를 받으면 이러한 조건들은 적용되지 않습니다.

저작권법에 따른 이용자의 권리는 위의 내용에 의하여 영향을 받지 않습니다.

이것은 [이용허락규약\(Legal Code\)](#)을 이해하기 쉽게 요약한 것입니다.

[Disclaimer](#)

A DISSERTATION FOR THE DEGREE OF DOCTOR OF  
PHILOSOPHY

Evaluation of Curing Shrinkage of the Photo-Curable Material  
and its Application for Photo-Curable Adhesives

광경화 수축현상의 분석기법 개발 및  
광경화 접착소재에 대한 응용 연구

Ji-Won Park

Advisor: Hyun-Joong Kim

PROGRAM IN ENVIRONMENTAL MATERIALS SCIENCE  
GRADUATE SCHOOL  
SEOUL NATIONAL UNIVERSITY

February, 2016

## Abstract

### Evaluation of Curing Shrinkage of the Photo-Curable Material and its Application for Photo-Curable Adhesives

Ji-Won Park

Program in Environmental Materials Science

Department of Forest Sciences

The Graduate School

Seoul National University

In this research, I designed measuring system for shrinkage of UV (ultraviolet) curable materials and carried out analyses of experimental factors to achieve the high reliability of the system. Throughout the process of system designing, I measured shrinkage of monomers that have different structures respectively. Based on the evaluation of monomer, shrinkage of composite materials whose properties were imitated from final products was measured along with the evaluation of factors of shrinkage.

As for internal factors, the geometry of specimens had a great impact on shrinkage. Particularly, significant reduction of axial shrinkage was observed

when they had a low aspect ratio. By modeling, I confirmed that the shrinkage at the flanking side of material would influence its axial shrinkage. In order to minimize the impact, a specimen that have an aspect ratio over 40 is needed.

The shrinkage of specimens varied according to contents of photo-initiator and UV intensity to affect the reactivity. The contents of photo-initiator and UV intensity could change the depth of curing in complex ways, causing shrinkage delay phenomena.

The properties of UV curing depending on system temperature, which was measured by photo-differential scanning calorimetry (DSC), varied according to glass transition temperature of specimens. It resulted from declining mobility caused by partial cross-linking through a curing process. Reactivity tended to increase up to a certain temperature and then decrease, which is because thermodynamic reaction outdo kinetic reaction as the temperature rises.

Although it is known that the reactivity of UV curing increases as the number of functionalities of monomers increases, the opposite outcome was obtained in this research. It was confirmed that the shrinkage and reactivity of di-functional monomer were relatively higher than those of hexa-functional monomer were. It would be related to the fact that materials composed of di-functional monomer has more flexible molecular structure and can maintain its mobility within the curing process.

Acrylate and methacrylate are the most structured to take advantage of the photo-curing system. The reactivity of both structures are excellent, and reactivity of acrylate is known to be higher than that of methacrylate. In the mono-acrylate system, methacrylate had an excellent reactivity, which could maintain the mobility of the polymer associated with the structure of methacrylate. Both shrinkage and reactivity of the materials were higher in multi-functional system. In particular, we are able to verify that the patterns of the results obtained from photo-DSC and from the shrinkage test are the same, which means that the evaluation using photo-DSC can predict the shrinkage evolution. Therefore, the complementary application of two methods is expected to be possible at measurement in curing system.

In the shrinkage evaluation using the isomer system, I confirmed that the reactivity was changed depending on the core structure. The molecules with a linear core structure and side chains expressed different curing characteristics according to properties such as the mobility and density of reactive site.

UV-polymerized adhesive was materialized by blending a pre-polymer that was pre-synthesized and multi-functional acrylate as a reactive diluent. The reaction was delayed in the case that the size of reactive diluent was small while its contents were high.

In curing materials such as dental adhesive, since their dimensional stability in the curing process is important and hardness after curing should be excellent, the system was designed to contain filler. UV curable adhesive system containing filler are implemented by manufacturing the acrylate including a nano-silica particle in the core structure. The shrinkage varies depending on blended materials. A nano-porous effect presented in the

condition that molecules with different sizes were mixed with each other. The effect can improve the reactivity of the system.

In this study, I propose the system to estimate volumetric shrinkage through measurements for axial shrinkage by designing the device to measure axial shrinkage. I analyzed internal and external factors that would affect shrinkage. The patterns of shrinkage can be predicted more accurately by controlling the factors. Various structural characteristics of materials have an effect on shrinkage, which was evaluated as the results for the reactivity and mobility of the materials. In the evaluation for products, it is possible to analyze the shrinkage change in photo-curing process through the simplified curing system and investigate the main factors influencing each system.

**Keyword:** volumetric shrinkage, axial shrinkage, modeling, photo-initiator, light intensity, acrylate, system temperature, UV curable adhesive, multi-functional monomer

**Student Number:** 2008-21297

# Contents

<b>1. Introduction</b>	<b>2</b>
1.1. UV Curing Technology and its Application	2
1.1.1. UV Curing Technology	2
1.1.2. UV Curing Technology and its Industry	3
1.1.3. Forecast on World Market of UV Curing Materials	13
1.1.4. UV Curing Mechanism	19
1.1.5. UV Curing Chemical	21
1.1.6. Problems UV Curable Material, the Need for UV Curing Behavior Analysis	28
1.1.7. Shrinkage	30
1.2. UV Curing Evaluation Method	35
1.2.1. Evaluation System using Thermo-chemical Behavior of UV Curing	36
1.2.2. Evaluation System using Mechanical Behavior of UV Curing	43
<b>2. Literature Review</b>	<b>45</b>
2.1. Research on Applied UV Curable Resin	45
2.2. Evaluation of UV Curing Behavior	49
2.3. UV Curing Behavior Research using Shrinkage Test	53
2.4. UV Curing Application and Shrinkage Test	59
<b>3. Objectives</b>	<b>63</b>
<b>4. Quantification of the Evaluation of Shrinkage</b>	<b>66</b>

4.1. Production of Equipment	66
4.1.1. Design of Test Equipment	66
4.1.2. Sensor Types and their Pros and Cons	73
4.1.3. The Principle of the Electrical Sensor	75
4.2. Basic Test of Shrinkage	79
4.3. Modeling of Material	95
4.3.1. Ideal Configuration and Shrinkage Phenomenon	99
4.3.2. Real Concave Model	107
4.4. Change of shrinkage in response to the external environment	122
4.4.1. Content of the initiator and shrinkage	122
4.4.2. UV Intensity and Shrinkage	136
4.4.3. Temperature and Shrinkage	160
<b>5. Change of Shrinkage as Function of the Change of the Material</b>	<b>181</b>
5.1. Change of shrinkage associated with differences in the molecular structure	181
5.1.1. Shrinkage rate changes in accordance with the number of functional groups	181
5.1.2. Tri-acrylate System based on TMPTA	189
5.2. Acrylate vs Methacrylate	196
5.2.1. MPEG-A vs MPEG-MA	200
5.2.2. NEO-DA vs NEO-DMA	208
5.2.3. HD-DA vs HD-DMA	213
5.2.4. TMP-TA vs TMP-TMA	220

5.3. Shrinkage of the different size in the molecule	227
<b>6. Evaluation of the Actual Material</b>	<b>238</b>
6.1. Adhesives by Photo Polymerization	240
6.1.1. Preparation of UV Curable Adhesives	240
6.1.2. UV Curing Behavior with Photo-DSC	244
6.1.3. Shrinkage Test	259
6.2. UV curable Adhesives – dental adhesives	267
6.2.1. Blending System of Multifunctional Acrylate	269
6.2.2. Filler Contained Acrylate System	278
<b>7. Conclusion</b>	<b>299</b>
<b>References</b>	오류! 책갈피가 정의되어 있지 않습니다.

### List of figures

Fig. 1-1. Classification of UV rays with a wavelength region.....	4
Fig. 1-2. UV curing sequence, 1) Formulation, 2) UV irradiation, 3) Initiation and 4) Curing [Brancher, 2015]. .....	5
Fig. 1-3. Schematic figure of UV ink application to take advantage of the UV curing system (GEW, 2015). .....	9
Fig. 1-4. UV curable adhesive for electric area (Permacol, 2015). .....	10
Fig. 1-5. U.S. electronic adhesives market revenue by product, 2012-2022 (USD million) [Grand View Research, 2015]. .....	16
Fig. 1-6. Comparison of material properties in accordance with the difference in the size and functionality of monomer [Miwon Specialty Chemical, 2015]. .....	23

Fig. 1-7. Comparison of multi-functional acrylate's properties in accordance with the functionality [Miwon Specialty Chemical, 2015].....	25
Fig. 1-8. Structure of extended acrylate (a) ethoxylated (b) propylated...	27
Fig. 1-9. Scheme of shrinkage occurring by UV curing.....	33
Fig. 1-10. Volumetric Shrinkage of monomer by blob linking .....	34
Fig. 1-11. Cell / lamp guide design and appearance of photo-DSC .....	38
Fig. 1-12. General result using photo-DSC (Park, 2011). .....	39
Fig. 1-13. Molecule structure changed by UV curing. ....	41
Fig. 1-14. General result using real-time FT-IR (Park, 2011).....	42
Fig. 2-1. Synthesis and evaluation of UV and thermal dual-curable resin [Park, 2009].....	47
Fig. 2-2. NIR system for analysis of real time shrinkage materials (Christian, 2015) .....	54
Fig. 2-3. Schematic drawing of the Linometer (Gee, 1993) .....	57
Fig. 2-4. The difference in axial shrinkage and volume shrinkage based on the c-factor (Lee, 2006) .....	58
Fig. 2-5. Evaluating of micro-shrinkage phenomenon by 3-D confocal laser .....	60
Fig. 4-1. Method of measuring the axial shrinkage with Linometer .....	70
Fig. 4-2. Design of improved Linometer – UV light parts- .....	71
Fig. 4-3. Design of Improved Linometer – Housing parts- .....	72
Fig. 4-4. Principle of eddy sensor (Measure Central, 2015).....	77
Fig. 4-5. Structure of eddy sensor (Measure Central, 2015).....	78
Fig. 4-6. Selected acrylate to the basic evaluation (a) caprolacton acrylate (CA) (b) nonyl phenyl acrylate (NPA) .....	81
Fig. 4-7. Graph of Shrinkage Test 1) UV exposure starting 2) Shrinkage	

initiating 3) Shrinkage increased and curing reaction and 4) Final reaction → Define Shrinkage.....	84
Fig. 4-8. Real-time shrinkage of caprolaction acrylate.....	85
Fig. 4-9. Real-time shrinkage of nonyl phenyl acrylate .....	86
Fig. 4-10. Shrinkage rate of caprolaction acrylate .....	87
Fig. 4-11. Shrinkage rate of nonyl phenyl acrylate .....	88
Fig. 4-12. Heat flow of mono-acrylate system.....	92
Fig. 4-13. Exothermic area of mono-acrylate system.....	93
Fig. 4-14. Scheme of meniscus (concave) form of between double side.	98
Fig. 4-15. Ideal configuration of shrinkage on contact mode .....	101
Fig. 4-16. Plotting graph of curl shrinkage versus diameter.....	104
Fig. 4-17. Ratio of curl volume on shrinkage .....	106
Fig. 4-18. Experiment configuration of shrinkage on contact mode.....	109
Figure 4-19. Specimens for evaluating the shrinkage caused by the sampling size.....	110
Fig. 4-20. Concave curl in a CCD actual contact mode that were taken using CCD .....	115
Fig. 4-21. Changing of shrinkage in accordance with the radius [MPEG-A] .....	116
Fig. 4-22. Exponential fitting analysis of the shrinkage by content of the initiator [MPEG-A] (R-square: 0.801).....	117
Fig. 4-23. Changing of shrinkage in accordance with the radius [MPEG-MA] .....	118
Fig. 4-24. Linear Fiting analysis of the shrinkage by content of the initiator [MPEG-MA] (R-square : 0.355).....	119
Fig. 4-25. Comparison of the correlation radius and shrinkage –close shape is acrylate, open shape is methacrylate -.....	120

Fig. 4-26. Wettability of the material and curl shape (a) acrylate (MPEG-A) (b) methacrylate (MPEG-MA).....	121
Fig. 4-27. Shrinkage of TMPTA depends on the photo-initiator contents. .....	126
Fig. 4-28. Shrinkage Rate of TMPTA depend on photo-initiator contents. .....	127
Fig. 4-29. Shrinkage behavior of TMPTA depend on Initiator contents.	129
Fig. 4-30. Shrinkage of PETA depend on photo-initiator contents. ....	131
Fig. 4-31. Shrinkage rate of PETA depend on photo-initiator contents..	132
Fig. 4-32. Shrinkage behavior of PETA depend on initiator contents....	134
Fig. 4-33. Polymer network formation with multi-functional monomer [Dusek, 2012].....	135
Fig. 4-34. Activation energy of endothermic/exothermic reaction .....	142
Fig. 4-35. Shrinkage of TMPTA depends on the UV intensity (PI 3 phr) .....	143
Fig. 4-36. Surface topology of the curing space (Lee, 2001).....	144
Fig. 4-37. Scheme of shrinkage delay effect.....	145
Fig. 4-38. Representation of gel curing profiles. In (a), laser penetrates deeply, but only lightly cross-links the gel. In (b), free radical initiation is localized in the upper portion of the solution (Lee, 2001) .....	146
Fig. 4-39. The shrinkage rate of TMPTA depends on the UV intensity (PI 3 phr) .....	149
Fig. 4-40. Shrinkage rate normalized by light intensity to the 0.6 order	150
Fig. 4-41. The shrinkage behavior of TMPTA depends on UV intensity	152
Fig. 4-42. Shrinkage of TMPTA depends on the UV intensity (PI 5 phr) .....	156

Fig. 4-43. The shrinkage rate of TMPTA depends on the UV intensity (PI 5 phr) .....	157
Fig. 4-44. Shrinkage initial time in accordance with the content of the initiator and UV intensity .....	158
Fig. 4-45. Normalized shrinkage rate by UV intensity.....	159
Fig. 4-46. Rate of polymerization as a function of time at various temperatures for .....	164
Fig. 4-47. Conversion degree ( $\alpha$ ) as a function of the glass transition temperature ( $T_g$ ) for the epoxy system (Urbaniak, 2011).....	165
Fig. 4-48. Structure of ethoxylated TMPTA .....	169
Fig. 4-49. Heat flow of TMPTA is accordance with the temperature ....	170
Fig. 4-50. Heat flow of EO6 TMPTA is accordance with the temperature .....	171
Fig. 4-51. Heat flow of EO9 TMPTA is accordance with the temperature .....	172
Fig. 4-52. Heat flow of EO15 TMPTA is accordance with the temperature .....	173
Fig. 4-53. Exothermic areas of tri-acrylate system (a) TMPTA (b) EO6 TMPTA (c) EO9 TMPTA (d) EO15 TMPTA.....	174
Fig. 4-54. Maximum heat flow of tri-acrylate system.....	176
Fig. 4-55. Normalized maximum heat flow of tri-acrylate system .....	177
Fig. 4-56. Scheme of maximum heat flow trend by $T_g$ .....	178
Fig. 4-57. Thermodynamic vs. kinetic control of reaction .....	179
Fig. 5-1. Structure of multi-functional acrylate (a) 1,6-Hexanediol diacrylate.....	184
Fig. 5-2. Shrinkage corresponding to the number of functional groups.	186
Fig. 5-3. Shrinkage rate corresponding to the number of functional groups	

.....	187
Fig. 5-4. Normalized Shrinkage rate by functionality number/molecular weight .....	188
Fig. 5-5. Shrinkage (a) TMPTA (b) EO6 TMPTA (c) EO9 TMPTA (d) EO15 TMPTA.....	192
Fig. 5-6. Theoretical shrinkage and experimental shrinkage by molecular weight .....	194
Fig. 5-7. Mobility of molecule depend on molecule's size.....	195
Fig. 5-8. Molecular structure of (a) MPEG-A (b) MPEG-MA .....	203
Fig. 5-9. Shrinkage of MPEG-A/MPEG-MA .....	204
Fig. 5-10. Heat flows of MPEG-A and MPEG-MA.....	205
Fig. 5-11. Exothermic areas (total heat dissipation) of MPEG-A and MPEG-MA.....	206
Fig. 5-12. Effect of metha methyl (a) Interfering role of packing, (b) The role of free available space .....	207
Fig. 5-13. Molecular structure of (a) NEO-DA (b) NEO-DMA .....	209
Fig. 5-14. Shrinkage of NEO-DA and NEO-DMA .....	210
Fig. 5-15. Heat flows of NEO-DA and NEO-DMA.....	211
Fig. 5-16. Exothermic areas (total heat dissipation) of NEO-DA and NEO-DMA.....	212
Fig. 5-17. Molecular structure of (a) HD-DA (b) HD-DMA .....	215
Fig. 5-18. Shrinkage of HD-DA and HD-DMA.....	216
Fig. 5-19. Heat flows of HD-DA and HD-DMA.....	217
Fig. 5-20. Exothermic areas (total heat dissipation) of HD-DA and HD-DMA.....	218
Fig. 5-21. Core structural differences between NEO-DA and HD-DA..	219
Fig. 5-22. Molecular structure of (a) TMP-TA (b) TMP-TMA .....	222

Fig. 5-23. Shrinkage of tri-acrylate TMP-TA and TMP-TMA .....	223
Fig. 5-24. Heat flows of TMP-TA and TMP-TMA .....	224
Fig. 5-25. Exothermic areas (total heat dissipation) of TMP-TA and TMP-TMA .....	225
Fig. 5-26. Comparison of the shrinkage evaluation and photo-DSC evaluation results.....	226
Fig. 5-27. Structural differences between the two materials (a) 1,4 butanediol structure (b) 1,3 butanediol structure .....	232
Fig. 5-28. Cross-comparison between four materials (a) 13B-DA and 13B-DMA (b) 14B-DA vs 14B-DMA (c) 13B-DA vs 14B-DA (d) 13B-DMA vs 14B-DMA.....	233
Fig. 5-29. Shrinkage rate of four materials .....	234
Fig. 5-30. Heat flow of di-functional system.....	235
Fig. 5-31. Mobility of the cured polymer which is based on the molecular structure .....	236
Fig. 6-1. Formulation of UV curing system (Hong, 2002).....	239
Fig. 6-2. Status of UV polymerized adhesives during the polymerization process .....	242
Fig. 6-3. Equipment of UV polymerization process.....	243
Fig. 6-4. Heat flow profiles of UV curable adhesives with PEG unit (a) 100 (b) 200 (c) 400 (d) 1000.....	250
Fig. 6-5. The peak height of UV curable adhesives with PEG .....	251
Fig. 6-6. Scheme of diluent role in the pre-polymer .....	252
Fig. 6-7. Highest peak time of UV curable adhesives. ....	253
Fig. 6-8. Highest peak time versus methacrylate contents. ....	254
Fig. 6-9. Calculated exothermic area based on neat.....	255
Fig. 6-10. Initial stage of heat flow profiles of UV curable adhesives...	256

Fig. 6-11. Initial stage of UV curing of UV curable adhesives with PEG 100.....	257
Fig. 6-12. Heat flow value change the rate of UV curable adhesives with PEG 100.....	258
Fig. 6-13. Shrinkage of UV curable adhesives with PEG unit (a) 100 (b) 200 (c) 400 (d) 1000.....	262
Fig. 6-14. Shrinkage of UV curable adhesives versus PEG concentration .....	263
Fig. 6-15. Approach time on specific shrinkage (2%) of UV curable adhesives.....	264
Fig. 6-16. Compare different two cases of structure by curing condition .....	265
Fig. 6-17. Shrinkage rate of UV curable adhesives with PEG unit (a) 100 (b) 200 (c) 400 (d) 1000 .....	266
Fig. 6-18. Shrinkage of binary monomer system.....	272
Fig. 6-19. Maximum shrinkage of binary monomer system.....	273
Fig. 6-20. Heat flow of binary monomer system .....	274
Fig. 6-21. Maximum heat flow of binary monomer system. ....	275
Fig. 6-22. Scheme of nano-porous effect of binary monomer system....	276
Fig. 6-23 Heat flow of binary monomer system are accordance with UV intensity .....	277
Fig. 6-24. Preparation of nano-silica with sol-gel reaction (Zhang, 2014) .....	283
Fig. 6-25. Preparation of nano-silica core, multi-functional acrylate.....	284
Fig. 6-26. Shrinkage of NSC-MF acrylate and PETA blending system.	285
Fig. 6-27. Shrinkage of NSC-MF acrylate and PETA blending system – black straight line is calculated shrinkage, red dot line is	

experimental shrinkage- .....	286
Fig. 6-28. Shrinkage of NSC-MF acrylate and TMPTA blending system .....	287
Fig. 6-29. Shrinkage of NSC-MF acrylate and TMPTA blending system – black straight line is calculated shrinkage, red dot line is experimental shrinkage- .....	288
Fig. 6-30. Shrinkage of NSC-MF acrylate and BIS-GMA blending system .....	289
Fig. 6-31. Shrinkage of NSC-MF acrylate and BIS-GMA blending system – black straight line is calculated shrinkage, red dot line is experimental shrinkage- .....	290
Fig. 6-32. Heat flow of NSC-MF acrylate and PETA blending system .	291
Fig. 6-33. The maximum heat flow of NSC-MF acrylate and PETA blending system – black straight line is calculated heat flow, red dot line is experimental heat flow-.....	292
Fig. 6-34. Heat flow of NSC-MF acrylate and TMPTA blending system .....	293
Fig. 6-35. The maximum heat flow of NSC-MF acrylate and TMPTA blending system – black straight line is calculated heat flow, red dot line is experimental heat flow-.....	294
Fig. 6-36. Heat flow of NSC-MF acrylate and BIS-GMA blending system .....	295
Fig. 6-37. The maximum heat flow of NSC-MF acrylate and BIS-GMA blending system – black straight line is calculated heat flow, red dot line is experimental heat flow-.....	296
Fig. 6-38. Island/bridge structure of mixture system with NFC MF acryalte and BIS-GMA.....	297



## List of tables

Table 2-1. Volumetric shrinkage of epoxy/clay composites.....	61
Table 4-1. Comparison of metal UV lamp and UV LED.....	69
Table 4-2. Advantages and disadvantages depending on the type of sensor	74
Table 4-3. Shrinkage test result of mono-acrylate system .....	89
Table 4-4. Photo-DSC test result of mono-acrylate system .....	94
Table 4-5. Shrinkage of side direction (per 0.1ml) .....	103
Table 4-6. Basic properties of MPEG-A and MPEG-MA.....	111
Table 4-7. Shrinkage test result of TMPTA depending on photo-initiator contents.....	128
Table 4-8. Shrinkage test result of PETA depending on photo-initiator contents.....	133
Table 4-9. The shrinkage test result of TMPTA depending on UV intensity .....	151
Table 4-10. Maximum heat flow and $\Delta T$ of the tri-acrylate system according to system temperature.....	175
Table 5-1. Basic information of multi-functional acrylate.....	185
Table 5-2. Theoretical shrinkage and experimental shrinkage.....	193
Table 5-3 Arrhenius $K_p$ the PLP parameters for various monomers determined by PLP-SEC (Bebe, 2008).....	198
Table 5-4. Basic properties of acrylate/methacrylate monomers .....	202
Table 5-5. Basic properties of di-acrylate monomers .....	231

# *Chapter 1*

Introduction

# 1. Introduction

## 1.1. UV Curing Technology and its Application

### 1.1.1. UV Curing Technology

The UV (ultraviolet) curing technology is a technique of forming a polymer structure by the chain reaction of a ring structure or a double bond as activating radical and cation of the initiator after exposure UV light [Hwang, 2011].

In general, UV curing technology is divided into UV polymerization technique and UV curing technology. The UV polymerization technique is similar to polymer technology to prepare general linear polymers, and this process has the advantage that it can be easily applied to the bulk polymerization. UV curing technology is the technique which forms a three-dimensional polymer structure with multi-functional monomers such as 1, 6-hexandiol diacrylate (HDDA), dipentaerithritol hexacrylate (DPHA) through cross-linking by UV initiation [Lee *et al.*, 2013].

### 1.1.2. UV Curing Technology and its Industry

Since chemical company, Bayer (Germany) developed a UV curing coating method in 1986; UV curing technology has been applied for curing of the coating film in the field of paint. Recently, it has been utilized as a technique for producing functional polymers such as adhesive, in cases of producing mobile devices, coating to manufacture, and making biomimetic products with nano-imprinting.

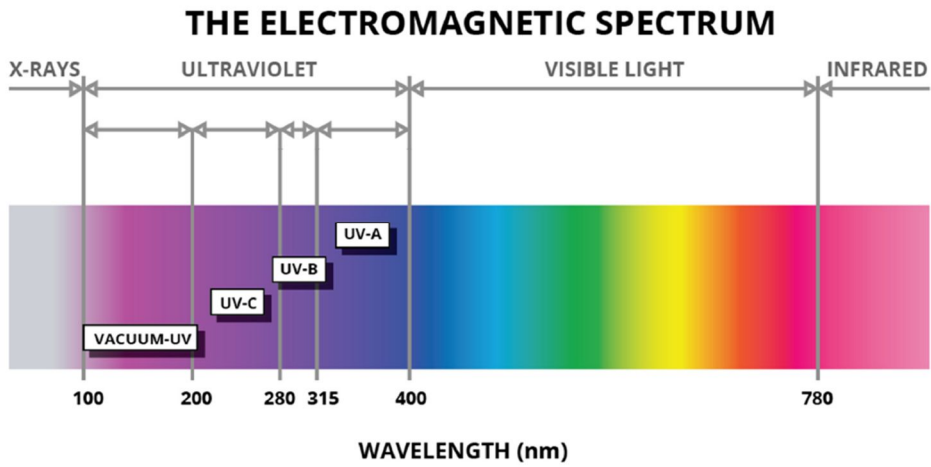


Fig. 1-1. Classification of UV rays with a wavelength region.

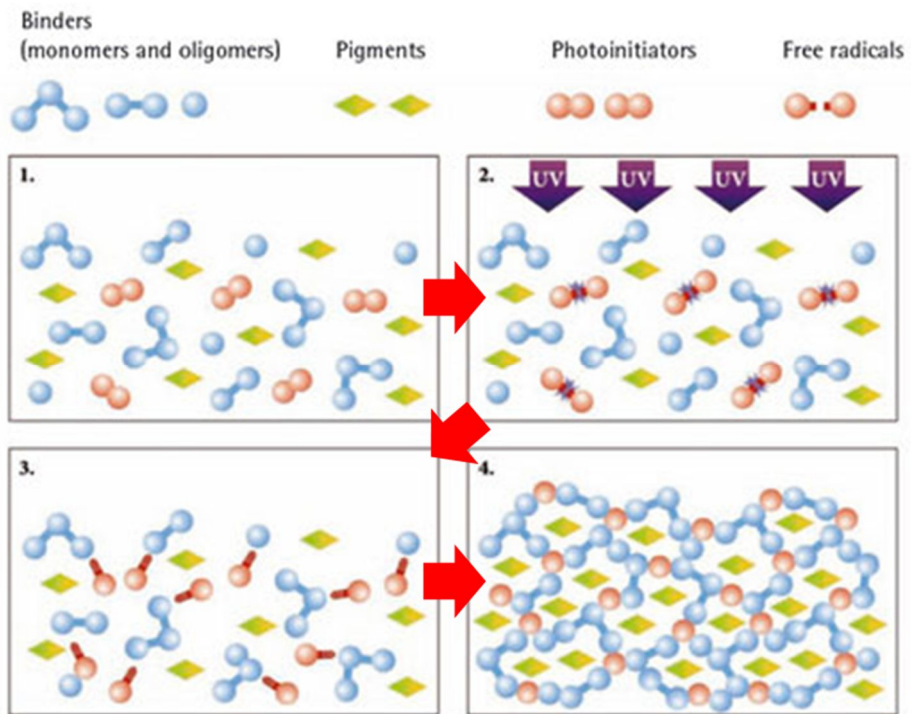


Fig. 1-2. UV curing sequence, 1) Formulation, 2) UV irradiation, 3) Initiation and 4) Curing [Brancher, 2015].

Because UV curing is unlike the common thermosetting technique - the reaction is advancing very quickly, the technology using UV source not only save energy in the process but also improve productivity. In addition, the manufacture of solvent-free process is possible and it is suitable for the manufacturing process environmentally friendly technologies. The general advantages of UV curing technology are given as follows.

- **Solventless process: non VOCs**
- **Room temperature processing**
- **Fast curing system: low energy consumption**
- **High speed process**
- **Small handling space**
- **Excellent finishing processing**

#### 1.1.2.1. Adhesion and Drying between Electronic Components and Optical Components

Because UV curable resin is cured instantaneously when irradiated with UV, it is considered as a key technology in the field of adhesive. Since the materials has useful features such as a little changing of volume after curing (compared thermal curing), transparency, and fast drying, it is often used in the adhesion of precision mechanical parts and optical components.

[Example]

Liquid crystal panel, bio-chips, cameras and prisms, pickup lens of the CD/DVD player (the part that recognizes the information of light reflected from the disk), hard disk magnetic component parts, speaker cones, parts of the engine internal magnet coil, motor, electronic components, and circuit board [USHIO Japan, 2013].

#### 1.1.2.2. Curing and Drying of Printing/Ink System

Recently, in the field of packaging industries implements were formed the unique appearance of various materials such as aluminum or a metal, and plastic. It has a form that is different from a flat structure; it has the drawback in coating and general printing. In order to realize the printing and drying on the exterior surface that is difficult by general materials, UV curing materials are adopted in the case. UV curing technology is also applied to accelerate the curing and drying for high productivity.

[Example]

Can/PET bottle of juice and beer, container of shampoo and cosmetics, tube such as toothpaste, card types such as a credit card or membership card, switch of OA equipment/appliances, keyboards, seal/stickers, and CD/DVD.

In addition, UV curing and drying devices have been used when processes need to print a large amount with high speed or a large-sized product such as package of candy, flyers and catalogs, and large posters.

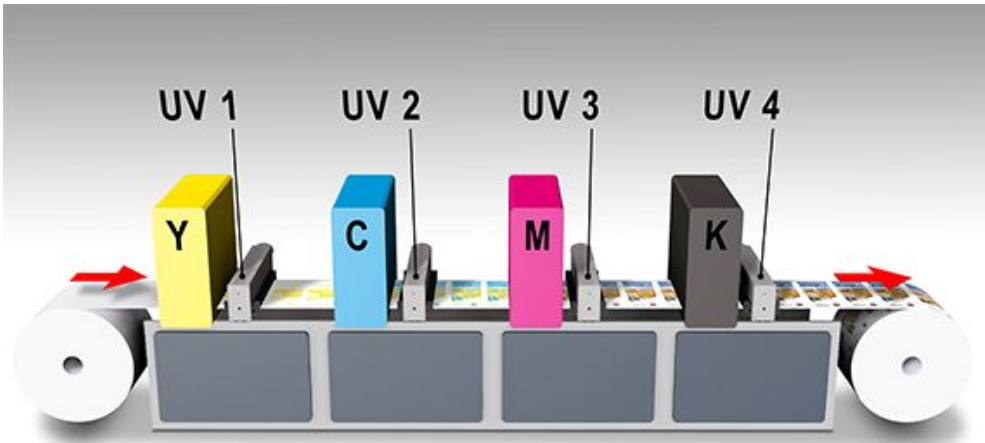


Fig. 1-3. Schematic figure of UV ink application to take advantage of the UV curing system (GEW, 2015).



Fig. 1-4. UV curable adhesive for electric area (Permacol, 2015).

### 1.1.2.3. Curing and Drying of General Coating

UV curing technology has been applied to the packaging process of products with new shape and design in the fields such as mobile phone and automotive, which are classified advanced integration/complex technology. In addition, UV curing and drying technology are used in the process such as surface protection construction, common plastics and coating of hard-coat for gloss/hardness. By the introduction of UV curing technology, it enables a new design and improving productivity.

[Example]

Lens, mirrors, body, and headlights of bike and automobile, plastic lens glasses, cellular phone, game consoles, toys, metal tone switch, system kitchen, furniture, exterior/interior tile and floor.

### 1.1.2.4. Other Specific Area

UV curing technology has been used in many areas other advanced industries. Coating of optical fiber, protective coating of identification, forming of a Fresnel lens (peeling after curing to put the resin into a mold),

mold keychain or dish (thick processing the transparent resin) and UV creates a model (3-dimensional CAD stereo lithography UV Curing technology has been used to cure the resin, as a technique for creating complex three-dimensional object).

### 1.1.3. Forecast on World Market of UV Curing Materials

In 2011, the merging market size of UV curable materials that include paint/coatings, inks, and adhesives was evaluated to increase up to \$ 6 billion or more as the UV curing market has grown steadily every year. One of features of the market is that more than 50% of the market shares an ink related industries in particular [Fuji Keizai, 2012].

The market size of UV curable coating material and coating agent reduced by process change of an optical disc and mobile phones. However, the market of adhesive, which was occupied small portion in the field of UV curable resin, has expanded significantly by the rapid development of the touch panel or smartphone and it drives the market growth. Rapid growth of the smartphone market in Korea has induced the rapid growth of the UV curable adhesive material market in particular.

In 2107, the market of UV curable coating materials and agent area will reduce to the level of 2012 or more. However, the market is expected to grow to \$ 6.5 billion or more because double-digit growth has continued in the market of adhesive from 2012.

#### 1.1.3.1. UV Curable Adhesives

Recently, optical adhesive material added its importance depending on the growth of the smart industry. The primary roles of the optical adhesive are to control the optical properties and to ensure the reliability of the final products. It is possible that various materials are applied to the adhesive system such as acrylate, silicone, urethane, and epoxy, etc. In particular, so acrylate material is used as a main raw material for the production of adhesives because it has a very wide option.

UV curing adhesives are expected to be the fastest growing product segment over the next seven years because of rising demand in medical devices. This particular segment is expected to grow at a CAGR of over 12% from 2015 to 2022 [Grand View Research, 2015].

Surface mount devices are the largest application and generated revenue worth USD 1,329.8 million in 2014. This is expected to be the fastest growing application segment over the forecast period. Rising electronics manufacturing capabilities in Europe and Asia Pacific is supposed to drive this segment growth over the forecast period.

Conformal coatings accounted for over 24% of the global market share and are anticipated to witness stagnant growth rate over the forecast period. High requirement for protecting circuit boards from corrosion and abrasion is a major factor contributing demand in the segment. These coatings also provide significant protection from external stress, which is also estimated to enhance product penetration.

Potting and encapsulation are expected to witness rapid growth over the forecast period owing to significant requirement in applications including relays, automotive power trains and fly-back transformers. Technological advancements coupled with increasing demand for consumer electronics including mobile phones and video games have furthered industry penetration in this segment.

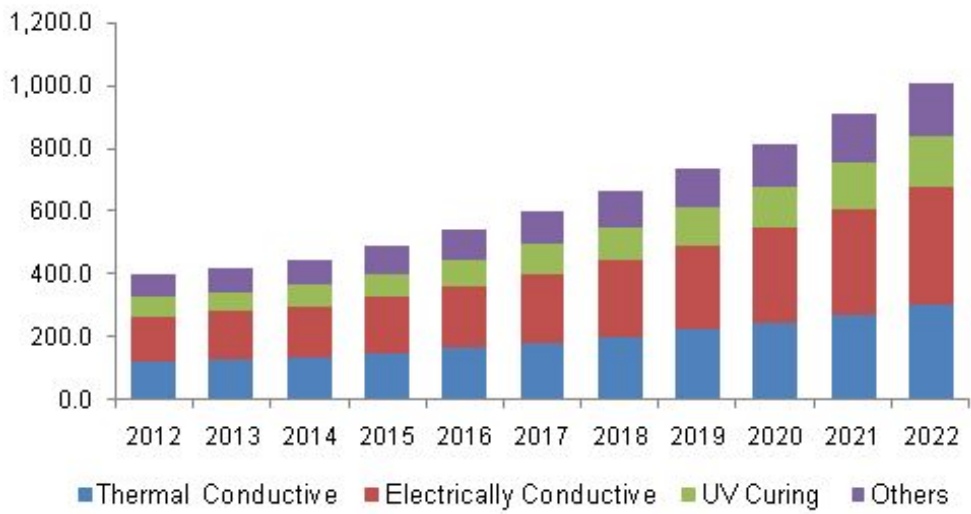


Fig. 1-5. U.S. electronic adhesives market revenue by product, 2012-2022 (USD million) [Grand View Research, 2015].

### 1.1.3.2. UV Bulk Polymerization

In general, the process of the solvent polymerization is used in the industries. The solvent polymerization process is designed in various solvent based. Therefore, it can be in a variety of polymerization conditions. There is an advantage that the process can be adjusted variously to the performance of the polymerized material based on the process condition. In recent years, however, the needs of polymerization processes, which do not use these solvents, are highlighted in response to various environmental issues.

The bulk polymerization process is the simplest form of the polymerization process. However, there are some disadvantages such as the heat control and the molecular weight control. Therefore, this process has been used very few times. To overcome these drawbacks, the UV curing technology was applied to the bulk polymerization process. By utilizing the UV technology, heating generation can be controlled. In addition, it can adjust the time of the polymerization. Therefore, it is possible to control the structure of the molecules variously. It is also possible to produce a high-performance adhesive through the secondary blending and curing process.

In the preparation process of the adhesives, UV is used in both the

polymerization process and the curing process. Especially the curing behavior in the secondary curing process gives a great influence on the physical properties of the adhesive. Curing behavior is the most significant factor in applying the process of the adhesive. The typical curing behaviors are having a cure rate and shrinkage. The cure rate is a major impact on process ability. When shrinkage increases, internal reliability of the product decreases. Therefore, analysis of these curing behaviors is essential. These properties are dependent on the reactive diluent that is used in secondary curing process. The diluent is not only used in controlling the curing properties but also did in controlling the viscosity and specific properties. Therefore, the selection and the use of the diluent are very important.

#### 1.1.3.3. Dental Adhesive

Dental adhesives and sealants market can be segmented based on the application fields such as denture bonding agents, pit and fissure sealants, restorative adhesives, luting cements, orthodontic bonding agents, tray adhesives and dental surgical tissue bonding (Duqum, 2012).

The major market drivers of dental adhesives and sealants market are

improper food habits, young generation in age group of 16 to 26 years is more aware about dental care and high buzz of oral care campaigns by governments and companies. Some of the major restraints of this market are low dental hygiene quotient in adults in the age group of 30 to 40 years and high treatment costs in North American and European countries (Transparency Market Research, 2012).

The largest markets for dental adhesives and sealants is observed in North America and Europe. While, Asia-Pacific area is the most attractive market since the awareness about oral hygiene is increasing in this area, especially in developing countries including China and India where most of the younger generation is investing in the dental care. In the rest of the World, it is also considered that the market for dental procedures grows; especially the most attractive markets are some of the countries of Latin America.

#### 1.1.4. UV Curing Mechanism

The UV curing process requires a light source, which directs UV or visible light onto the formulated product. Photo-initiators absorb the UV energy

from the light source, setting in motion a chemical reaction that quickly, in fractions of a second, converts the liquid formulation into a solid, cured film.

The bulk of the formulation is composed of monomers and oligomers. Monomers are low molecular weight materials. They can be mono or multi-functional molecules, depending on the number of reactive groups (usually acrylate) they possess. Functional monomers become part of the polymer matrix in the cured coating because their reactive functional groups undergo polymerization during exposure to UV light.

Monomers also function as diluents in the formulations, used to adjust system viscosity, and are sometimes referred to as reactive diluents. Oligomers, conversely, tend to be of higher molecular weight, viscous materials where the molecular weight ranges from several hundred to several thousand grams/ molecule or even higher. Usually, the type of oligomer backbone determines the final properties of the coating such as flexibility, toughness, etc. These backbones can be epoxy, polyether, polyester, polyurethane or other types. The functional groups that provide linkage between molecules are located at both ends of the oligomer molecules. The functionality found to be most effective is the acrylate functional group (Ciba, 2002).

### 1.1.5. UV Curing Chemical

Most materials utilized in UV curable systems has the unsaturated structure. There are the materials having the structure such as acrylate, methacrylate, vinyl, and allyl. Among these various types of materials, acrylate is most frequently used at currently.

The reasons of using the acrylate are as follows;

- 1) It is possible to reproduce a variety of structures
- 2) The producing cost is low
- 3) The manufacturing process is simple

These acrylates vary according to their structure and properties. The width of its performance that depending on the type and form is very wide.

#### 1.1.5.1. Structure and Basic Properties of Acrylate

Acrylate material can be implemented as the form with a variety of structures by changing the core structure. It is possible to make a difference in molecular weight under the same side-chain structure or implement to vary the number of functional sites as having the same site. The basic properties of acrylate with these various structures changes depending on the size of the structure and the number and type of functional groups. Figure 1-6 presents the fundamental change in the physical properties according to the structural differences of acrylate. The choice of materials depends on these differences in performance. In particular, it is important to select materials in accordance with the viscosity and reactivity required on the UV curing process. Therefore, analysis for the change in the physical properties of the materials is needed essentially.

		Reactivity	Viscosity	Adhesion	Toxicity
Mono-functional monomer		Slow	Low	Good	High
Di-functional monomer		↓	↓	↓	↓
Multi-functional monomer		Fast	High	Poor	Low
For same functionality	Low MW monomer	Slow	Low	Good	High
	↓ High MW monomer	↓ Fast	↓ High	↓ Poor	↓ Low
For same functionality	Acryl monomer	Fast	Low	Poor	High
	↓ Methacryl monomer	↓ Slow	↓ High	↓ Good	↓ Low

Fig. 1-6. Comparison of material properties in accordance with the difference in the size and functionality of monomer [Miwon Specialty Chemical, 2015].

#### 1.1.5.2. Curing Properties of Multi-functional Acrylates

In UV curing system using an acrylate, the multi-functional acrylate plays an important role in controlling the physical properties. Generally, it acts as a key factor in determining the physical properties of the polymer film because it has an excellent reactivity and a higher cross-linking density as compared to mono-acrylate. The Figure 1-7 shows how the basic physical properties of the multi-functional acrylate changes depending on the number of functional groups.

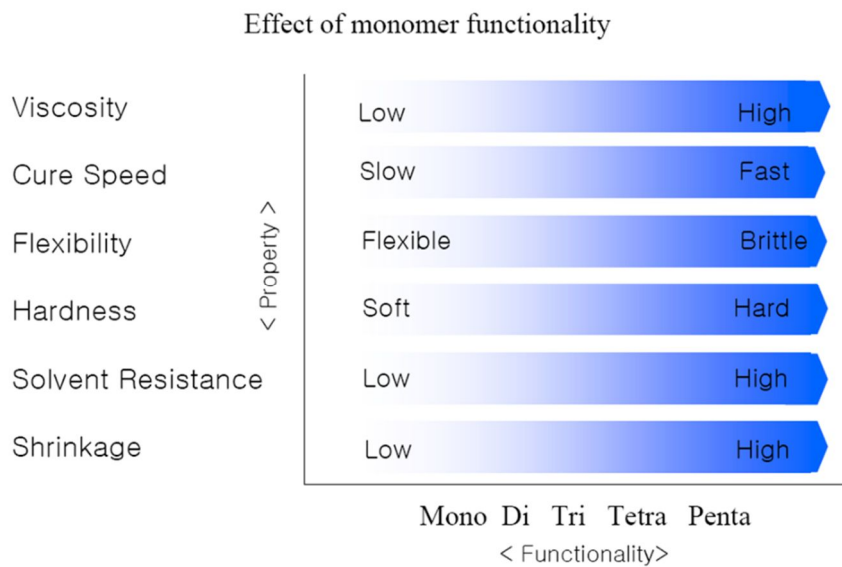


Fig. 1-7. Comparison of multi-functional acrylate's properties in accordance with the functionality [Miwon Specialty Chemical, 2015].

### 1.1.5.3. Changing of the Characteristic due to the Extension of the Molecular Structure

A variety of structures of acrylate can also make a change in the molecular size as well as in the functional groups freely. Ethoxylation and propylation are representative methods to be able to alter these structures. Each method that links the ethylene glycol or propylene glycol structure repeatedly to reproduce the final structure has different characteristics. Basic properties of ethoxylated monomer are characterized as hydrophilic, fast-curing, good diluent, and chemical-resistant, and it is more water-soluble, faster-curing, surface-curing, more flexible, and lower toxicity according to the increasing of ethoxylated structures. On the other hand, propoxylated monomer is hydrophobic, hardness, and chemical resistant, and it is slow cured and more flexible and has the decreased modulus according to the increasing of propoxylated structures

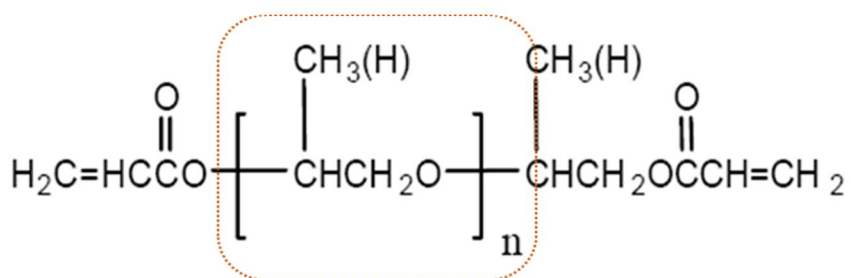
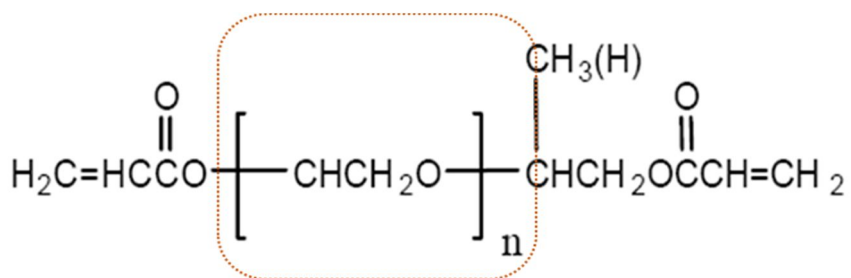


Fig. 1-8. Structure of extended acrylate (a) ethoxylated (b) propylated.

### 1.1.6. Problems UV Curable Material, the Need for UV Curing Behavior Analysis

The UV curing technology is expected the stable growth of a market by taking advantage of the advanced feature, there is a tendency that its scope is expanding. However, various problems have also been reported as the range of its use has been expanding.

The UV curing technology has some problem such as response to early hours, high exothermic and rapid shrinkage of the material. Further, it is not possible to reach 100% conversion rate of the material, thus the unreacted functional groups remain. This phenomenon occurs a change in physical properties and appearance change of material, and that can be cause problems of reliability of the product of a long-term perspective. Because the curing behavior is different according to the various conditions -inside and outside- of materials, accurate prediction is difficult. The following are those mentioned disadvantages of UV curable materials in general.

- **Difficulty in maintaining the smoothness of the surface**
- **Complex condition of Variable viscosity/thickness**
- **Oxygen inhibition effect**

- **Poor curing of thick film, deep coating**
- **Adhesion failure occurs (Adhesion to the substrate)**
- **A secondary reaction is produced by uncured material**

Therefore, it is needed to develop the system to solve all of the problems and the advanced model to predict future changes associated with the use of the product. By these require, many groups have researched analyzing tool of the characteristics of the material from developing the raw material to final products. Methods of more accurately predict the UV curing behavior, in particular, has evaluated continued until recently.

### 1.1.7. Shrinkage

The definition of “Shrinkage” is the amount by which anything decreases in size, value, weight, etc. In case of casting/molding industries, that means a slight dimensional reduction brought about by the reduction in volume of the cast or molded material as it cools and solidifies. When shrinkage of a part will present fitting problems, e.g., interchangeably, the casting pattern/mold cavity is made slightly larger.

Shrinkage has been studied in various fields. Especially, it has been investigated in a direction to maximize the stability and minimize external defects of the product in connection with industrial productivity. For example, the research on the change in appearance of the product has been conducted in the field of extrusion and injection-molding of polymeric material, accumulated variable results depending on external factors such as injection velocity, injection temperature, the difference between internal and external temperature, and cooling rate, and applied mass production techniques. The shrinkage control is the most important part of the application of the UV curable material. UV curing materials, which rapidly shrink in the curing process, the theoretical shrinkage level is over 20%. This

shrinkage behavior can induce warpage of the material and adapted to generate an internal stress. These phenomena linked to problems with the finished product.

A variety of materials to apply the curing system, particularly, resin and cement with the photo-curing system, are applied in the field of dentistry. The photo-curable resin and cement are used variously in dentistry because they have the advantages such as fast-curing, excellent surface properties, and high strength. However, the photo-curable resin is considered as a substance that should be handled very carefully because it has a high shrinkage, which results in the decreased surface adhesiveness (degradation of surface binding force) and the physical damage of cured materials. Therefore, the shrinkage of photo-curing resin should be lower, which demands to reduce the degree of conversion or reactivity of the resin. However, this can cause problems such as the transition phenomenon of uncured resin materials or the delays of setting time of the resin.

The volume shrinkage of acrylates and methacrylate occurs during polymerization and is due to the replacement of long-distance connections via weak Van der Waals force by strong short covalent bonds between the carbon atoms of different monomer units (Figure 1-9 and 1-10). This volume

shrinkage causes serious problems, including a large build-up of internal stress, which results in defect formation, and dimensional changes, which are responsible for decreased mechanical properties shrinkage of UV Oligomers and Monomers (Moeck, 2014). Volume shrinkage is one of the main drawbacks of UV cured coatings and can lead to premature coating failures

However, the mechanism of light-curing system is directly related to the shrinkage of photo-curable materials. The shrinkage is a phenomenon that occurs as each space of monomer units overlaps during curing. The shrinkage increases linearly as curing of each monomer progresses. The factors affecting the curing mechanism are divided into internal factors such as molecular structure and features and the number of functional groups in materials and external factors such as the amount of initiators and the intensity and wavelength of light. Therefore, it is an important factor in handling the materials to analyze the curing mechanisms according to internal and external factors and the relationship between shrinkage and them.

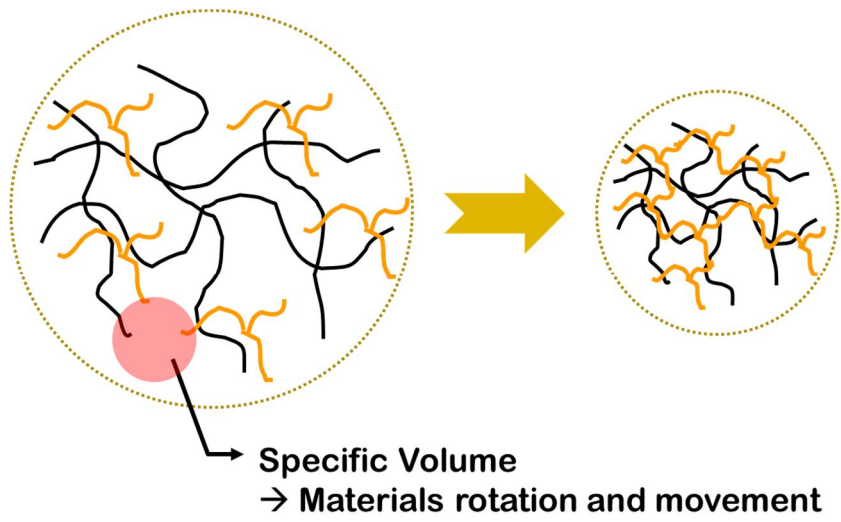


Fig. 1-9. Scheme of shrinkage occurring by UV curing

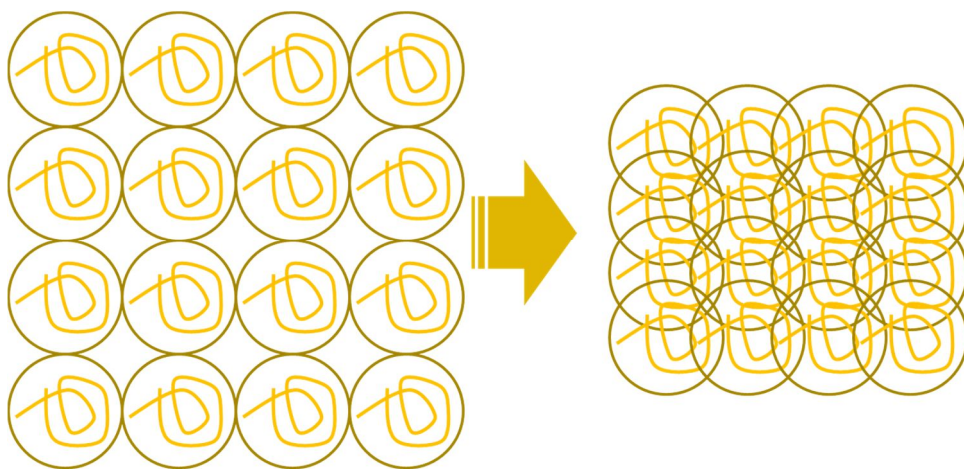


Fig. 1-10. Volumetric Shrinkage of monomer by blob linking

## 1.2. UV Curing Evaluation Method

To evaluate the curing behavior of the molecule, approaching viewpoint from the physical and chemical is possible. It is possible to divide into two methods that is determined by changes of the appearance of the material and physical properties and the micro viewing that method for measuring the change in energy due to changes in the transition stage /the changing of binding structure forms of intermolecular. Evaluate the UV curing behavior also applicable similarly, it is identifiable two methods - evaluating the mechanical behavior and evaluating the thermo-chemical behavior.

To measure the mechanical behavior of the material according to UV curing, there is a method of measuring shrinkage that was the volume change of the material caused by the curing and methods of measuring the shear stress/viscosity that is depends on the change in rheological behavior by material curing.

To measure the thermo - chemical behavior the material with UV curing, there are two methods typically. After UV initiation, Fourier transform infrared spectroscopy (FT-IR) can measure a change in the chemical bonds, especially some kinds of bond such as double bonds in particular. Another

tool such as photo-differential scanning calorimetry (DSC) can measure exothermic by the chain reaction - for example, the binding energy varies in the reaction that the double bond changed to one strand - depending on the structure changes.

Recently, the method of measuring real-time UV curing behavior is highlighted, the measurement method described above are changes to a method for real-time measurement.

#### 1.2.1. Evaluation System using Thermo-chemical Behavior of UV Curing

Generally, real-time FT-IR and photo-DSC are used to measuring method for analyzing the thermo-chemical behavior on UV curing process. They have been used as analytical techniques for chemical for a long time and were applied very quickly to analysis of UV curing behavior.

##### 1.2.1.1. Photo-Differential Scanning Calorimetry

Photo-DSC with the structure as shown in the Figure 1-11 is a device that measures the difference in energy, generated between the specimen and

reference. The biggest difference from the general DSC, the most DSC measurements is running a temperature ramp condition, in other hand almost a case of photo-DSC is running on the isothermal test condition. Therefore, photo-DSC measuring the heat of reaction of the material according to the energy influx of external in constant temperature conditions that differ from the DSC which of measure 1st/2nd transition point. The Figure 1-12 shows the photo-DSC measurements in general. The curve that means the heat - flow will be rises the moment the UV is irradiated. The curve of beyond the highest point, it is decreased with the form descending in a curve. The height of the peak is constant for the reaction rate in the unit time. As the height of the peak is high, the reaction rate by UV be faster.



Quartz Window    PCA Outer Lid    PCA Inner Lid    PCA Platforms

Fig. 1-11. Cell / lamp guide design and appearance of photo-DSC

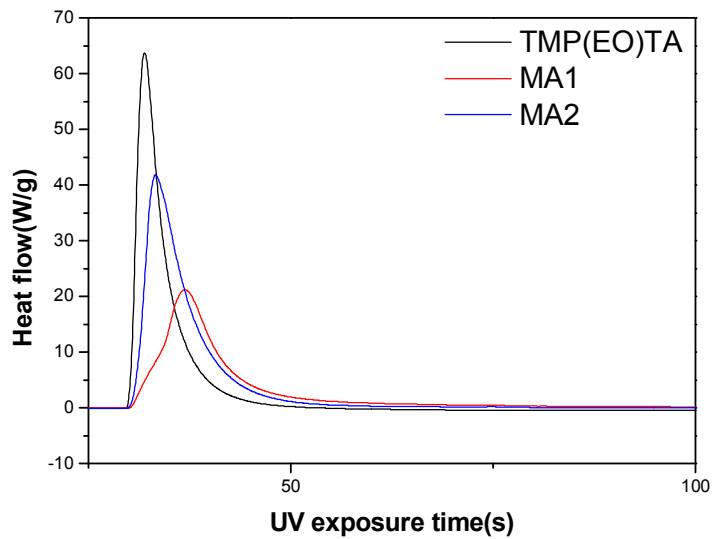


Fig. 1-12. General result using photo-DSC (Park, 2011).

#### 1.2.1.2. Real-time Fourier Transform Infrared Spectroscopy

Real-time FT-IR have the same structure as the general IR, however, it is a device for a high speed repeat, scan process scanning and reading very quickly change the molecular structure through high-frequency (250 scan/s). If the change of the molecular structure occurs as shown in Figure 1-13 and 1-14, real-time FT-IR can be work scanning for measuring the reaction structure is possible. Generally, it becomes possible to measure by building a system of the reflection type of the ATR method. FT-IR has advantage to confirm the change in the molecular structure itself.

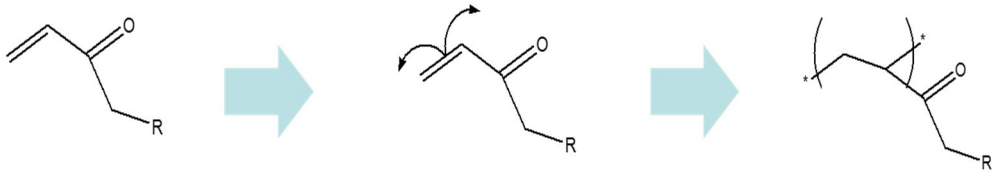


Fig. 1-13. Molecule structure changed by UV curing.

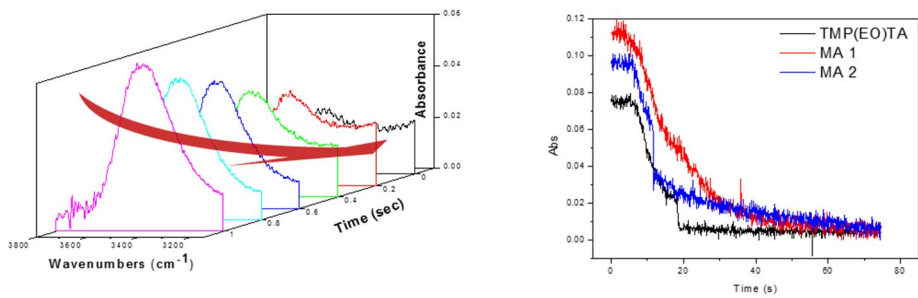


Fig. 1-14. General result using real-time FT-IR (Park, 2011).

### 1.2.2. Evaluation System using Mechanical Behavior of UV Curing

Meanwhile, a method of measuring mechanical behavior has started to be introduced recently, that have received a lot of attention because the methods has advantages which can be observed the perspective macroscopic mechanical- physical changes from raw materials to end products.

Measurement of the rheological behavior is a technique for measuring the visco-elastic behavior of the polymer. The technique for analyzing the characteristics of the molecules varies according to molecular condition or general environment such as temperature, impact velocity, and frequency. It is a technology that can setting limits the scope of industrial application the materials. General rheometer will measure a phenomenon that viscosity is increased by UV curing and analysis process of changing molecular from semi-liquid or solid state into a solid state. ARES (advanced rheometric expansion system, TA, USA) is a general tool measure rheological property of materials. Storage modulus, loss modulus and tan delta are derived from the experimental results.

# *Chapter 2*

## Literature Review

## 2. Literature Review

### 2.1. Research on Applied UV Curable Resin

Recently, the several studies have reported on the expanded application of UV curable resin such as composite curing system.

Hwang, *et al.*, [2011] reported research about the synthesis of UV curable urethane material and its application in the automotive field, the change of material properties-before and after curing-, and analyzed the overall UV curing behavior. The effects of polycarbonate diols on the UV curing behavior and their physical properties were evaluated according to their molecular weight. The UV curing behavior was analyzed using FT-IR and photo-DSC.

Park, *et al.*, [2009] developed and evaluated dual-curing type UV curable material utilized in the manufacturing process of the display (Figure 2-1). Complete curing of the UV curable material is impossible through a single curing method because there is a limit to control the conversion rate. Therefore, tools quantifying the curing system is essential. They introduced

an additional curing system promoted by thermal curing. Dual-curable adhesives were prepared using various epoxy acrylate oligomers, a reactive diluent, photo-initiators, a thermal-curing agent, and a filler. The UV and thermal-curing behaviors of the dual-curable adhesives were investigated using photo-DSC and FT-IR-attenuated total reflection spectroscopy in aspects of the determination of gel fraction, pendulum hardness, and adhesion strength.

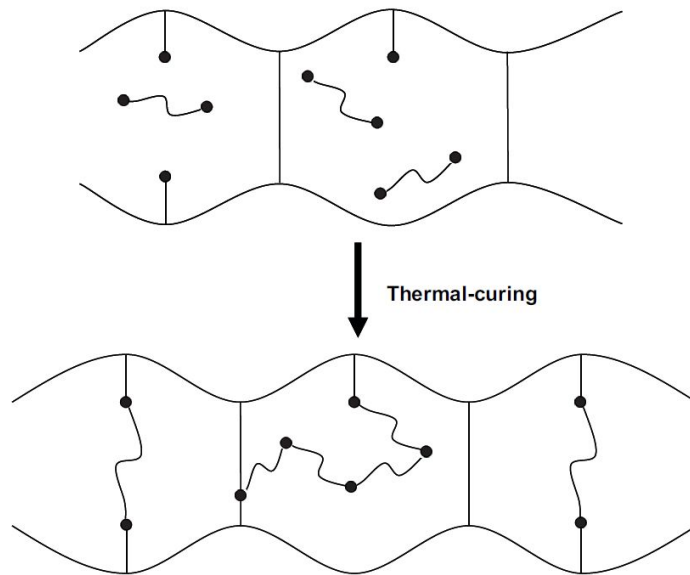


Fig. 2-1. Synthesis and evaluation of UV and thermal dual-curable resin  
[Park, 2009].

Zhenglong, *et al.*, [2010] introduced thiol and multi-functional systems to ensure the curing rate of UV curable coating materials. They presented a novel approach to the preparation of UV curable polyurethane coatings combined multi-functional thiol- and ene-terminated polyurethane with aqueous dispersions. By the synergistic combination of polyurethane dispersion synthesis and thiol-ene chemistry, the strategies for the preparation of new UV curable polyurethane coatings were developed. The measurements such as photo-DSC, real-time FT-IR, dynamic mechanical analysis (DMA), and tensile test are used to investigate photo-polymerization and mechanical behavior of UV curable polyurethane coatings.

Lee, *et al.*, [2013] studied about adhesive material applied to the semiconductor manufacturing process. The rapid change of product properties was possible through the formation of a three-dimensional structure in the newly introduced UV curing system; it ensured excellent heat resistance. They employed semi-interpenetrated (IPN) structured polymer networks by UV curing using acrylate-terminated dual-curable urethane, epoxy adhesive, dipentaerythritol hexaacrylate (DPHA), and hydroxydimethyl acetophenone as a photo-initiator.

Lu, *et al.*, [2015] researched technology for carbon composite materials using a UV curing system. Since UV curing system has a fast conversion rate from liquid to solid, characteristics of system are generally excellent. However, there are disadvantages such as incomplete curing in shadow area. Thus, the challenge is the non-UV transparency of the composite materials. This research considered to adhere UV resin to damaged panels to form hard patches for fast repair and introduced a new UV curing system.

Martin-Gallego [2015] also used gold-functioned graphene as a conductive filler in UV curable epoxy resin. They analyzed the change of fundamental curing properties to control characteristics of the curing system including a filler.

## 2.2. Evaluation of UV Curing Behavior

Zekeriya *et al.*, [2011] used the photo-DSC to analyze the role and function of photo-initiator affecting the curing behavior of UV curable materials. By photo-DSC technique, they assessed the behavior of photo-initiated radical polymerization between the mixture of 80 wt% of epoxy diacrylate (EA) and

20 wt% of tripropylene glycol diacrylate (TPGDA) and 2-mercaptothioxanthone (TX-SH) as a photo-initiator according to temperature.

Aruma *et al.*, [2007] analyzed the UV kinetics of a UV curable material derived from castor oil by photo-DSC and predicted its mechanical properties before and after curing through dynamic mechanical studies. A ricinoleic acid amide-di-functional acrylate synthesized from that oil- was rapidly polymerized as well as non-irritant and non-pungent. Cross-linking networks were formed by photo-polymerization with the monomer as varying the amount of reactive diluents such as TPGDA and trimethylol propane triacrylate (TMPTA) to modify the viscoelastic characteristics of the networks.

In order to analyze the energy transfer system and curing behavior of polymer composite materials and nanoparticle, Nearingburg *et al.*, [2011] used the photo-DSC. Opto-thermal properties of the polymer and nanoparticle composite were measured by the photo-DSC. A specimen was characterized in isothermal mode according to the presence and absence of optical illumination

Combing the real-time FT-IR and photo-DSC, Duygu, *et al.*, [2011] analyzed the curing behavior of multi-functional acrylates. Photo polymerization reactions were performed under different initiator concentration and UV light intensity.

Carola *et al.*, [2009] also used both the real-time FT-IR and photo-DSC complexly to analyze the curing behavior of UV curable epoxy resin. Lower rate in cross-linking reactions and higher conversion degree were obtained in photo-DSC experiments with real-time FT-IR. A limited amount (10 wt %) of HBP influenced to a certain extent of curing kinetics of the epoxy resin followed by FT-IR

Cho, *et al.*, [2007] was referred to the introduction of an *in situ* system for measuring the curing behavior of the UV curable material. The curing process of UV curable cationic adhesives containing cycloaliphatic epoxide, oxetane, and  $\epsilon$ -caprolactone polyol was investigated using a sensor composed of two indium tin oxide (ITO) that coated glass plates separated by a Teflon spacer, which measures the electrical conductivity and capacitance of the resin specimen. The experimental results showed that, as the photo-initiator concentration increased, the relative conductivity rapidly

decreased, indicating an increase in the percentage of cure conversion and the cure rate, as confirmed by photo-DSC analysis

### 2.3. UV Curing Behavior Research using Shrinkage Test

Christian, *et al.*, [2015] reported quantitative determination and time-resolved monitoring for shrinkage during UV-polymerization progressed with near infrared (NIR) spectroscopy (Figure 2-2). Conversion rate is measured by observing the change in the C = C double bond structure of acrylate in the light with wavelength range of  $1620\text{ cm}^{-1}$  according to the difference in wavelength between the UV and NIR with the evaluation of shrinkage phenomena,

Le, *et al.*, [2014] researched about the influence on color of materials in the shrinkage evaluation of UV curing molding products. The results show that shrinkage evolution depends on the absorption action of the color of materials on the light and the inhibition of the nonnative component.

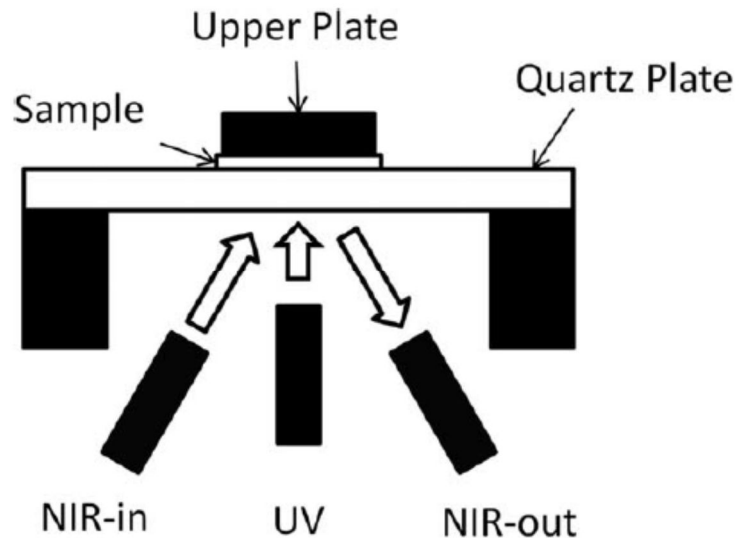


Fig. 2-2. NIR system for analysis of real time shrinkage materials (Christian, 2015)

Gee, *et al.*, [1993] introduced linimeter, which is proposed as a measuring system to predict volumetric shrinkage through axial shrinkage (Figure 2-3).

Lee, *et al.*, [2006] analyzed the relationship between volumetric shrinkage and axial shrinkage (Figure 2-4). The measuring instrument was developed to predict the volumetric shrinkage from the assessment of axial shrinkage. The degree of shrinkage is determined by the aspect ratio of specimen and the adhesion condition of substrate. At least 6 C-factor (aspect ratio), volumetric shrinkage can be interpreted immediately from results of axial shrinkage after the adhesion with substrate is complete.

Carlos Alvarez-Gayosso, *et al.*, [2004], to measure the shrinkage phenomenon of light curing material, introduce real-time shrinkage meter. Measuring the variation of shrinkage in accordance with the characteristics of the material. In the shrinkage measurement of real time, changes in contraction rate can be observed.

Sufyan Garoushia, *et al.*, [2008], in the curing process of composite materials reinforced with short glass fiber, confirmed the shrinkage phenomenon and the accompanying formation of IPN structure. For

composite material, shrinkage of the material is not applied directly, anisotropic effected by of the filler.

Rhodes, K. *et al.*, [2000], study the shrinkage phenomenon and the problem of adhesion stress due to rapid curing characteristics that light curing system. To implement low shrinkage/low stress, introduce new material and curing system.

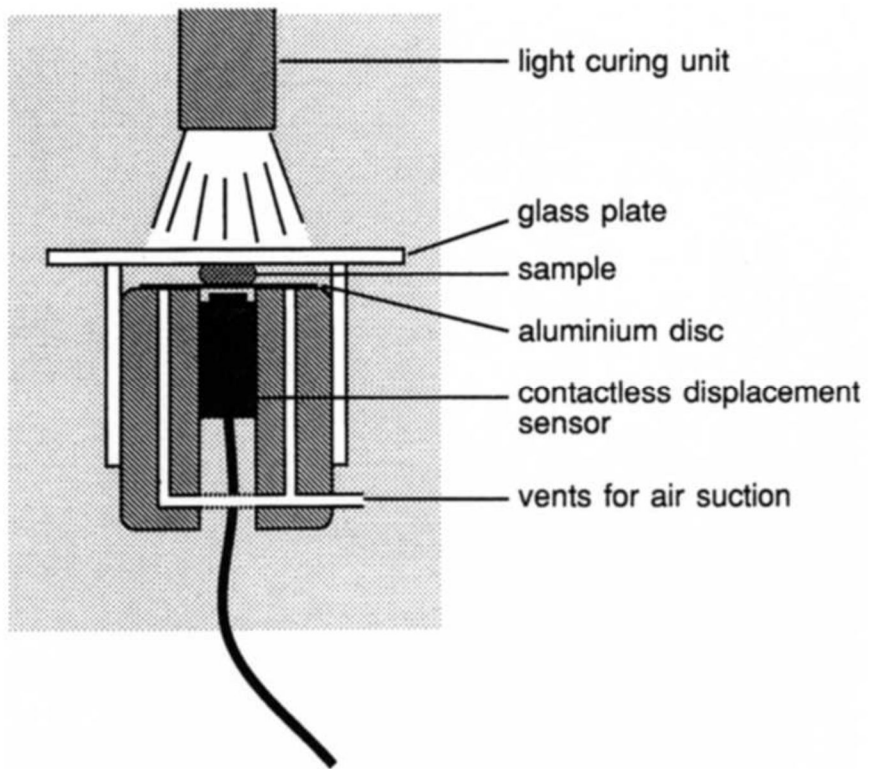


Fig. 2-3. Schematic drawing of the Linometer (Gee, 1993)

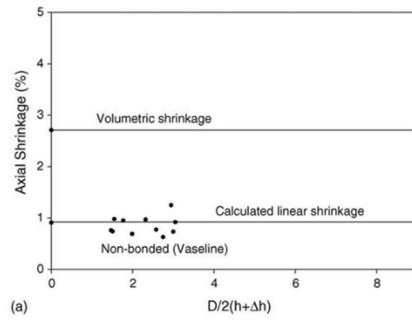
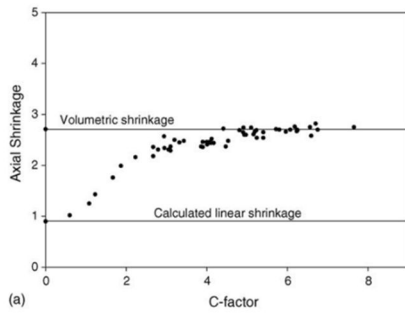


Fig. 2-4. The difference in axial shrinkage and volume shrinkage based on the c-factor (Lee, 2006)

## 2.4. UV Curing Application and Shrinkage Test

Katsuo *et al.*, [2015] designed a fine forming structure that uses a curable silicone resin. By utilizing 3-D confocal laser, micro-shrinkage phenomenon occurring after curing were evaluated (Figure 2-5).

Poonima *et al.*, [2015] introduced dilatometer to measure the volume change of epoxy/clay composites. As the particles that influence the reactivity are adopted, shrinkage varies with the reactivity of the change (Table 2-1).

Moeck *et al.*, [2014] also introduced a variety of UV curable oligomers and proposed application fields in accordance with the basic physical properties of each material. Especially in order to control the problem of shrinkage in areas where the material is applied, it proposes a technique, such as a blend of materials.

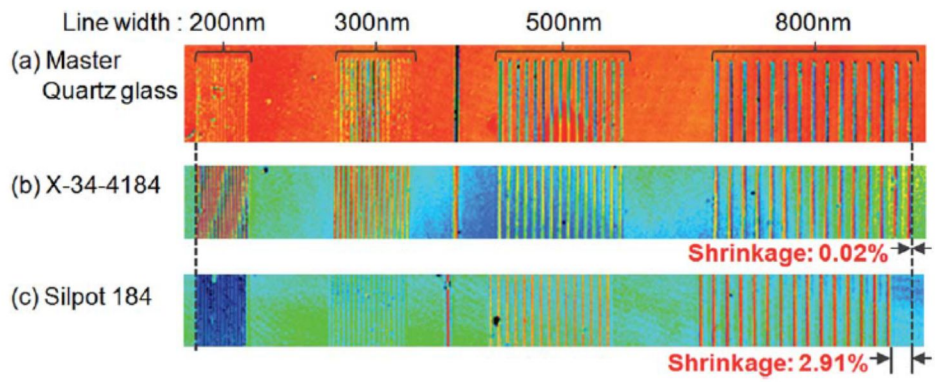


Fig. 2-5. Evaluating of micro-shrinkage phenomenon by 3-D confocal laser

Table 2-1. Volumetric shrinkage of epoxy/clay composites

System	$\Delta V$ based on $\Delta v_{e0}$	$\Delta V$ based on $\Delta v_{to}$	$\Delta V_{\text{normalized}}$ based on $\Delta v_{e0}$
Epoxy	5.16	7.27	7.27
Epoxy/15 phr CTBN	4.87	7.16	8.23
Epoxy/3phr clay	5.08	7.76	7.99
Epoxy/3phr clay/15 phr CTBN	4.71	7.69	9.07

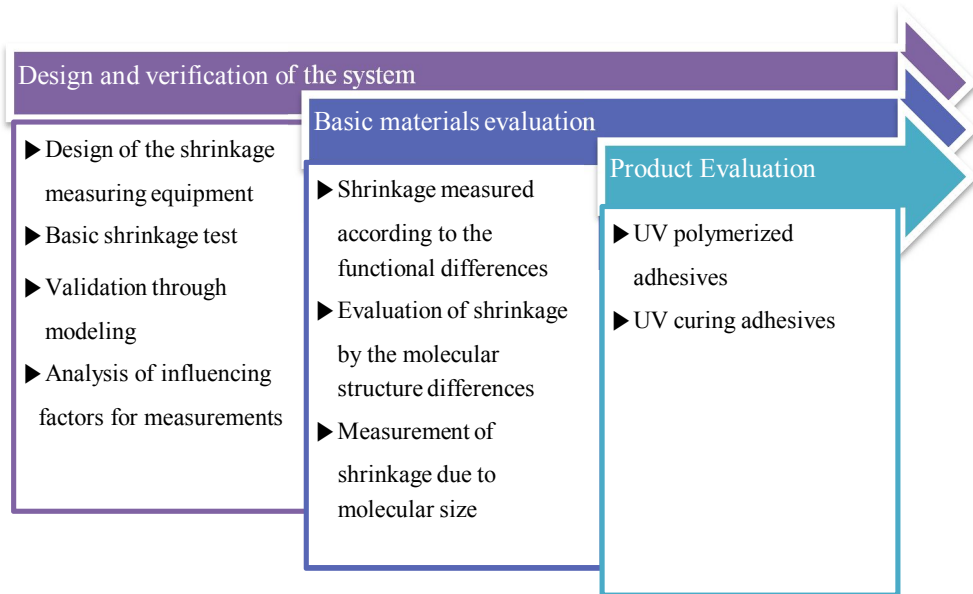
# *Chapter 3*

## Objectives

### **3. Objectives**

Shrinkage is pointed out as the biggest problem of the UV curing system. In order to solve these problems, a system for measuring the shrinkage has been introduced continuously. It has been introduced a feature of the test method such as range of error, the object to be measured, the system of elements, however, the exact description of the internal and external factors did not mention. In addition, shrinkage measurements are limited to a simple monomer or finished products, and accurate analysis for several variables of shrinkage changes based on the material characteristics have not been progressed.

Therefore, I designed a useful system for evaluating shrinkage factors in the shrinkage measurement and analyzed the internal and external variables. To analyze deviation occurring from the photo-DSC, I will propose a complementary method. Based on this system, I analyzed the shrinkage according to the characteristics possessed by the basic materials. In addition, I evaluated the effect of materials characteristics on curing behavior and shrinkage. Finally, I will explain the causes of the shrinkage characteristics of the actual products by analyzing the shrinkage properties with a material structure that replicated the shape of the final product.



# *Chapter 4*

Quantification of the Evaluation of Shrinkage

## 4. Quantification of the Evaluation of Shrinkage

### 4.1. Production of Equipment

#### 4.1.1. Design of Test Equipment

Common material will shrink constantly and independently to the direction. It is extremely difficult to measure the value as a volume. The shrinkage phenomenon can be changed in a variety by internal and external factors of the material. However, the axial shrinkage can be measured through a change in length. This can be explained by the following equation. Based on the equation below, axial shrinkage of material is calculated to be equivalent to one-third of the volume shrinkage.

$$\text{Volume A (original Cubic; edge length is X)} = X^3$$

$$\text{Volume B (shrinkage Cubic; edge length is X-a; a is linear shrinkage)} = (X-a)$$

<sup>3</sup>

$$= X^3 - 3aX^2 + 3a^2X - a^3 \text{ (} a^2 \text{ and } a^3 \text{ are can ignored because a is small)}$$

$$= X^2 (X-3a)$$

**(eq. 4-1)**

Nevertheless, according to such Lee [2006] and Park [2014], it is announced that the axial shrinkage and the volumetric shrinkage are approximately the same depending on the experimental conditions. The axial shrinkage almost reaches the volumetric shrinkage if the aspect ratio of the material is large, especially.

Shrinkage was measured by Linometer (Plustek, Taipei, Taiwan). First, the designated amount of specimen was loaded onto a stainless steel plate and covered with a sliding glass. They were placed on the displacement measurement sensor and transducer, and the slide glass on the top was fixed. When shrinkage of the specimen occurs by UV irradiation, the stainless steel plate was moved up and the moving distance was recorded according to the time. Finally, this axial shrinkage in vertical direction was transformed into a volume data and the estimate of volumetric shrinkage was calculated (Figure 4-1).

The optical measurement system using the half-mirror device was introduced to measure light intensity on the area where shrinkage actually occurs. The N<sub>2</sub> purging system also was done to address an oxygen interference problem with the radical curing method.

There are many types of light source to implement the UV curing system. Metal lamps and LED are used typically. The lamps have light sources with multi-wavelength bands and their main wavelength bands varies depending on the base materials. Whereas, the LED has a fixed wavelength band. In addition, there are several differences between them (Table 4-1).

In this study, we applied UV LED with a short-wavelength of 385 nm. I was designed such that its spectrum range was 5 nm, the maximum output was 150 mW at the reference surface which it reached, and the output control was able up to 255 stages.

Figures 4-2 and 4-3 are blueprints for implementing the measurement device. Its design that implements the light source is shown in Figure 4-2. UV proceeds in the direction of the arrow from the UV source to the sample. A configuration form of the overall equipment is shown in Figure 4-3. A cut-off structure was adopted to maximize the exterior of the element through the housing.

Table 4-1. Comparison of metal UV lamp and UV LED

Halogenic UV lamp	UV LED
Hot source & high pressure	Cold source & no pressure
High voltage: high energy consumption	Low voltage
Life cycle: 2,000 h	Long life cycle
Warm up: 90-30 min	Instantaneous on/off
Process environmental	Flexibility
Ozone	Non ozone

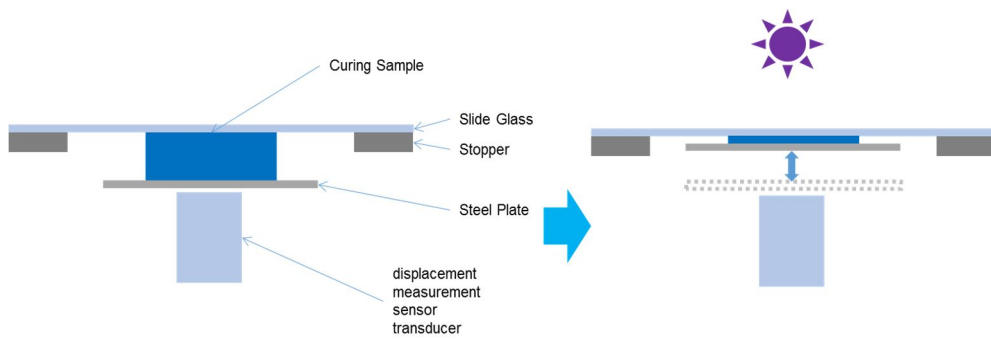


Fig. 4-1. Method of measuring the axial shrinkage with Linometer

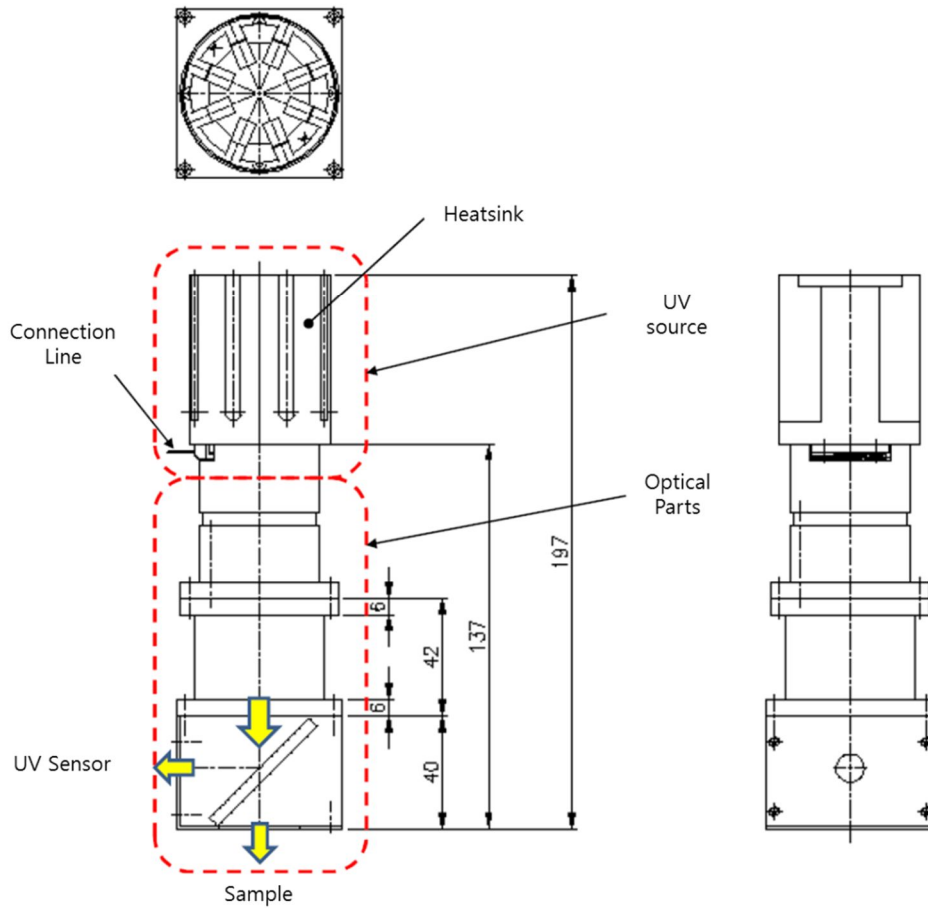


Fig. 4-2. Design of improved Linometer – UV light parts-



#### 4.1.2. Sensor Types and their Pros and Cons

There are different kinds of sensors, and the measurement methods are different depending on the types of sensors. Moreover, it is necessary to select a sensor optimized for the system since the strength and weakness of each method is different. Several sensors types have different characteristics of sensors for measuring the distance difference (Table 4-2).

Table 4-2. Advantages and disadvantages depending on the type of sensor

Sensor type	Advantages	Range	Disadvantages
Ultrasound-wave	The wide receiving Low cost	1,000 um>	Precise measurement is difficult Severe changes due to external wavelength
Infrared	High utilization category External damage is small	50 um>	Low resolution, The application limit of the permeable material
Laser	Accurate measurement Easy to use	0.1 um>	High cost
Eddy current	Accurate measurement Low cost Do not sensitive to temperature	0.01 %>	The applicable limit of the metal Resistance design needs
Capacitive	Ultra high resolution	0.001 %>	High cost Resistance design needs

#### 4.1.3. The Principle of the Electrical Sensor

Eddy-Current sensors operate with magnetic fields. The driver creates an alternating current in the sensing coil at the end of the probe (Figure 4-4). This makes an alternating magnetic field with induction of small currents in the target material; these currents are called as eddy currents. The eddy currents generate an opposing magnetic field, which resists the field by the probe coil. The interaction between magnetic fields is dependent on the distance between the probe and the target. As the distance changes, the electronics sense the change in the field interaction and produce a voltage output which is proportional to the change in distance between the probe and target (Figure 4-5). The target surface must be at least three times larger than the probe diameter for normal calibrated operation; otherwise, special calibration may be required (Measure Central, 2015).

The sensing field of a non-contact sensor probe engages the target over a certain area with respect to the spot size. The spot size is always proportional to the diameter of the probe and the target size should be larger than one. The ratio between probe diameter and spot size is significantly different for capacitive and eddy-current sensors. These

different spot sizes result in different minimum target sizes (Measure Central, 2015).

Capacitive sensors use an electric field for sensing. This field is focused by a guard ring on the probe resulting in a spot size about 30% larger than the sensing element diameter. A typical ratio of sensing range to the sensing element diameter is 1:8. This means that for every unit of range, the sensing element diameter must be eight times larger. For example, a sensing range of 500  $\mu\text{m}$  requires a sensing element diameter of 4000  $\mu\text{m}$  (4 mm). This ratio is for typical calibrations. High resolution and extended range calibrations will alter this ratio (Measure Central, 2015).

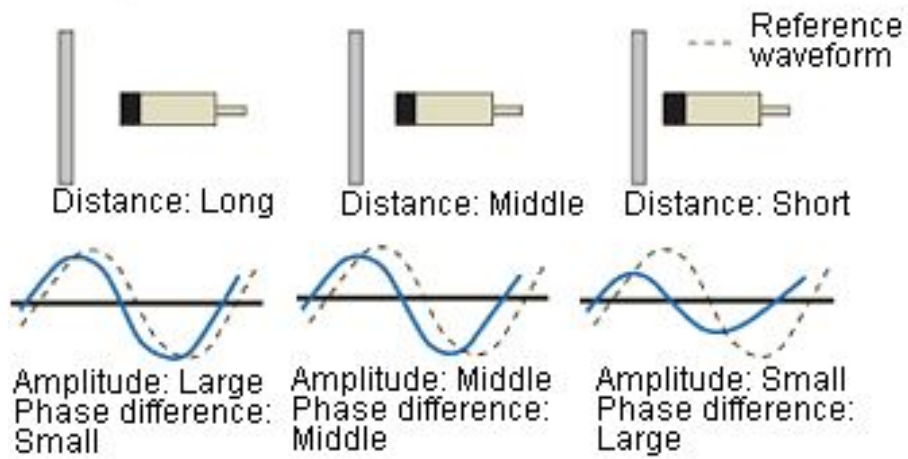


Fig. 4-4. Principle of eddy sensor (Measure Central, 2015)

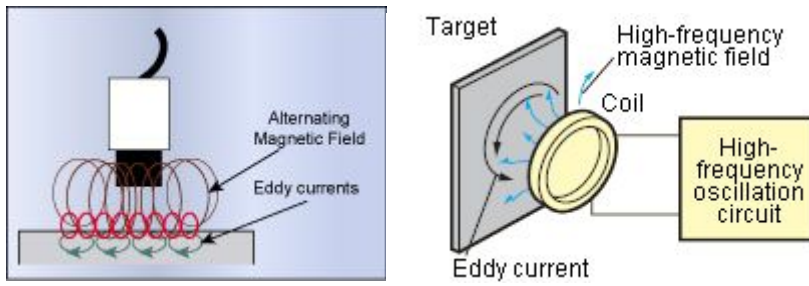


Fig. 4-5. Structure of eddy sensor (Measure Central, 2015)

## 4.2. Basic Test of Shrinkage

Shrinkage rate tests was conducted with the device designed previously. To set up how to analyze the result beforehand, mono-acrylate system was adopted for the basic test, and caprolacton acrylate (CA) and nonyl phenyl acrylate (NPA) were used as the materials (Figure 4-6).

Materials used in this study have acrylate as a functional group. While each material is chain-reacted and hardened by the initiator of the radical, each acrylate causes exothermic reaction. By measuring a heat flow per unit mass of each material, the conversion ratio of acrylate can be estimated. The photo-DSC was used to measure the heat flow of acrylate.

Shrinkage is determined by various factors of molecules. Typical shrinkage is proportional to the following simple formula.

$$\text{Shrinkage (\%)} = \frac{FN \times CR}{Mn} \quad (\text{Eq 4-1})$$

FN is functionality number of monomers, CR is the conversion ratio of curing system,  $M_n$  is the molecular weight. Figure 4-7 presents the results from measurement for shrinkage rate simultaneously, and each interval on the graph shows UV exposure starting, shrinkage initiating, shrinkage increase and curing reaction, and the final reaction phase. In the final reaction phase, the definitive shrinkage of the tested material is determined.

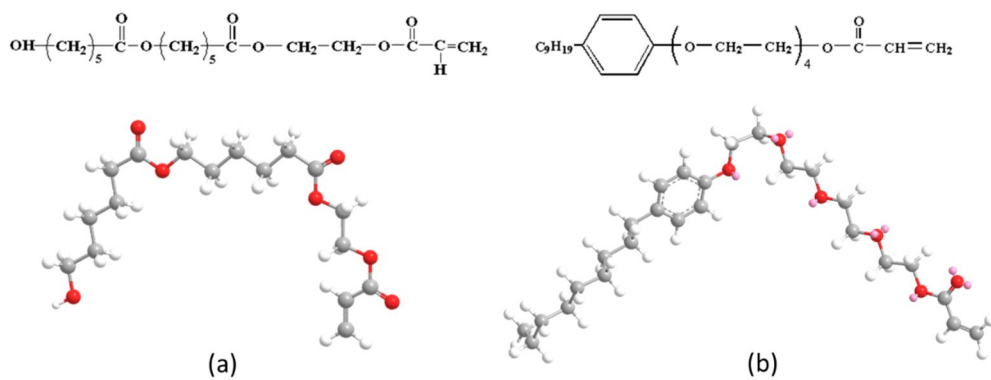


Fig. 4-6. Selected acrylate to the basic evaluation (a) caprolactone acrylate (CA) (b) nonyl phenyl acrylate (NPA)

The conversion ratio depends on the internal factors of the molecular structure and external factors such as a reaction rate and UV condition. Figures 4-8 and 4-9 shows the result of real-time shrinkage of CA and NPA those have mono-acrylate as a functional group. The final shrinkage of the two materials are the average of 3.35% and 2.6%. Thus, relative shrinkage based on the test result is 1:0.77. Molecular weight of CA and NPA are 344 and 450. Relative shrinkage per unit mass (mole equivalent) is 1:1.009. In terms of actual molecular weight, shrinkage of the two materials are not different significantly. These results show that the shrinkage over time, so the slope of the graph means shrinkage rate. Shrinkage rate is interpreted as curing rate of the material, and the result can be used to predict the degree of curing.

Figures 4-10 and 4-11 shows the results that were derived from Figures 4-8 and 4-9 by dividing the shrinkage to delta time ( $\Delta t$ ). The results mean the shrinkage rate (%/s) represented at each reaction point. The shrinkage rate at initial reaction was a negative result, which reflects features of this method to measure shrinkage. The shrinkage was detected after the transition of curing by UV occurred from surface to bottom at the direction of the thickness. Initially, the reaction caused the instantaneous thermal expansion

effect, which made the negative result. Although both materials are the same mono-acrylate materials, they are significantly different in reaction rate.

We can confirm how fast two materials shrink from the results for the shrinkage rate and infer the reaction rate from maximum peak time. Comprehensive analysis is listed in Table 4-3

The two results correspond to 52.1% and 60.4% of the theoretical shrinkage. The theoretical shrinkage rate is based on the assumption that molecule structure is uniform and conversion ratio reaches to 100%. As polymers formed, however, bulked groups played a role to inhibit next polymerization. Therefore, molecular weight could not increase infinitely. In addition, the confrontation of the side chain of acrylate made it impossible to reach the theoretical rate.

The difference between theoretical and experimental shrinkage of the two materials can be explained by the bulk property of side chain of NPC. Because side chain of CA can move freely, it may form more various

structures than when it moves as a monomer unit or polymerization unit.

This leads to wider shrinkage rate difference.

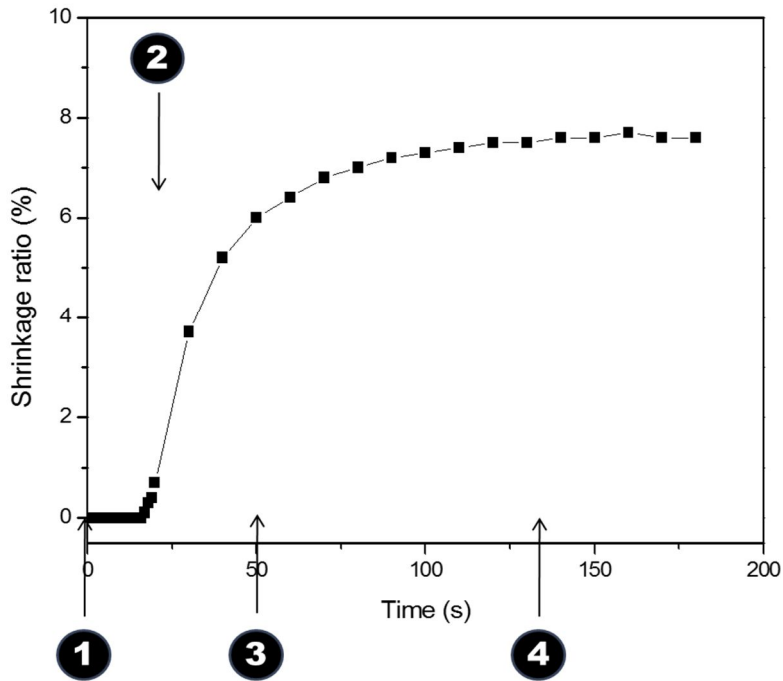


Fig. 4-7. Graph of Shrinkage Test 1) UV exposure starting 2) Shrinkage initiating 3) Shrinkage increased and curing reaction and 4) Final reaction → Define Shrinkage

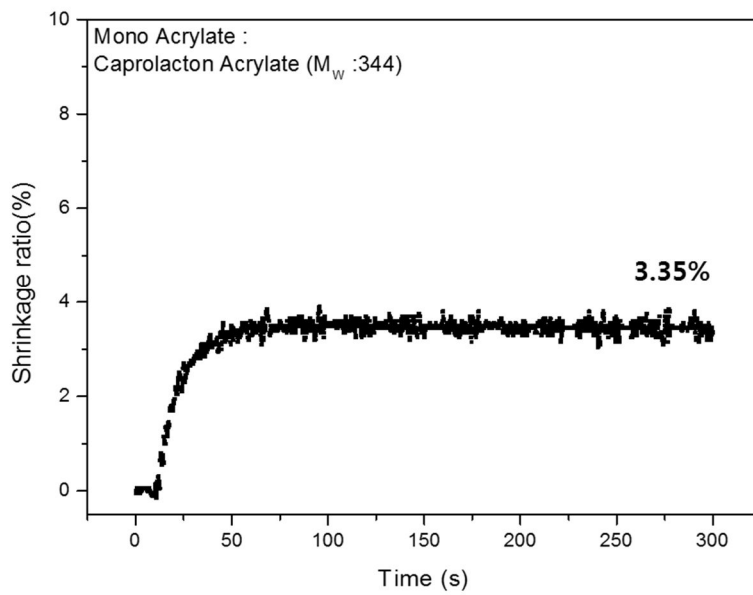


Fig. 4-8. Real-time shrinkage of caprolacton acrylate

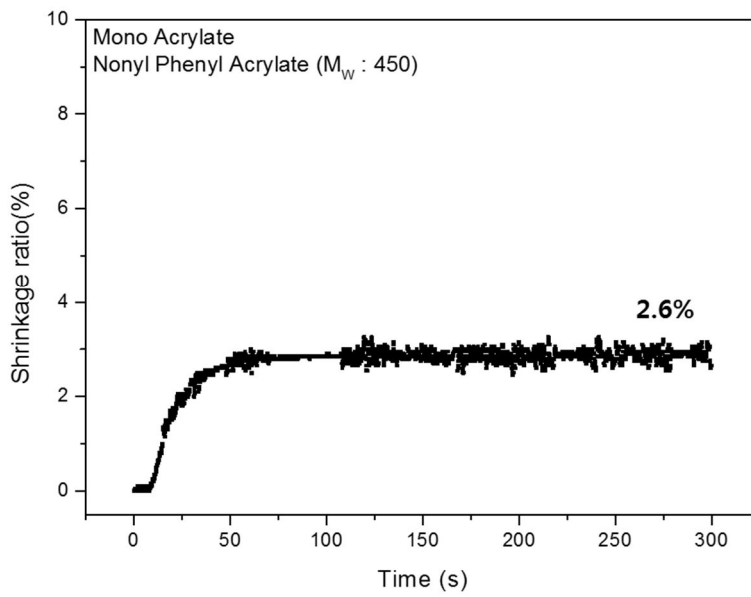


Fig. 4-9. Real-time shrinkage of nonyl phenyl acrylate

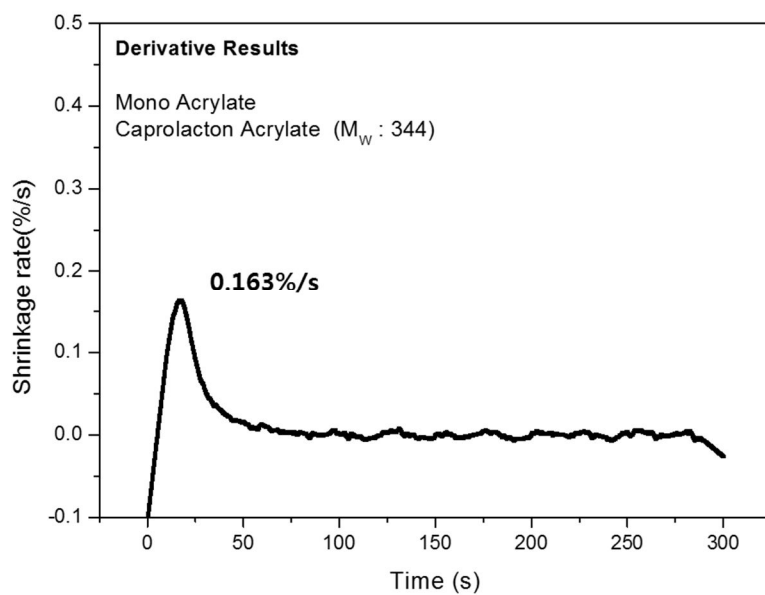


Fig. 4-10. Shrinkage rate of caprolacton acrylate

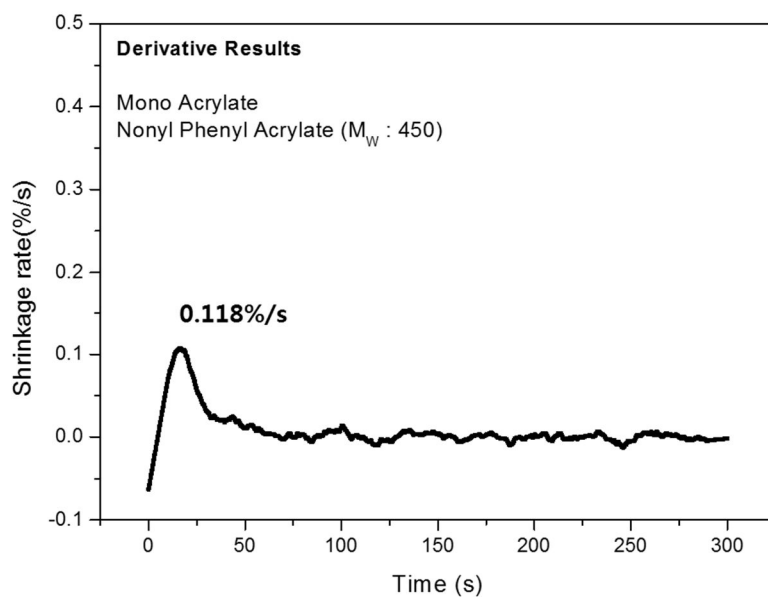


Fig. 4-11. Shrinkage rate of nonyl phenyl acrylate

Table 4-3. Shrinkage test result of mono-acrylate system

	Caprolacton acrylate	Nonyl phenyl acrylate
Molecule weight	344	450
Theoretical maximum shrinkage (%)	6.43	4.30
Axial shrinkage (%)	3.35	2.60
Maximum shrinkage rate (%/s)	0.163	0.118
Peak approach time (s)	18.1	15.3
Experimental ratio/theoretical ratio	52.1	60.4

Figure 4-12 is the measurement of real-time heat output using the photo-DSC. When UV lamp was opened, heat output dramatically increased. After a period of time (about 60s), the output was stabilized. The peak means the heat flow at moment, and the conversion of functional group during the curing-period can be estimated by integrating peaks of the period.

Figure 4-13 shows the integral value of heat flow calculated from Figure 4-12; as time went on, the result converged to a certain level (229.9 J/g in caprolacton acrylate and 116.8 J/g in nonyl phenyl acrylate). The two materials have different numbers of functional group at each unit mass. Thus, the number of functional group per unit mass can be calculated through the following formula.

$$\begin{aligned}
 & \textit{Advanced result of B} \\
 & = \frac{\textit{Converge result B}}{\textit{Converge result A} \times \textit{unit mass reactor number of B}}
 \end{aligned}
 \tag{E}$$

q  
4-  
2)

(Ex 0.8  $\cong$  (201J/g) / (331J/g  $\times$  0. 76))

The acrylic reactor number of unit mass was 1: 0.76; the convergence of advanced graph 1: 0.67 can be obtained by calculating with the value of the reactor number. Since the shrinkage rate was different as 1:077, we can conclude that the difference between exothermic area gained by photo-DSC and the shrinkage rate was not significantly different.

Figures 4-8 to 4-13 show the correlation between distance and speed in shrinkage and heat flow. Especially, shrinkage measurement system analyzes shrinkage directly corresponding to the distance while the photo-DCS system analyzes heat output of materials corresponding to the speed; the results from two systems could be interpreted complementary to each other. The photo-DSC system is not only used as a tool to determine the conversion rate in advanced prediction model but also used as an indirect prediction system for shrinkage.

While shrinkage indicate the bulk characteristics of the material, photo-DSC shows the reaction of the molecular units. Thus, the differences in results between two methods depend on the structural differences of the material.

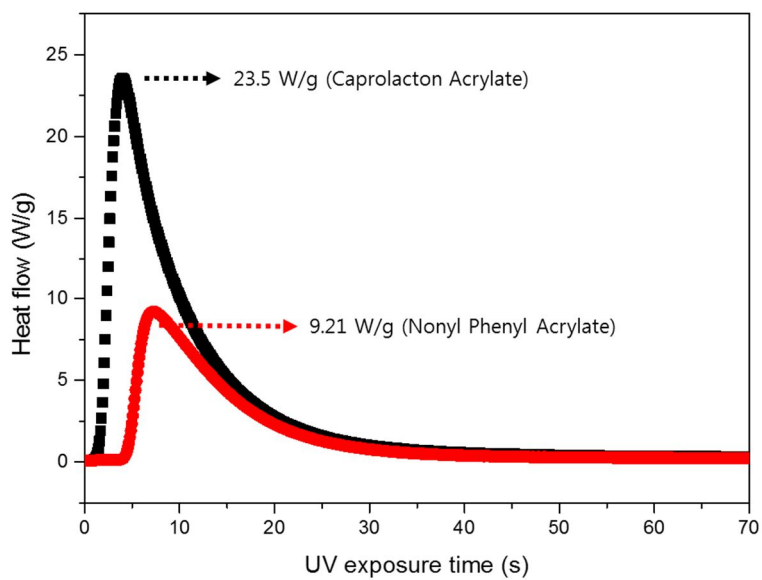


Fig. 4-12. Heat flow of mono-acrylate system

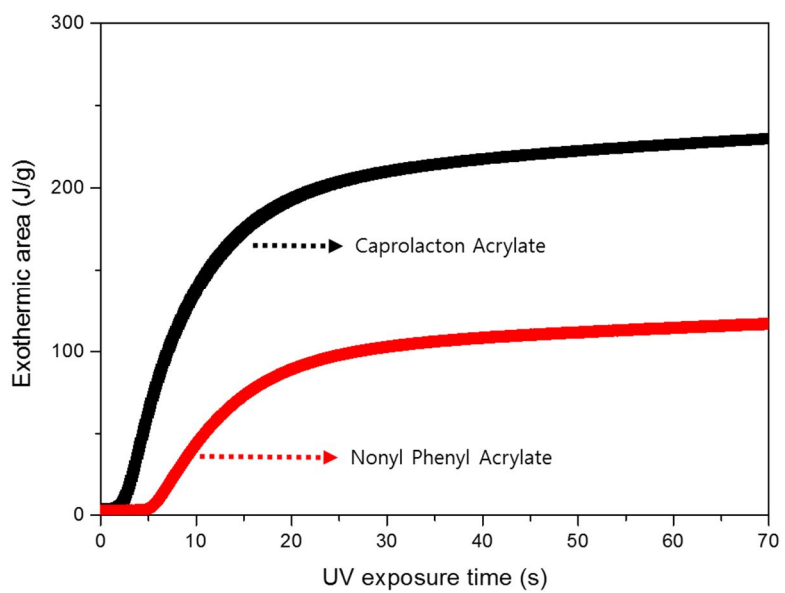


Fig. 4-13. Exothermic area of mono-acrylate system

Table 4-4. Photo-DSC test result of mono-acrylate system

	Caprolacton Acrylate	Nonyl Phenyl Acrylate
Molecule weight ( $M_n$ )	344	450
Maximum heat flow (W/g)	23.50	9.21
Peak approach Time (s)	3.97	7.27
Exothermic Area (J/g, at 70s)	229.9	116.8

### 4.3. Modeling of Material

Since the volume shrinkage rate is known to be faster as three times than axial shrinkage, it is possible to presume the volume shrinkage rate from axial shrinkage rate with a simple calculation. However, the result of axial shrinkage model suggested by Gee [1993] contradicted the expected value. Although several environmental factors and curing ratio could partially contribute to this difference, there are limitation to explain it.

According to previous research by Lee (2006), the condition in sampling process affects the measurement of axial shrinkage rate. Thus, the change of condition could hinder the estimation for volumetric shrinkage from axial shrinkage while axial and volumetric shrinkage measurements are stable in the maintenance of same condition. However, some materials showed unstable results even under the same condition.

This study was conducted on variables of shrinkage process and their interpretation by modeling the shrinkage rate test for explaining the differences in measurements.

Real fluid gets wet while surface energy has a certain angle under different

environments. If a new contact side is formed on the other side of wet structure, new type of wet structure is created. The material made from this process has two fixed sides and mobile sides

This structure generally forms meniscus structure and has a convex or concave structure depending on surface energy level. If we assume that the specimen figure has a vertical structure (Figure 4-14.), we can expect the figure of the non-contact area through the formula underneath.

$$(nr^2h\rho) \times g = mg = T \times 2\pi r \times \cos \alpha \quad (\text{Eq 4-3})$$

- ✓  $T$  is the surface tension
- ✓  $r$  is the radius of the tube (so that  $2\pi r$  is the total length of the meniscus)
- ✓  $m$  is the mass of the liquid
- ✓  $\rho$  is the specific gravity of the liquid
- ✓  $g$  is the acceleration due to gravity
- ✓  $h$  is the height to which the liquid rises

$$h = \frac{T \times 2\pi r \times \cos \alpha}{\pi r^2 \rho \times g} = \frac{2T \cos \alpha}{\rho g r} \quad (\text{Eq 4-4})$$

This meniscus structure is affected by surface tension and viscosity of the material, and it forms concave curl structure when its energy is below the surface level.

The basic modeling set up and the test to identify the curl structure and shrinkage rate factors was conducted.

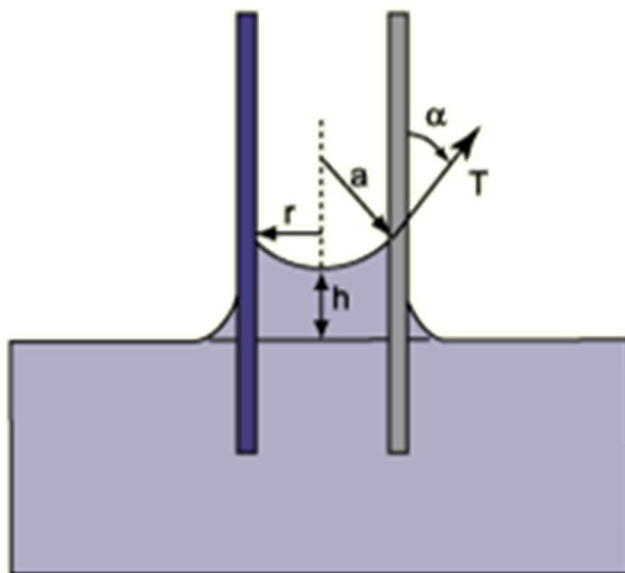


Fig. 4-14. Scheme of meniscus (concave) form of between double side.

#### 4.3.1. Ideal Configuration and Shrinkage Phenomenon

In assumption that the surface energy of resin and the contact surface energy are equal, the materials is not significantly impacted by air interaction, and its adhesion to the surface is stronger than gravity, we can expect the shape like (a) of Figure 4-15.

The author calculated the shrinkage rate when the materials curing assuming the followings.

- **Assume 1: Curl = demi sphere**
- **Assume 2: Regular shrinkage**
- **Assume 3: Do not move on contact area**
- **Assume 4: Do not move on up-down side**

We can calculate the shrinkage volume with Eq.4-5 when it shrinks from side direction and it has a semicircular shrinkage shape. a and b are marked on Figure 4-15. Since it has a rotational shape around the central axis, the volume can be calculated from integral with integration range from  $-a$  to  $a$ .

$$\int_{-a}^a \pi(\sqrt{a^2 - x^2} + b)^2 dx =$$

$$\frac{3\pi a^2 b \sin^{-1}\left(\frac{x}{|a|}\right) + 3\pi b \sqrt{a-x} x \sqrt{x+a} - \pi x^3 + (3\pi b^2 + 3\pi a^2)x}{3}$$

(Eq.4-5)

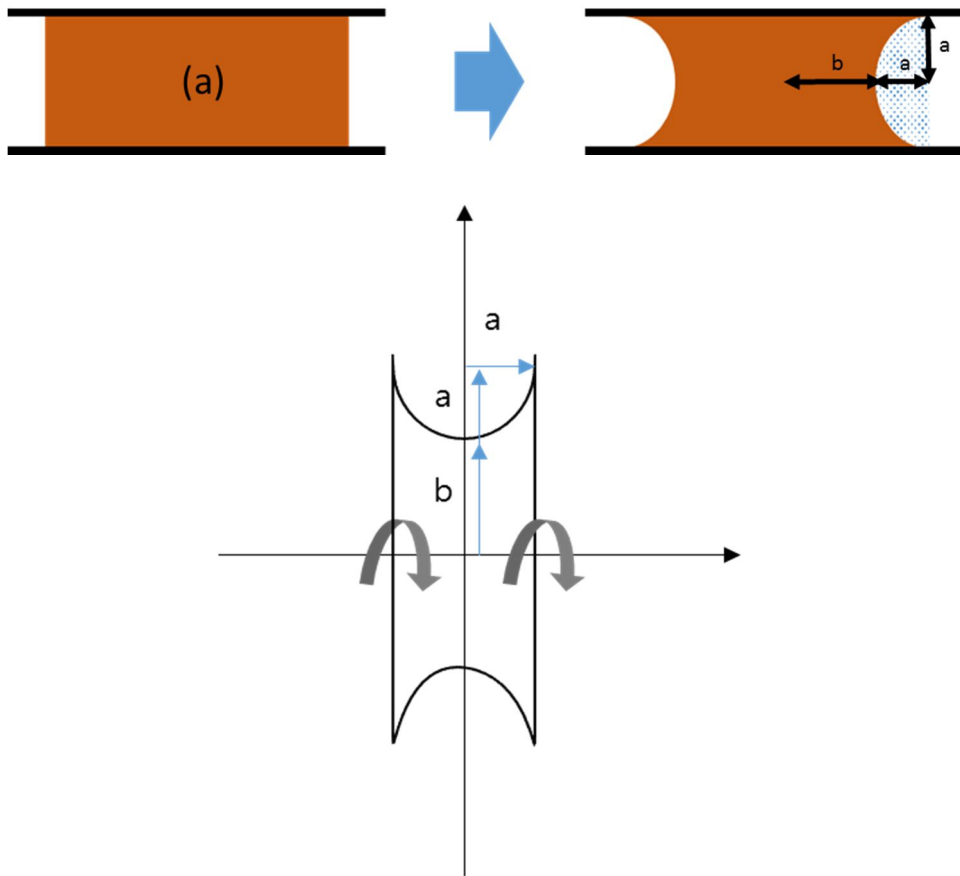


Fig. 4-15. Ideal configuration of shrinkage on contact mode

The author firstly set the volume constant and calculated the shrinkage ratio of curl according to the changes of radius, other than any other variant following the shrinkage process. From the Table 4-5, we can confirm that the curl ratio is disproportional to the radius.

When the radius gets smaller than a certain level, volume change exceeds the theoretical shrinkage rate, and there are deviations in shrinkage rate even when the radius remains fixed.

The curl ratio plays a significant role when the curl moves freely and its vertical mobility is defined. We can confirm that the radius of the specimen is very important regarding volume shrinkage rate analysis of axial shrinkage rate (Figure 4-16).

The outcome suggests that even if the aspect ratio exceeds 15, the shrinkage from the curl is over 10%. According to Lee (2006), the shrinkage rate reaches the limit within aspect ratio of 5 to 6. Therefore, the experimental results significantly differ from ideal model. The main ground for this inconsistency comes from two factors: The experiment did not consider

vertical shrinkage, and the curl from surface energy occurs in the real contact mode.

Table 4-5. Shrinkage of side direction (per 0.1ml)

Radius (mm)	Area (mm <sup>2</sup> )	Thickness (mm)	In-curl volume (mm <sup>3</sup> )	Reduced volume (mm <sup>3</sup> )	<b>Ratio (curl/total, %)</b>
50	7854	0.013	0.1000	0.0000	<b>0.020</b>
25	1963	0.051	0.0998	0.0002	<b>0.160</b>
20	1257	0.080	0.0997	0.0003	<b>0.312</b>
15	707	0.141	0.0993	0.0007	<b>0.739</b>
10	314	0.318	0.0975	0.0025	<b>2.483</b>
9	254	0.393	0.0966	0.0034	<b>3.398</b>
8	201	0.497	0.0952	0.0048	<b>4.818</b>
7	154	0.650	0.0929	0.0071	<b>7.145</b>
6	113	0.884	0.0888	0.0112	<b>11.212</b>
5	79	1.273	0.0811	0.0189	<b>18.919</b>
4	50	1.989	0.0651	0.0349	<b>34.940</b>

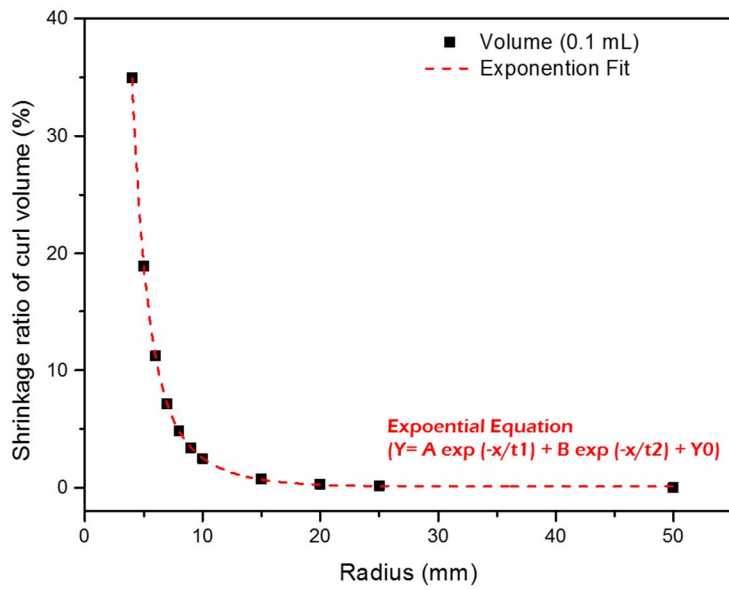


Fig. 4-16. Plotting graph of curl shrinkage versus diameter

The author calculated the curl shrinkage rate, assuming that real material can move vertically and has a constant shrinkage rate.

In the hypothesis, since the curl's mobility is fixed as a semi - sphere, the portion of the curl ratio gets lower as the vertical shrinkage is happening. Nevertheless, under the assumption that the side moves freely, the shrinkage differs by 0.72% when radius is 8 mm and shrinkage is low (under 5%) or high (over 20%). As the shrinkage gets lower, the difference becomes bigger, so this inhibits precise prediction of volume shrinkage (Figure 4-17).

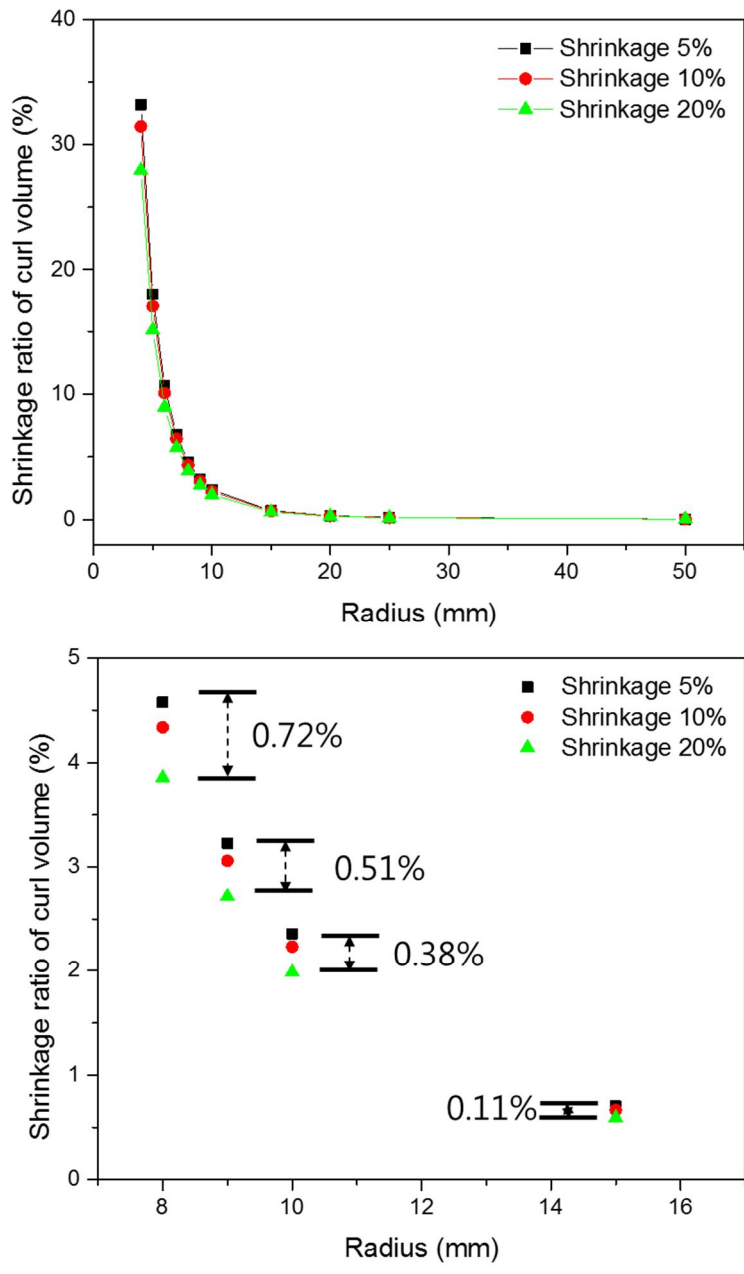


Fig. 4-17. Ratio of curl volume on shrinkage

#### 4.3.2. Real Concave Model

In the ideal structure, axial shrinkage change is important, as shrinkage gets smaller. However, this underestimates the effect of the side mobility.

Most real materials have concave structures, so they make a contact with some curl structure, and curing is proceeding with this state. As Figure 4-18 shows, curing is taking place in every direction, the sides without a contact face start to wither along the loop boundaries.

The materials with low viscosity have high initial mobility and high reaction rate, so these materials shrink faster and smaller (Ellakwa, 2007), and the strong shrinkage stress from this process leads to deformation (Charton, 2007).

To confirm this shrinkage phenomenon, the author used two materials with the same functional group and similar molecular structure. The chosen materials are Methoxy Polyethylene Glycol (550) Monoacrylate (MPEG-A)

and Methoxy Polyethylene Glycol (550) Monomethacrylate (MPEG-MA) in the Figure 4-19.

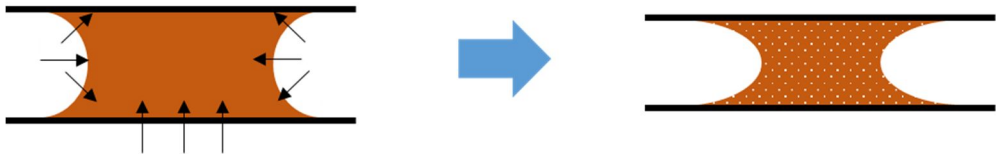


Fig. 4-18. Experiment configuration of shrinkage on contact mode

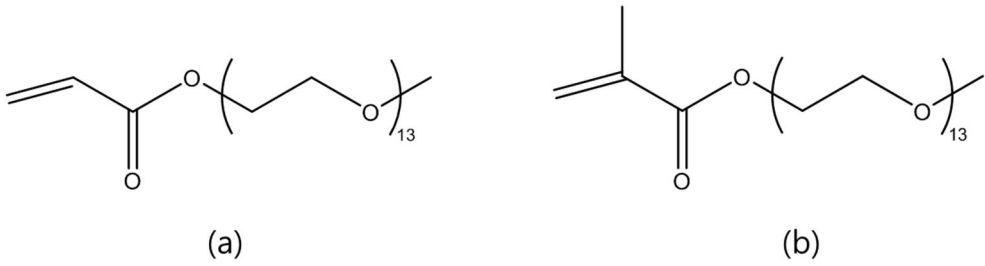


Figure 4-19. Specimens for evaluating the shrinkage caused by the sampling size  
(a) Methoxy Polyethylene Glycol (550) Monoacrylate [MPEG-A]  
(b) Methoxy Polyethylene Glycol (550) Monomethacrylate [MPEG-MA]

Table 4-6. Basic properties of MPEG-A and MPEG-MA

Materials	Abbreviations	Functionality Number	Viscosity (cps@ 25°C)	T <sub>g</sub> (°C)
Methoxy Polyethylene Glycol (550) Monoacrylate	MPEG-A	1	50	-50
Methoxy Polyethylene Glycol (550) Monomethacrylate	MPEG-MA	1	39	-65

Since the two materials have very low viscosity, they have a very low wetting angle. The author tried to produce thin film as thin as possible to secure more than a certain level of aspect ratio. The minimum specimen thickness was 400  $\mu\text{m}$  considering the properties of Eddy sensor and environmental factors like noise of current signal. The displacement error range of Eddy sensor was set to 0.2  $\mu\text{m}$ , and this error range is equivalent to 0.1% of specimen thickness.

It is impossible to get to the specimen with precise thickness because the specimens are fluid state. The specimen radius is calculated from the measured diameter after a certain quantity of specimen spread along the airfoil. The radius range was set to be from 4.8 mm to 8.8 mm, and the curing conditions were additionally set of 4 variables for assuring independence from external variables. The control variable was the portion of photo-initiator, and it is known that reaction increases as more photo-initiator is included. (Kamble, 2009)

The aspect ratio is calculated by the following formula, and the ratio was from 24 to 44 in this experiment.

$$\text{Aspect ratio} = \frac{\text{Thickness } (\mu\text{m})}{\text{Width } (\mu\text{m})} \quad (\text{Eq 4-6})$$

The author observed the shapes from the side with CCD (Charge Coupled Device) to confirm the concave structure. The consistent angle of curl is confirmed in Figure 4-20.

The shrinkage rate change of MPEG-A (Figure 4-21 and 22) verifies the proportional increase of the shrinkage rate with respect to radius. This coincides with the previously discussed ideal model, which predicts diminishing impact of curl as the radius gets smaller. Although the rate change depends on curing rate, it is affected by radius regardless of curing rate.

Narrowing down to the factor of curl, the response rate increases as more initiator added and then curing rate would increase (Hwang, 2001). Curing rate indicates the degree of reaction among functional groups. Higher curing rate means a higher reaction rate of acrylate, so shrinkage rate increases as curing rate hikes. When the reaction rate surpasses a certain degree, the shrinkage from free side would accelerate.

Nevertheless, although the shrinkage rate of MPEG-MA tends to increase with respect to radius, radius factor showed unstable results (Figures 4-23 and 24). The maximum shrinkage of MPEG-A was 2.7%, while that of MPEG-MA was only less than 1%. Because the shrinkage rate of MPEG-MA is very low, the sampling effect is critical. In addition, due to the lower viscosity of MPEG-MA, the open area of concave structure is wider and less affected by curling and other factors (Figure 4-25).

In the test based on mono-acrylate with low viscosity, it was found that shrinkage changed depending on the radius. The change in shrinkage was proportional to the length of the radius, which signifies the material differences made the differences in the outcomes (Figure 4-26).

In fact, UV curable resin has a diverse range of viscosity, which has a major impact on the utilization of products. For instance, as the viscosity decreases, processes such as coating could be performed more rapidly while problems such as over-flow occur more. Therefore, the control of viscosity is considered as essential.

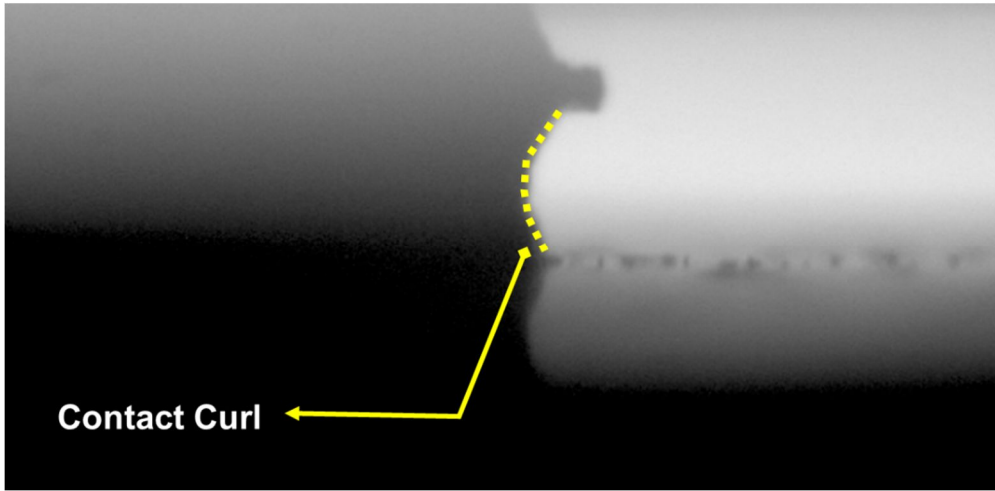


Fig. 4-20. Concave curl in a CCD actual contact mode that were taken using CCD

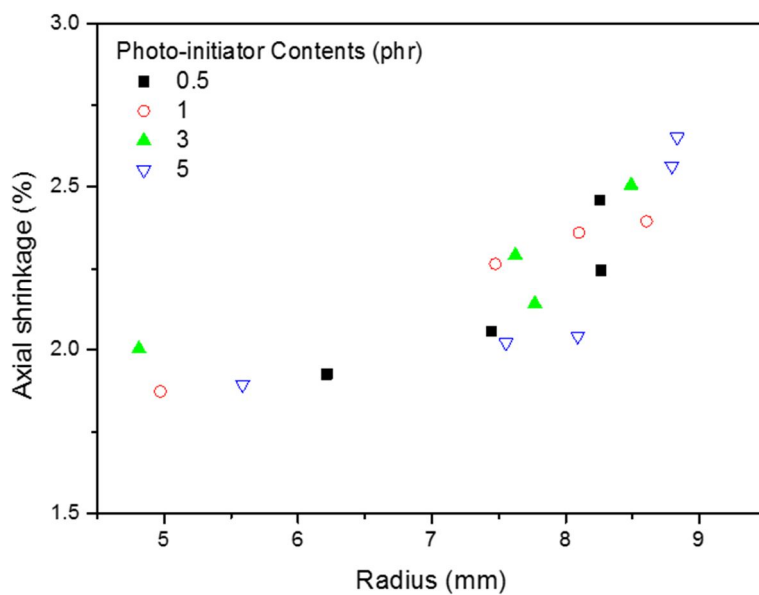


Fig. 4-21. Changing of shrinkage in accordance with the radius [MPEG-A]

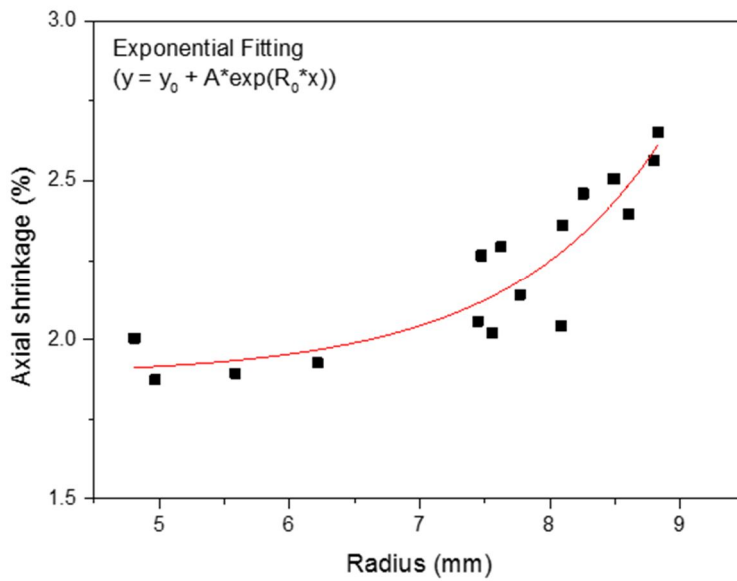


Fig. 4-22. Exponential fitting analysis of the shrinkage by content of the initiator [MPEG-A] (R-square: 0.801)

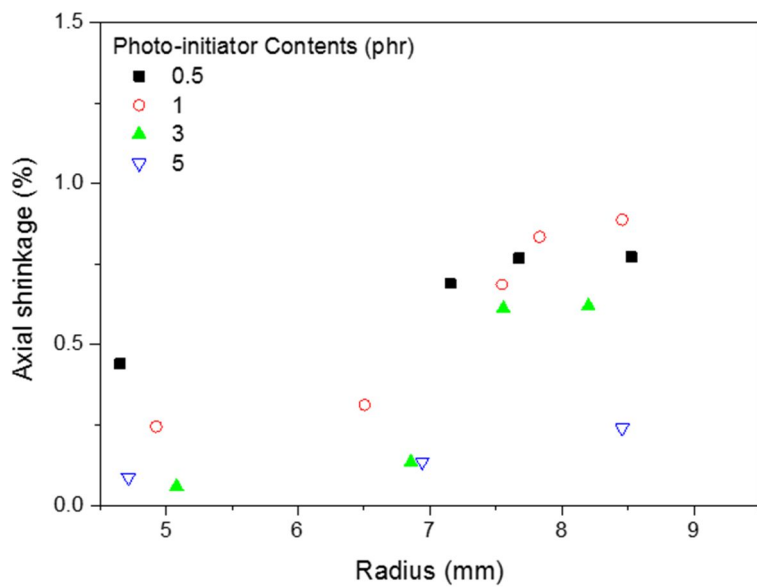


Fig. 4-23. Changing of shrinkage in accordance with the radius [MPEG-MA]

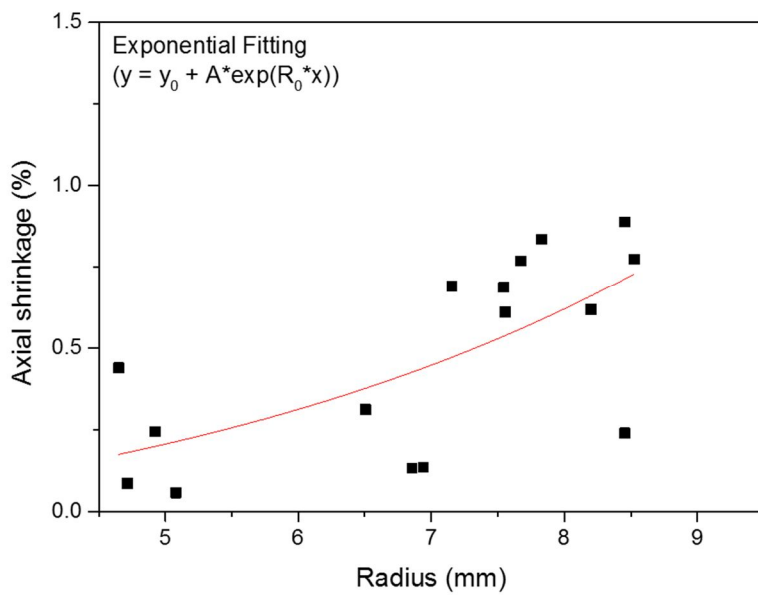


Fig. 4-24. Linear Fitting analysis of the shrinkage by content of the initiator [MPEG-MA] (R-square : 0.355)

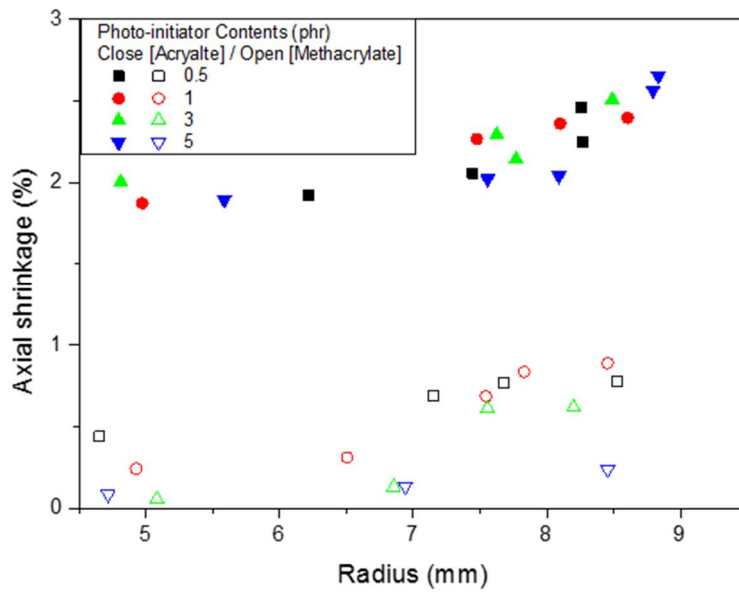
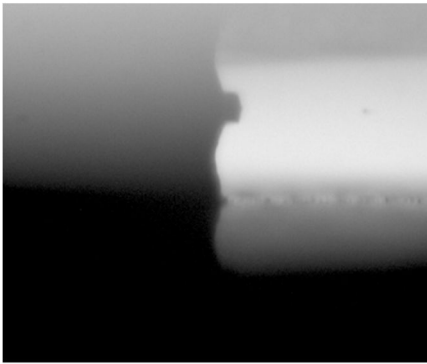
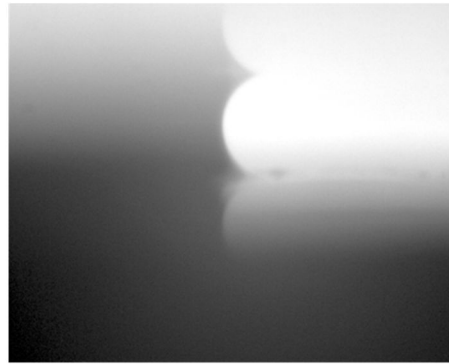


Fig. 4-25. Comparison of the correlation radius and shrinkage –close shape is acrylate, open shape is methacrylate -



(a)



(b)

Fig. 4-26. Wettability of the material and curl shape (a) acrylate (MPEG-A)  
(b) methacrylate (MPEG-MA)

#### 4.4. Change of shrinkage in response to the external environment

##### 4.4.1. Content of the initiator and shrinkage

There exist many more factors affecting the shrinkage rate other than exterior shapes. The type of photo-initiator, its portion, the source of light, and its intensity are known factors affecting curing rates. The type of photo-initiator and source of light must be taken into account to optimize UV curing system.

The radical-based basic reaction process is as follows.

##### Initiation



##### Propagation



##### Termination

*combination*



*disproportionation*



The general expressions for rate of polymerization ( $R_p$ ), kinetic chain length ( $U$ ), and instantaneous degree of polymerization ( $DP_n$ ) are:

$$R_{pol} = k_p[M][P_{tot}] = k_p[M] \left( \frac{2fk_d[I]}{k_t} \right)^{1/2} \quad (\text{Eq 4-7})$$

$$v = \frac{R_p}{R_{term} + R_{tr}} = \frac{k_p[M]}{k_t[P_{tot}] + k_{tr}^{mon}[M] + k_{tr}^{sol}[S]} \quad (\text{Eq 4-8})$$

$$DP_n^{inst} = \frac{k_p[M]}{(k_t + 0.5k_{tc})[P_{tot}] + k_{tr}^{mon}[M] + k_{tr}^{sol}[S]} \quad (\text{Eq 4-9})$$

The reaction rate of initiator and the portion of monomer determine the reaction rate. The principal factors contributing to the formation of radical of initiators are the portion of initiators and the energy given from outside. The speed of formation of radical is proportional to the two precious factors, then the reaction rate increases as more initiators are added or more intense light is given.

The conversion ratio is known to be proportional to reaction rate (Cho, 2014). Shrinkage rate is directly affected by conversion ratio, and different reaction rate leads to different shrinkage rate.

The author observed shrinkage rate change as photo-initiator concentration and light intensity are manipulated to test the shrinkage rate change with respect to external variables other than properties of the material itself.

As a low viscosity of mono-acrylate system is proven that it may hamper precise shrinkage test, the author selected high viscosity material which is expected to have an elastic shrinkage rate. Trimethylolpropane triacrylate (TMPTA) and pentaerythritol triacrylate (PETA) are selected for this test

The portion of photo-initiator was set to be 0.5, 1, 3, 5 phr, and the intensity of light was fixed to  $10 \text{ mW/cm}^2$  with deviation of 10%.

TMPTA system verifies that shrinkage rate increases as more photo-initiator is included. (Figures 4-27 and 28). The UV curing rate gets faster and its reaction terminates early, according to the proportion of photo-initiator.

Even though the portion of photo-initiator increases from 3 to 5 phr, overall shrinkage rate and shrinkage speed do not show significant difference.

However, some shrinkage rate tends to decrease as a peak height approach gets faster. This is explained by the curl effect on shrinkage speed.

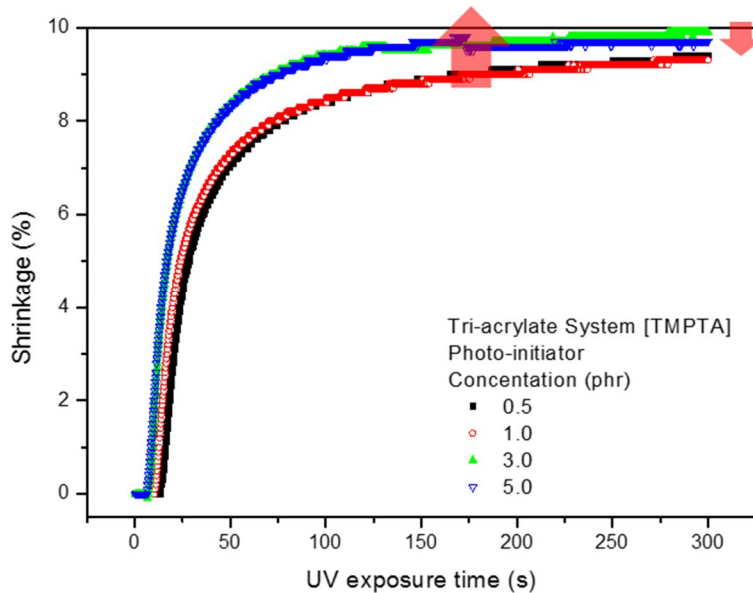


Fig. 4-27. Shrinkage of TMPTA depends on the photo-initiator contents.

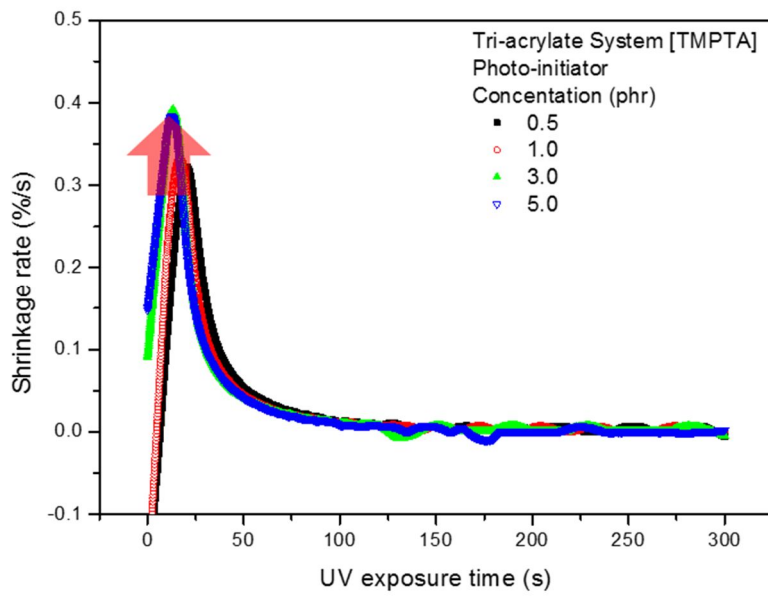


Fig. 4-28. Shrinkage Rate of TMPTA depend on photo-initiator contents.

Table 4-7. Shrinkage test result of TMPTA depending on photo-initiator contents

Photo-initiator contents (phr)	Shrinkage (%)	Maximum shrinkage rate (%/s)	Peak approach time (s)
0.5	9.4	0.322	20.5
1	9.3	0.334	16.9
3	9.9	0.391	13.2
5	9.7	0.383	12.8

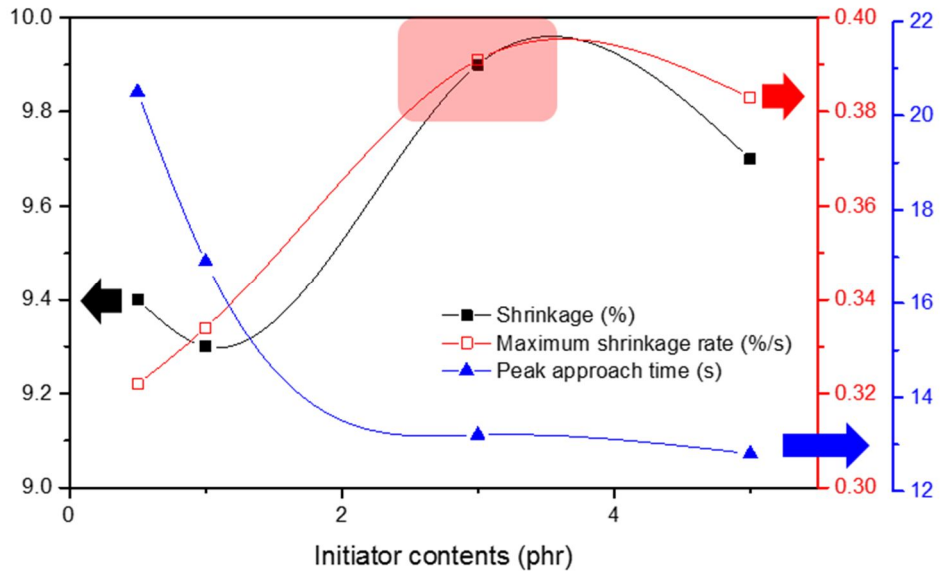


Fig. 4-29. Shrinkage behavior of TMPTA depend on Initiator contents.

PETA shows distinctive properties compared to previously mentioned TMPTA. The shrinkage rate change with respect to the photo - initiator was twice bigger (d% 1.1) than that of TMPTA (d%, 0.5%), and the difference was even wider when compared to overall shrinkage rate (Figure 4-30 and 4-31).

PETA has high viscosity and high cohesion to molecular hydrogen. Hydroxyl group functions as chain transfer and as cross-link between molecules, and it boosts the overall reaction rate (Lee, 2004).

Multi-functional group, however, this hydroxyl group plays as a disturbance factor in a chain reaction. Multi-functional group forms 3-dimensional structure as the radical reaction persists, and these structures cage unreacted site (Dusek, 2012). While this cage effect is happening, chain transfer of hydroxyl group would terminate the reactions rather than maintain them.

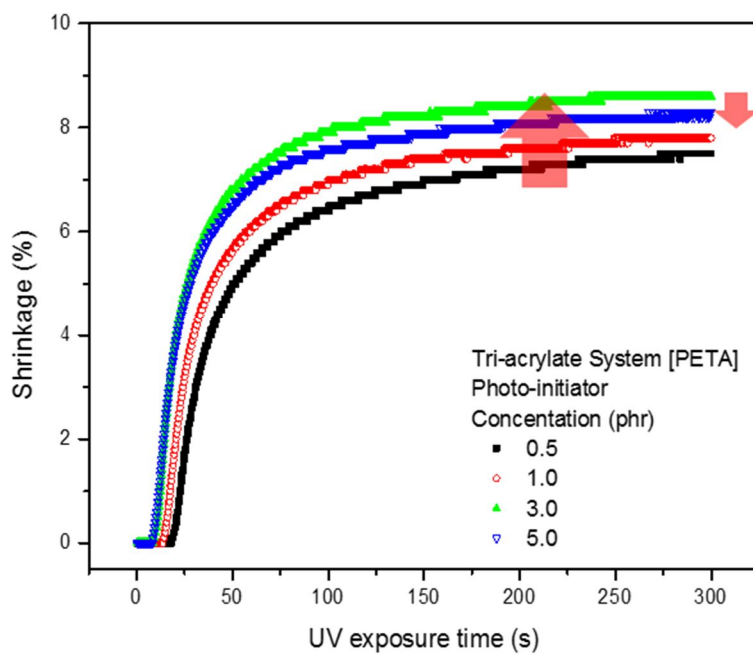


Fig. 4-30. Shrinkage of PETA depend on photo-initiator contents.

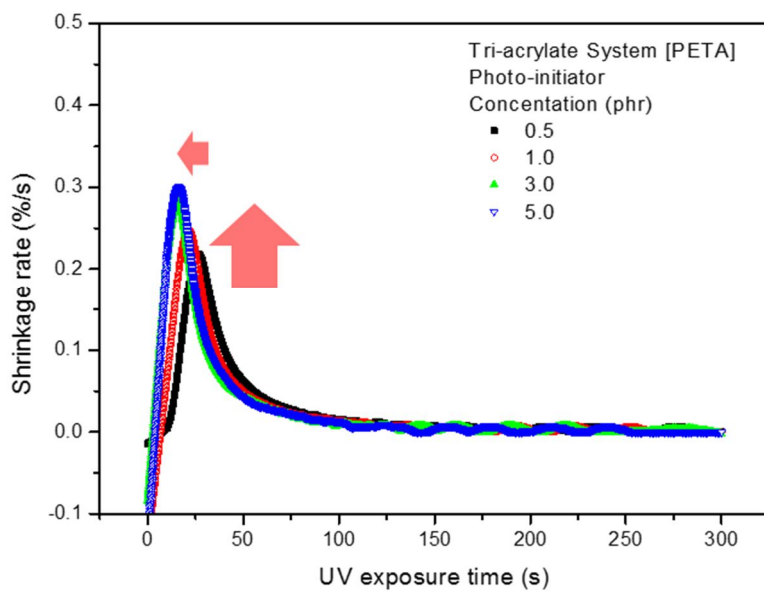


Fig. 4-31. Shrinkage rate of PETA depend on photo-initiator contents.

Table 4-8. Shrinkage test result of PETA depending on photo-initiator contents

Photo-Initiator Contents (phr)	Shrinkage (%)	Maximum Shrinkage rate (%/s)	Peak approach time (s)
0.5	7.5	0.219	26.4
1	7.8	0.248	21.4
3	8.6	0.282	15.8
5	8.3	0.3	16.3

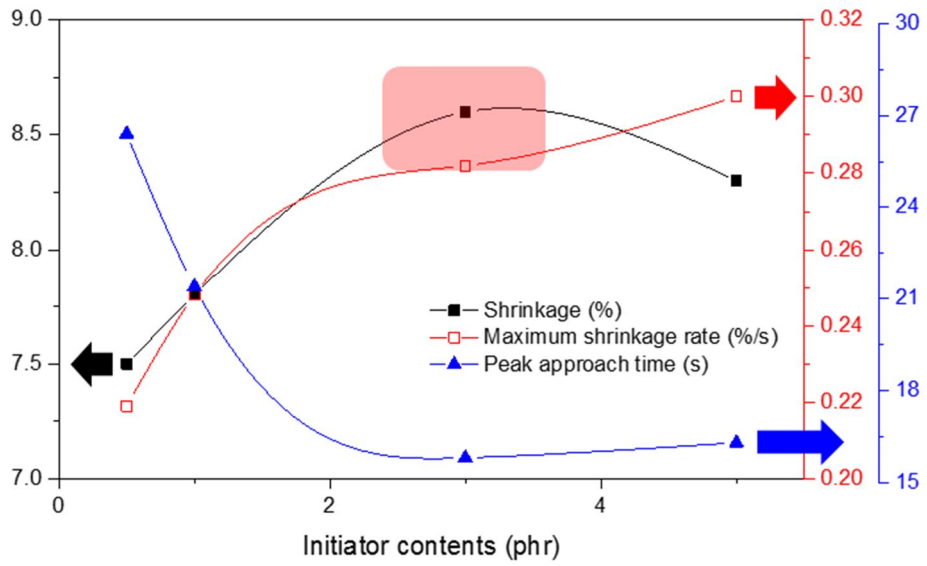


Fig. 4-32. Shrinkage behavior of PETA depend on initiator contents.

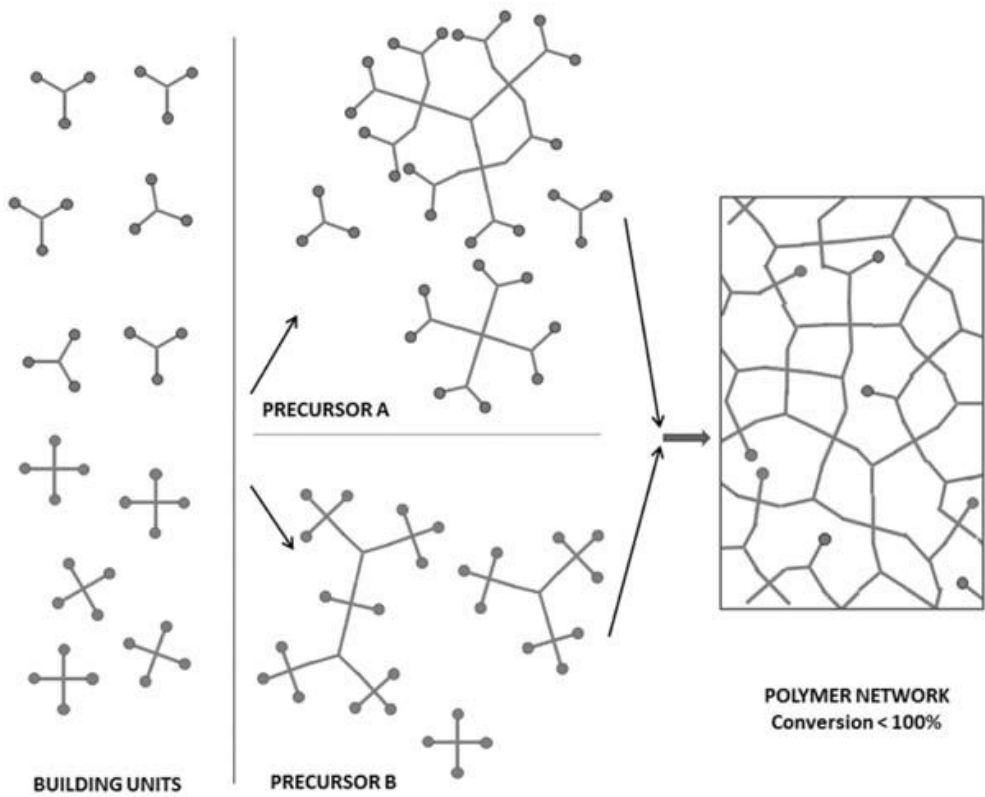


Fig. 4-33. Polymer network formation with multi-functional monomer  
 [Dusek, 2012]

#### 4.4.2. UV Intensity and Shrinkage

Since photo-initiators get activated to form radicals by UV, UV intensity plays crucial role in controlling activation energy regarding radical initiation. Although the activation energy in endothermic and exothermic reaction differs (Figure 4-34), it is common to be involved to exceed activation energy to react toward the right.

$$R_p = \frac{k_p}{k_t^{1/2}} [M] (\phi \epsilon I_0 [A] b)^{1/2} \quad (\text{Eq 4-10})$$

$k_p$  is the propagation kinetic constant,  $k_t$  is the termination kinetic constant,  $[M]$  is the molar concentration of monomer,  $\phi$  is the initiator efficiency,  $I_0$  is the incident light intensity in light quanta per area second,  $\epsilon$  is the absorption coefficient of the initiator,  $[A]$  is the molar concentration of initiator, and  $b$  is the thickness of the resulting specimen (Odian, 1991).

In addition, one can calculate the overall activation energy ( $E_a$ ) of the reaction by assuming that the reaction rate follows an Arrhenius-type behavior. The combination of the Arrhenius equations for the propagation and termination kinetic constants gives an expression for the effect of

temperature on the polymerization rate. It can be expressed as

$$\ln R_p = \ln[A] + \ln \left[ R_i^{1/2} [M] \right] - \left( \frac{E_a}{RT} \right) \quad (\text{Eq 4-11})$$

Where T is the absolute temperature, A is a constant of proportionality, R is the gas constant,  $R_i$  is the rate of initiation, and [M] is the monomer concentration (Odian, 1991).

TMPTA was used to confirm shrinkage change with respect to intensity, and the condition was set to be 3 phr, 5 phr whose shrinkage rates were highest. The intensity was initially set to be 100% and then lowered to 50%, 25%, 10%. When it is 100%, the intensity was 10 mW/cm<sup>2</sup>, and its deviation was within 10%.

Figure 4-32 is a graph that shows measurement results of a shrinkage corresponding to the UV intensity. It ensures that the changes trend is different which compare changing of the content of the photo-initiator. Change the amount of shrinkage is showing a deviation of more than 3% - from 6.8 percent to 9.8 percent-. Because the UV dose direct impact on the activation energy.

Stand out point of Figure 4-34 is shifting to the right as the growing point of the initial graph by reduce amount of light. When the time of 100% and 10%, measurement time of initial shrinkage is respectively 7.3s and 46.2s. There is a difference about 38.9 seconds. When started actually exposure to UV, it does not cure began after being delayed about 38.9 seconds.

The occurrence of these delay effects of shrinkage, can be interpreted from two points of view. The first is the system different to typical coating, the experimental conditions has relatively thick thickness. UV is absorbed only the upper, not transmitted to the lower area. Since initiation of photo-initiator is activated by absorbing, UV, and thus to go down to the lower with UV decreases gradually from the top.

$$C_d = D_p \ln\left(\frac{E_{max}}{E_C}\right) \quad (\text{Eq 4-12})$$

$C_d$  is the cure depth,  $E_{max}$  is the energy dosage per area,  $E_C$  represents a “critical” energy dosage, and  $D_p$  is the “depth of penetration” of the laser beam into the solution, which is inversely proportional to the molar

extinction coefficient and concentration of photoinitiator. (Jacobs, 1992/1996). This empirical equation has been used in the literature “*Rapid Prototyping and Manufacturing (Jacobs, 1992)*” to analyze experimental data on cure depth versus laser writing speed to determine  $D_p$  and the empirical constant  $E_c$  (Lee 2001). The logarithmic dependence on  $E_{max}$  arises in both cases, and  $D_p$  is inversely proportional to  $\epsilon$  and  $[PI]$  as

$$D_{dp} \Leftrightarrow \frac{2}{2.303\epsilon[PI]} \quad (\text{Eq 4-13})$$

The thickness capable of transmitting on the basis of the above equation, has a system that is inversely proportional to the amount of the initiator in proportion to the Energy. Decreasing of light intensity role as a failure factor that UV is going down to the bottom. Since the Cure depth is proportional to the log scale of the maximum amount of light, it is possible to calculate as follows.

$$\begin{aligned} C_{d10} &= D_p \ln (E_{max10}/E_c) \\ &= D_p \ln (E_{max100} \times 0.1 / E_c) \\ &= D_p [\ln (E_{max100}/E_c) + \ln (0.1)] \\ &= D_p (C_{d100} - 2.303) \end{aligned} \quad (\text{Eq 4-14})$$

Consequently, when light intensity is lower, depth that can be reached by light is reduced to dramatically, in the results, the total amount of energy must reach a more constant. Figure 4-35 is 3-dimensional cure depth profile based on the energy and the photo-initiator. Cure depth in accordance with the total amount of light changes very large when conditions of the initiator is constant.

Therefore, the phenomenon that the lower area reaction is delayed by a low amount of light is occurring. As a result, shrinkage delayed phenomenon is occurring too. Generally, depth profiling of shrinkage is very important because photo-DSC is a test tool that measures the energy release of the molecular units, however, shrinkage is to evaluate the bulk properties of the whole case of the shrinkable material. Figure 4-37 is a scheme of the process of curing transferred from top to bottom when these cure depth problems occur.

The second reason is that the internal stress was not generated properly due to the slow cure speed corresponding to the low light. Because light intensity is weak, activation of the initiator at a point become weaker and the overall cure speed decreased. The amount of initiator to be totally activated is reduced by radical termination stimulate.

Thus the polymer of the point that is a hardened comes to have a low cure density. Therefore, it does not move the plate in the early stages of cure accordingly the internal shrinkage stress becomes weaker. Then, the stress is eliminated internally or induce curing in the side parts. Figure 4-38 is an image related cure formation of the polymer when the light quantity is weak. Depending on the time, UV has reached down to the bottom position, a difference in the curing density of the polymer is generated itself. Therefore, shrinkage is decreased as compared with the case UV intensity is strong.

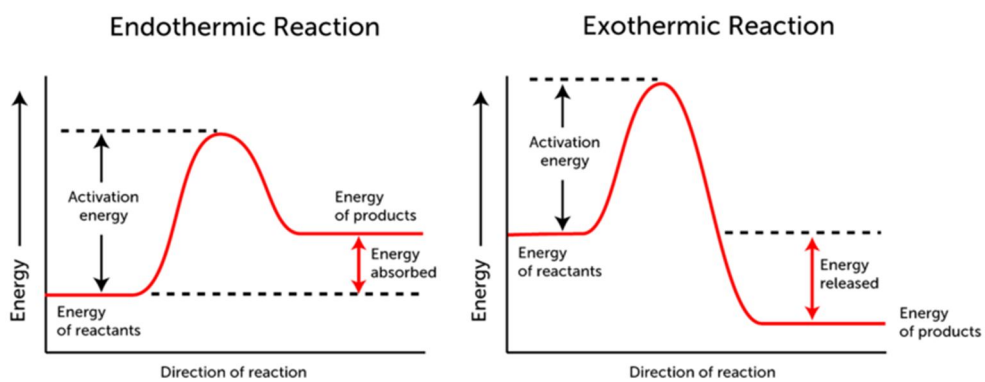


Fig. 4-34. Activation energy of endothermic/exothermic reaction

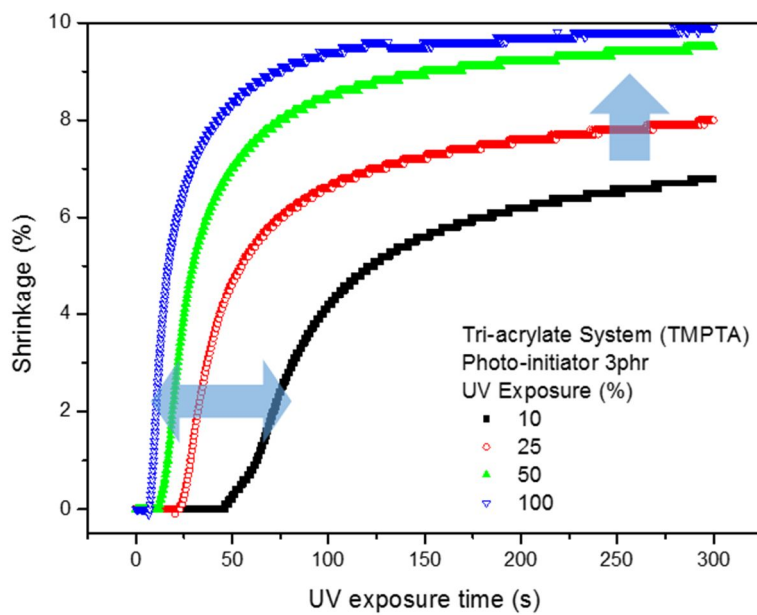


Fig. 4-35. Shrinkage of TMPTA depends on the UV intensity (PI 3 phr)

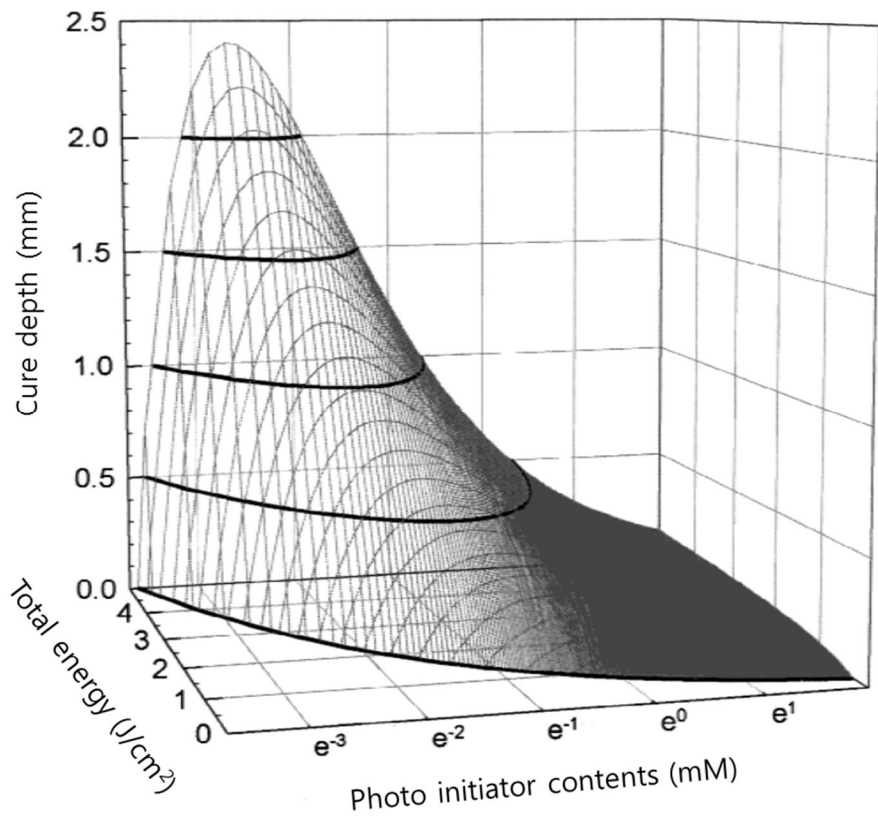


Fig. 4-36. Surface topology of the curing space (Lee, 2001).

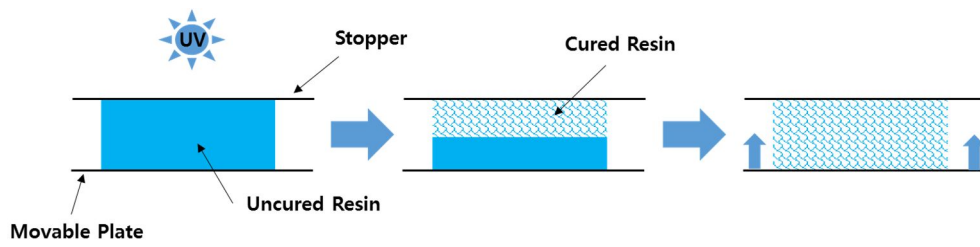


Fig. 4-37. Scheme of shrinkage delay effect

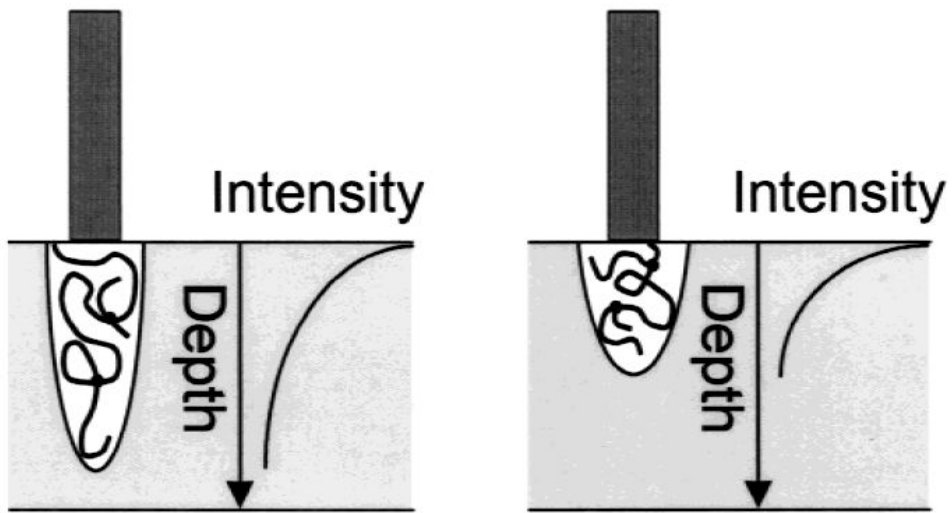


Fig. 4-38. Representation of gel curing profiles. In (a), laser penetrates deeply, but only lightly cross-links the gel. In (b), free radical initiation is localized in the upper portion of the solution (Lee, 2001)

The result of calculating the basis of shrinkage rate of shrinkage of the evaluation results is shown in Figure 4-39. Shrinkage rate has increased to dramatically depend on light intensity, Peak approaching time is rapidly advanced also. Peak time can be interpreted in delay due to the bulk properties that described above.

Shrinkage rate, when compared with the results of photo-DSC, is possible to use as an index that can describe the rate of reaction. Above mentioned Eq 4-14 predicted, the maximum rate of polymerization increased as one raised the incident light intensity.

$$R_p \propto (I_0)^\alpha$$

(Eq 4-15)

The when  $\alpha$  is 0.5, classic rate equation suggests when bimolecular termination occurs. In this experiment,  $\alpha$  is to obtain a result that is proportional with 0.5-0.6, Figure 4-40 is showing the results of re-calculate by calculating the initiator power factor as 0.6.

0.6 suggests that a combination of bimolecular and unimolecular termination is happening in the polymerization. In general,  $\alpha$  in multi-functional acrylate

systems known becomes from 0.5 to 1.0 (Decker and Moussa, 1990), from the evaluation of shrinkage, it is possible to analogize these initiator power factor.

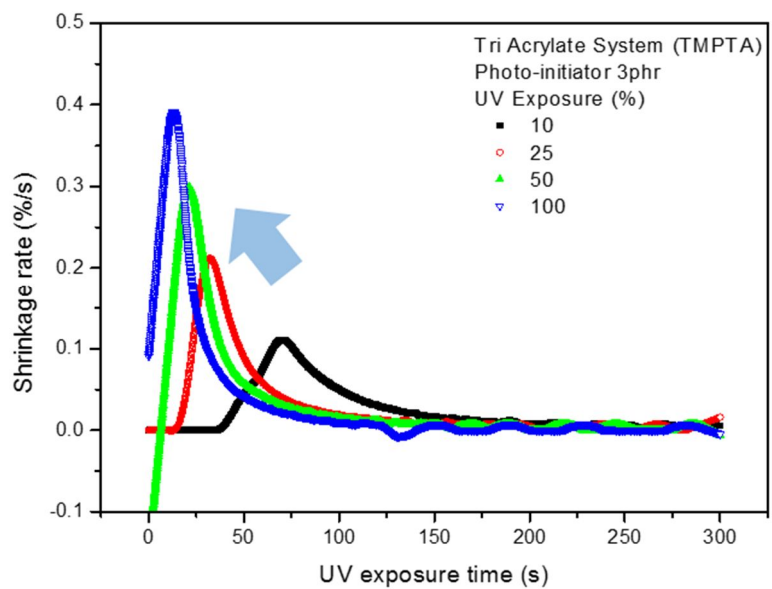


Fig. 4-39. The shrinkage rate of TMPTA depends on the UV intensity (PI 3 phr)

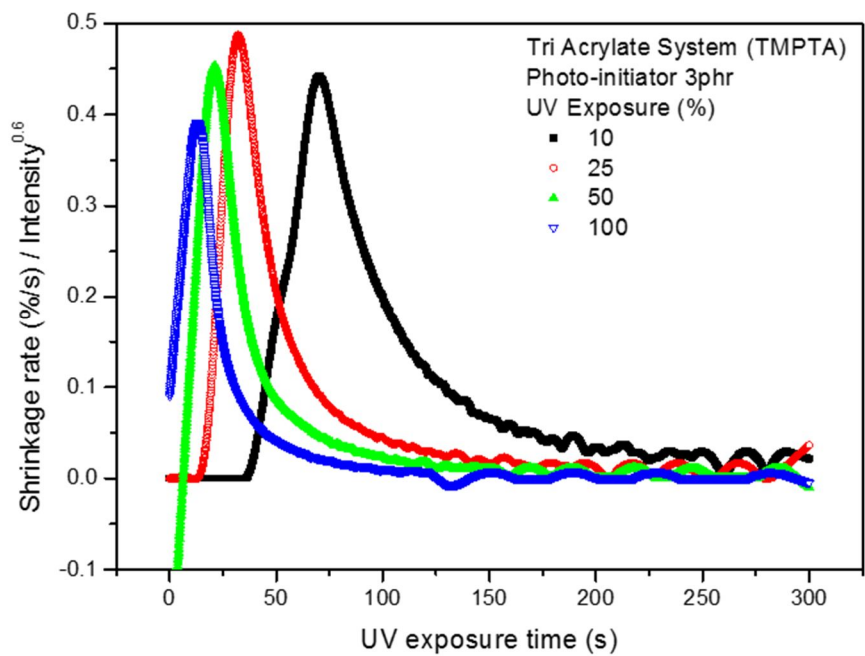


Fig. 4-40. Shrinkage rate normalized by light intensity to the 0.6 order

Table 4-9. The shrinkage test result of TMPTA depending on UV intensity

UV Intensity (%)	Shrinkage (%)	Maximum shrinkage rate (%/s)	Peak approach time (s)
10	6.8	0.111	70.3
25	8	0.212	32.2
50	9.5	0.299	21.2
100 (10mW/cm <sup>2</sup> )	9.9	0.391	13.2

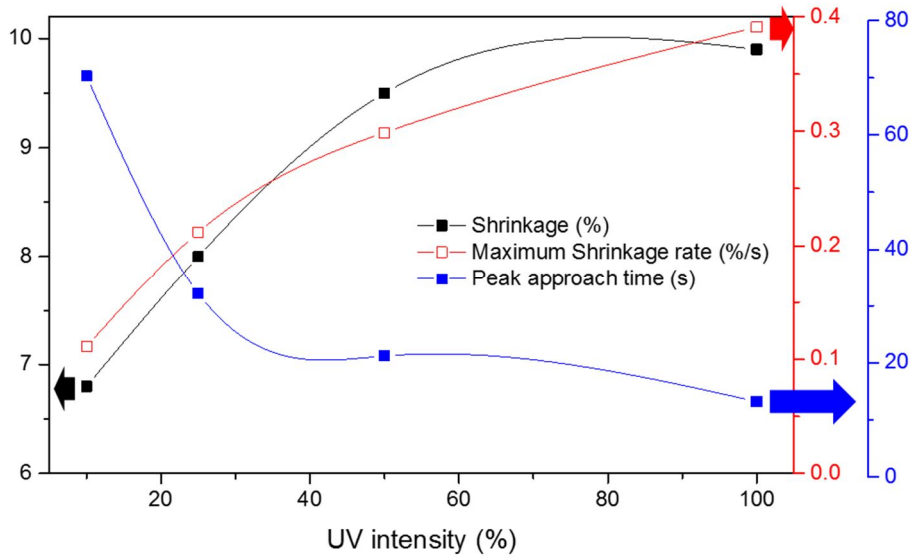


Fig. 4-41. The shrinkage behavior of TMPTA depends on UV intensity

Even increased content of photo-initiator, tend corresponding to the light amount is the same. As the UV intensity is increased, the shrinkage rate is also increasing. In addition, the difference in the shrinkage rate has largely occurred, the evaluation, delay phenomenon of shrinkage has appeared.

$D_p$  (depth of penetration) is inversely proportional to the amount of the photo-initiator, in a system where the content of the initiator is increased, the delay effect becomes greater. Looking at Figure 4-42, when the content of the initiator is 5 phr, it can be confirmed that the delay effect of the 10% condition is further increased. Photo-initiator have a more significant effect on absorbing the UV and the delay effect becomes larger in low light.

However, it is possible to verify that the initial time is pulled rather comes to light intensity increases. The result is reflected a feature of the test method for measuring the bulk characteristics. It is described in Figure 4-38, transmittance goes up and partially cure rate decreases at low content of the initiator. Therefore, not progress fast cure that can cause shrinkage phenomenon, a low curing density phenomenon also takes place at the same time.

It was calculated  $E_c$  based on the largest retarding condition that 10% of the intensity. Cd is the same since the thickness of the specimen is constant, it is  $\epsilon$  also the same, hence the same base material is used

- $E_{\max 10(3p)} = \text{UV intensity} \times \text{time} = 1 \text{ (mW)} \times 46.2 \text{ (s)}$

$$D_{p10(3p)} = 2 / 2.303 \times \epsilon \times [3]$$

$$\begin{aligned} C_{d10(3p)} &= D_{p10(3p)} \ln (E_{\max} / E_c) \\ &= (2 / 2.303 \times \epsilon \times [3]) \ln (46.2\text{J} / E_c) \end{aligned}$$

- $E_{\max 10(5p)} = \text{UV intensity} \times \text{time} = 1 \text{ (mW)} \times 58.8 \text{ (s)}$

$$D_{p10(5p)} = 2 / 2.303 \times \epsilon \times [5]$$

$$\begin{aligned} C_{d10(5p)} &= D_{p10(5p)} \ln (E_{\max} / E_c) \\ &= (2 / 2.303 \times \epsilon \times [5]) \ln (58.8\text{J} / E_c) \end{aligned}$$

$$C_{d10(3p)} = C_{d10(5p)}$$

$$(2 / 2.303 \times \epsilon \times [3]) \ln (46.2\text{J} / E_c) = (2 / 2.303 \times \epsilon \times [5]) \ln (58.8\text{J} / E_c)$$

$$[3] \ln (46.2\text{J} / E_c) = [5] \ln (58.8\text{J} / E_c)$$

$$(46.2\text{J} / E_c) = (58.8\text{J} / E_c)^{5/3}$$

$$\therefore E_c = 32.1 \text{ J}$$

(Eq 4-16)

Using these formulas, in the present system, it is possible to infer the "critical" energy dosage which role as a variable.

And analyzed the correlation of curing rate and intensity through a normalized of shrinkage rate in the previous 3 phr system. These trends also acts the same on 5 phr system, Figure 4-45 is a result of the normalized maximum shrinkage rate of each system to  $I_0^{0.6}$ .

Both shrinkage rate and shrinkage are larger at the content of the photo-initiator is 3 phr. This can be to understand about the non-regular shrinkage phenomena such as the curl and maintenance the space between the molecules are occurring by internal factors in terms of the decrease  $v$ . A sporadic curing property's role that will pull the time of measuring shrinkage in the case of light intensity has risen. Thus, despite shrinkage and shrinkage rate is low in the 5 phr system, shrinkage occur time is more rapid.

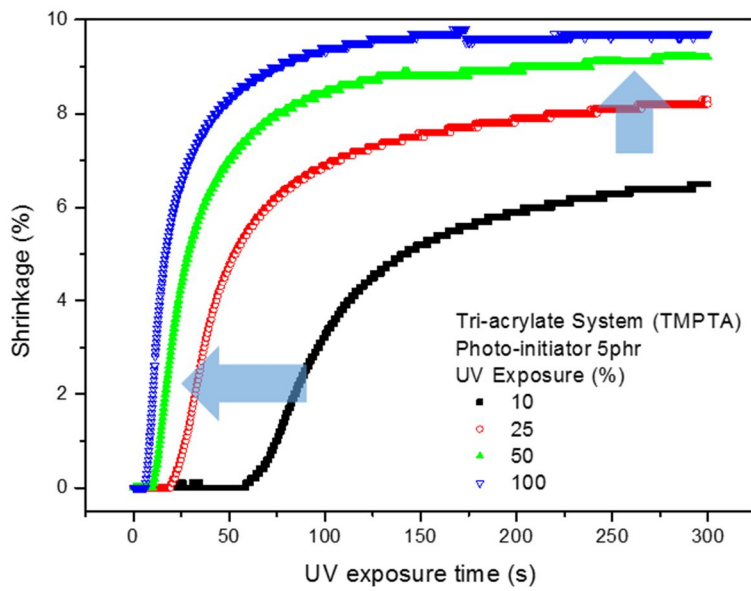


Fig. 4-42. Shrinkage of TMPTA depends on the UV intensity (PI 5 phr)

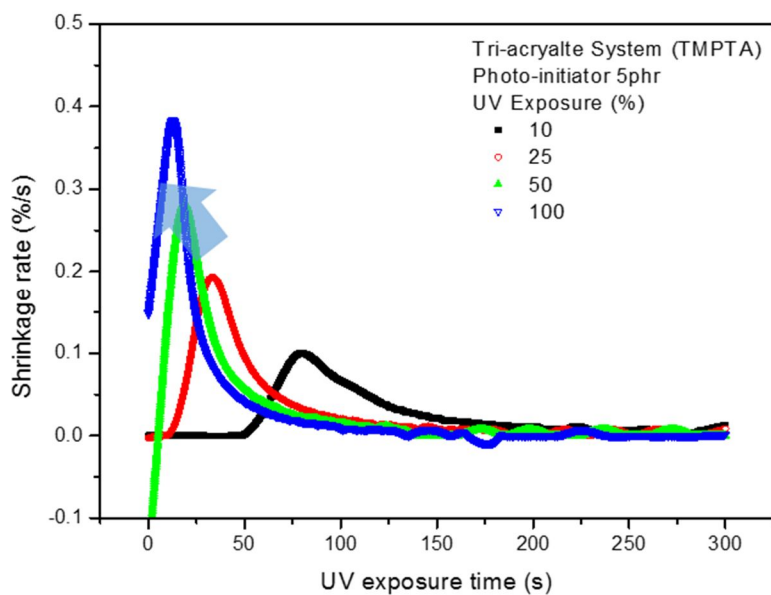


Fig. 4-43. The shrinkage rate of TMPTA depends on the UV intensity (PI 5 phr)

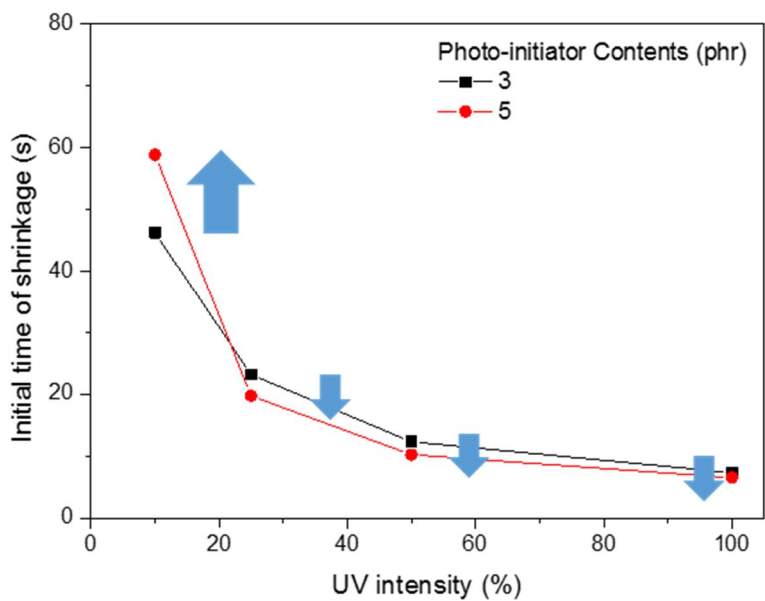


Fig. 4-44. Shrinkage initial time in accordance with the content of the initiator and UV intensity

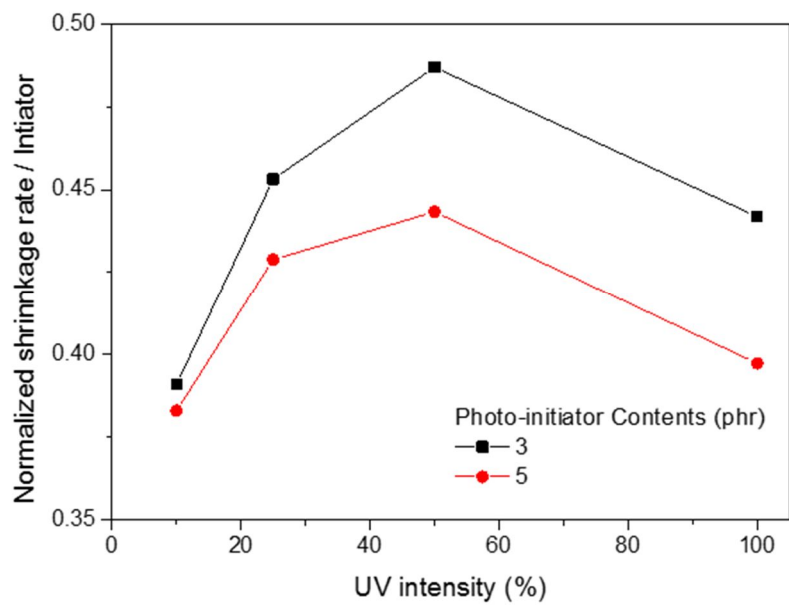


Fig. 4-45. Normalized shrinkage rate by UV intensity

#### 4.4.3. Temperature and Shrinkage

Reactivity increased with molecule's activity and reaction rate increased 2 times as temperature increase to 10 degrees.

Generally, the reaction rate of the UV curing system is to be increased with the temperature increasing. However, in the case where such hydroxy group is present in the molecular structure, it becomes attraction decreases between molecules at the temperature increases, and reactivity decreased too.

Figure 4-46 is a result of analyzing the difference in change by the presence or absence of hydroxy group when the temperature is changed under the same curing conditions (Lee, 2004). On same molecular structure system, a hydroxy group acts as the main factors that increase the reaction rate.

The  $T_g$  (glass transition temperature) is one of the most important parameters of a polymeric system.  $T_g$  determines the temperature boundary of significant changes in the enthalpic, viscoelastic, dilatometric etc. properties of all glass-forming materials. The relationship between  $T_g$  and conversion

degree in the curing reaction ( $\alpha$ ) of curing materials is a central concept in analyzing cure phenomena.

The  $T_g$  of polymeric materials is changed by converting ratio from monomer to polymer. Generally, the portion referred to as the  $T_g$ , of molecular weight is assumed to be infinite. In other words, it is changed that  $T_g$  depending on the degree of curing of the material.

The empirical DiBenedetto equation (DiBenedetto, 1949) gives a one-to-one relationship between  $T_g$  and  $\alpha$ .

$$\frac{T_g - T_{g0}}{T_{g\infty} - T_{g0}} = \frac{\lambda\alpha}{1 - (1 - \lambda)\alpha} \quad (\text{Eq 4-17})$$

$T_{g0}$  is the glass transition temperature of the uncured resin ( $\alpha = 0$ ),  $T_{g\infty}$  is the glass transition temperature of the fully reacted resin ( $\alpha = 1$ ),  $\lambda$  is a structure-dependent parameter with value between 0 and 1.

From an extension of the Couchman equation, Pascault and Williams showed that  $\lambda$  is equal to the ratio  $\Delta C_{\infty} / \Delta C_{p0}$ .  $\Delta C_{p0}$  is the change of the isobaric specific heat capacity at the glass transition of uncured resin,  $\Delta C_{\infty}$

is the change of the isobaric specific heat capacity at the glass transition of fully reacted resin (Figure 4-47).

Owing to enthalpy relaxation, the values of the glass transition temperature ( $T_g$ ) for partially reacted polymers may depend on the thermal history of specimens and the heating rate used for measurements. Use of the theoretical relations between  $T_g$  and the extent of reaction ( $x$ ) of a thermoset must take this fact into account. The original DiBenedetto equation has been re-evaluated as a convenient constitutive equation for expressing  $T_g$  versus  $x$ . An extension of Couchman's approach for the expression of the compositional variation of  $T_g$  enabled us to derive the same functionality as given by the DiBenedetto equation. Thus, the DiBenedetto equation may be regarded as based on entropic considerations applied to a model of the thermosetting polymer consisting of a random mixture of a fully reacted network with the initial monomers in an amount which depends on the particular conversion level. These two equations have been applied successfully to different copolymers (Pascault, 1990).

Although the initial reaction maintains a rubbery state because the  $T_g$  of the raw material is low. However,  $T_g$  is increased as the curing proceeds, the phenomenon that to be converted rubbery to glass is processed. These changes in conditions can influence the reactivity since influences on the

flowability of the material. Especially, there is also described in these  $T_g$  problems that why experimental conversion does not reach 100% (Moeck, 2014).

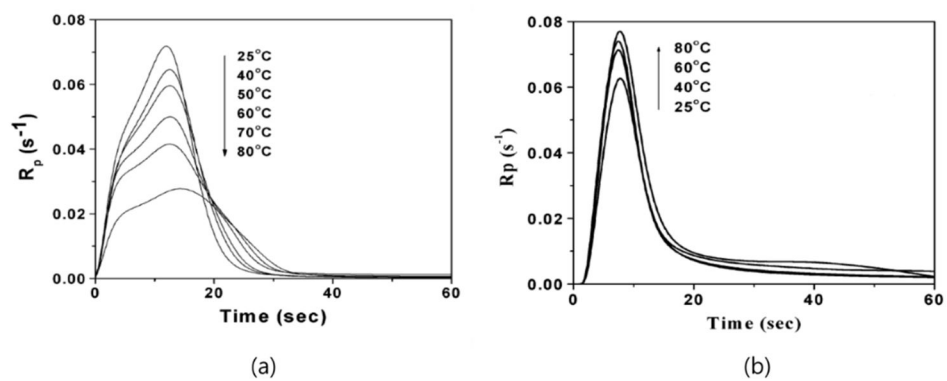


Fig. 4-46. Rate of polymerization as a function of time at various temperatures for  
 (a) Hydroxyethyl acrylate, (b) 1,6-hexanediol diacrylate (Lee, 2004)

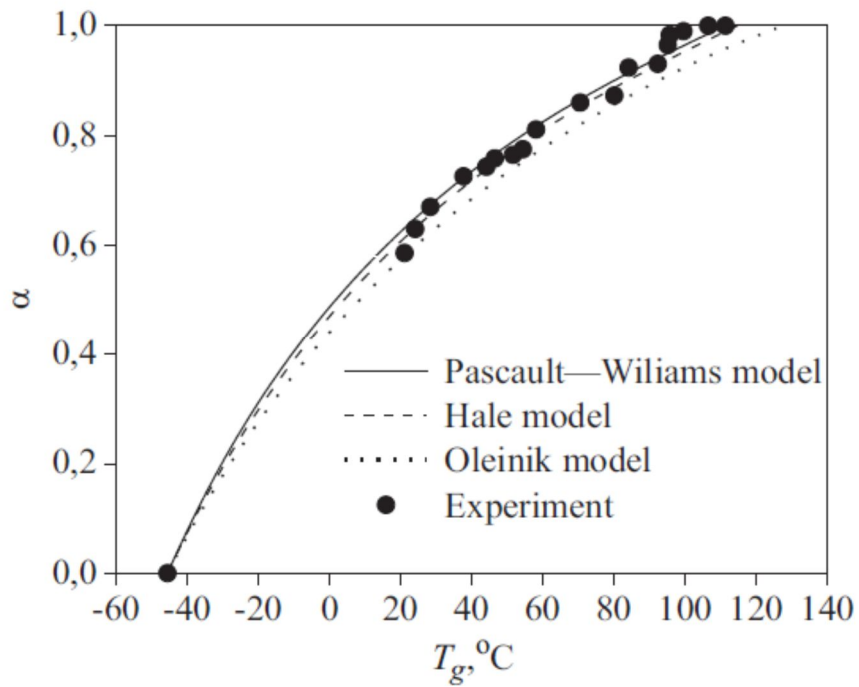


Fig. 4-47. Conversion degree ( $\alpha$ ) as a function of the glass transition temperature ( $T_g$ ) for the epoxy system (Urbaniak, 2011)

Photo-DSC are utilized to confirm the relationship between reactive changes and  $T_g$ . Before the shrinkage test and the photo-DSC, evaluation has been described as to be able to flow out the results with each other. Bulky properties cannot be confirmed directly on the basis of reactivity change it is inferred that effect of  $T_g$ /temperature on the actual shrinkage.

TMPTA and ethoxylated TMPTA were selected to evaluate it. The change in  $T_g$  of clarity that depending on the molecular structure, they have the same functional groups, so error is expected to be the smallest.

Ethoxylated TMPTA is classified by its molecular structure according to the level of the extended ethoxy structure. In this study, three materials extended to each chain every 2, 3, and 5 are used. Figure 4-48 shows the molecular structure of ethoxylated TMPTA.

In order to assess the impact of temperature, temperature was adjusted to -50, 25, 0, 25, and 50 °C. The intensity of UV was fixed 10 mW/cm<sup>2</sup> and error range was 10%.

Figures 4-49, 4-50, 4-51, and 4-52 present the heat-flow of TMPTA, EO6 TMPTA, EO9 TMPTA, and EO15 TMPTA, respectively. As the temperature rose, the reaction rate also increased.

The increment of reaction rate decreased as the order of TMPTA, EO6 TMPTA, EO9 TMPTA, and EO15 TMPTA. In aspect of heating value, the change of maximum heat flow from  $-25^{\circ}\text{C}$  to  $50^{\circ}\text{C}$  was up to five times more (Table 4-10). In addition, they decreased as the molecular weight increased in the test for the total heating value (Figure 4-53).

The graph was normalized as based on molecular weight since the actual density of acrylate differed among the materials (Figure 4-55). Each graph has a peak in a constant position, which is arranged in accordance with the order of the glass transition temperature ( $T_g$ ) of the materials.  $T_g$  of the materials were  $62^{\circ}\text{C}$ ,  $-7^{\circ}\text{C}$ ,  $-19^{\circ}\text{C}$ , and  $-32^{\circ}\text{C}$ , respectively.

As the reaction progresses in a certain part of materials and accordingly  $T_g$  increases in that part, the local reduction of mobility is induced. Eventually, Such reduced mobility decreases the reactivity of the material. Therefore, the rising of ambient temperature is an important factor to increase the reactivity of the material reduces (Figure 4-56).

However, the reactivity tends to decrease as the temperature rises further. The kinetic reaction has the main impact in the low temperature. However, temperature rise leads the thermodynamics reaction to accompany the reverse reaction and reactions related to by-products, and consequently, the heating value reduces. This is the reason for Figure 4-57.

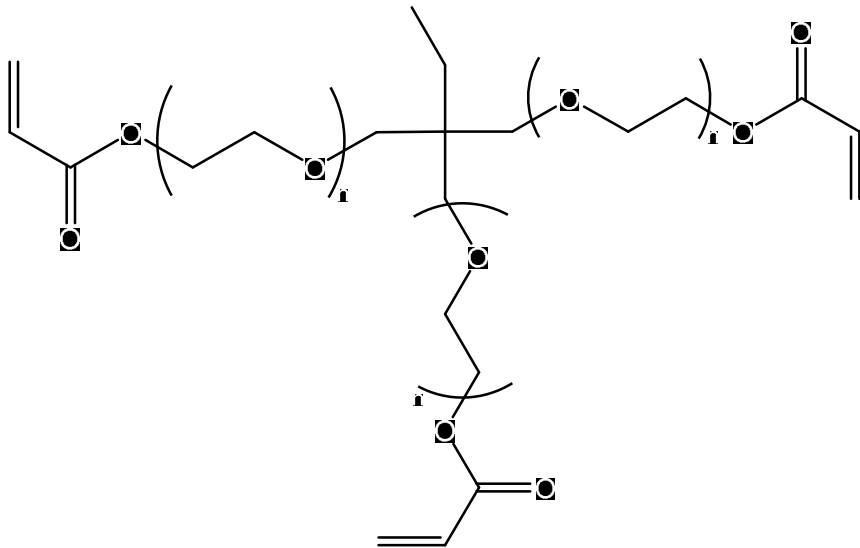


Fig. 4-48. Structure of ethoxylated TMPTA

- (a) Trimethylolpropane triacrylate:  $n=0$
- (b) Ethoxylated 6 trimethylolpropane triacrylate :  $n=2$
- (c) Ethoxylated 9 trimethylolpropane triacrylate :  $n=3$
- (d) Ethoxylated 15 trimethylolpropane triacrylate :  $n=5$

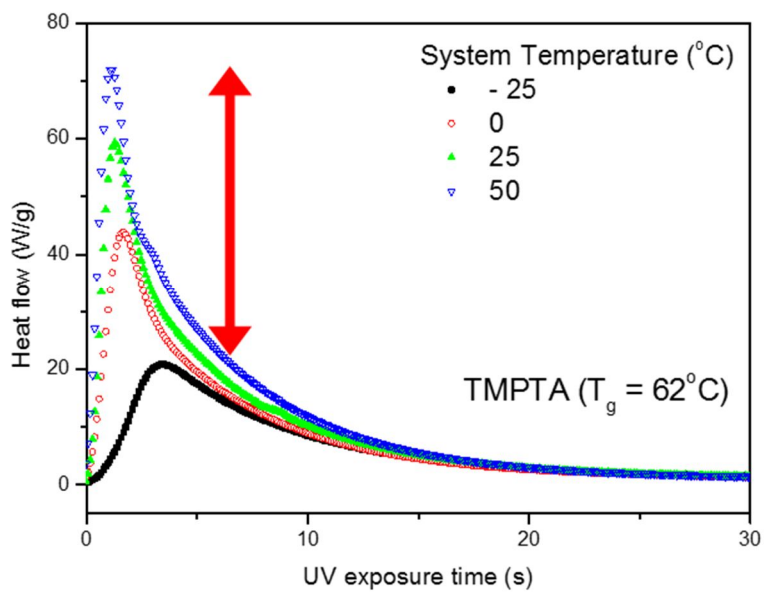


Fig. 4-49. Heat flow of TMPTA is accordance with the temperature

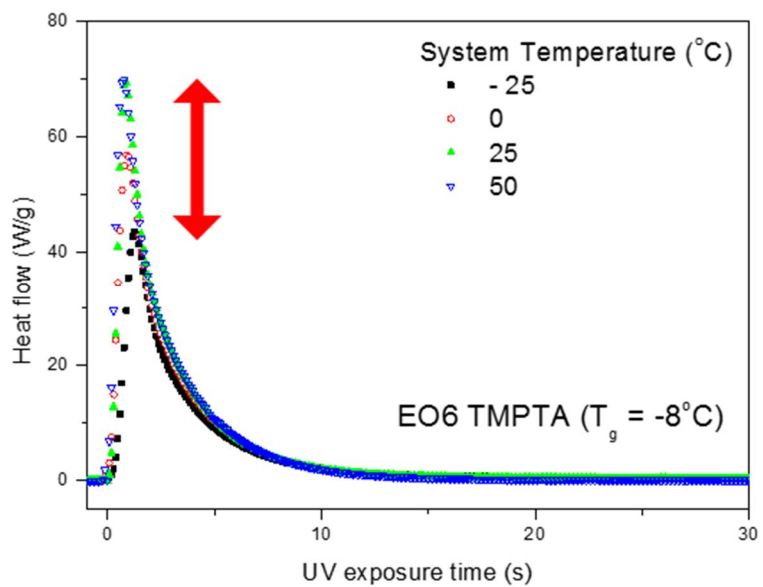


Fig. 4-50. Heat flow of EO6 TMPTA is accordance with the temperature

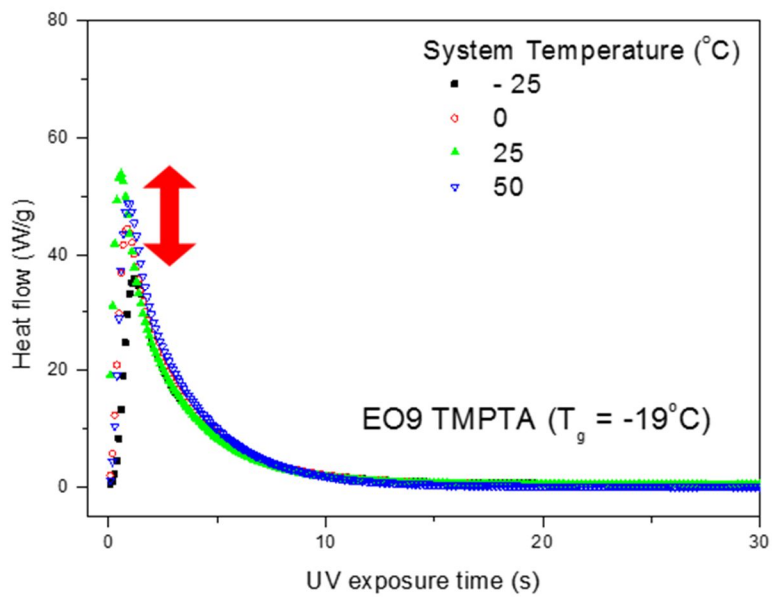


Fig. 4-51. Heat flow of EO9 TMPTA is accordance with the temperature

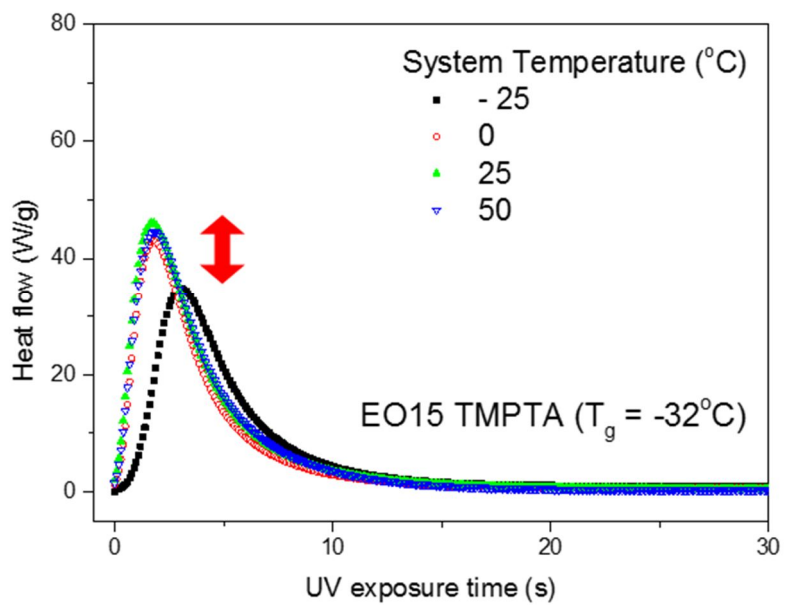
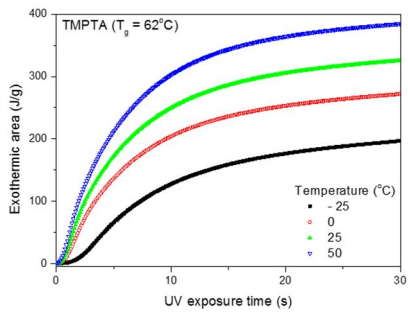
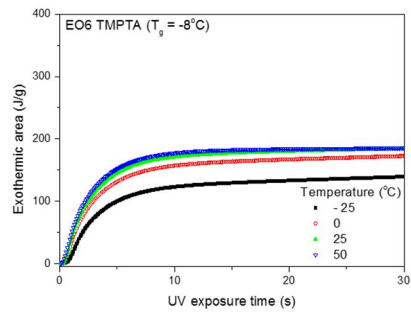


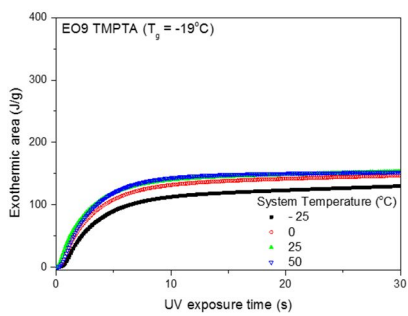
Fig. 4-52. Heat flow of EO15 TMPTA is accordance with the temperature



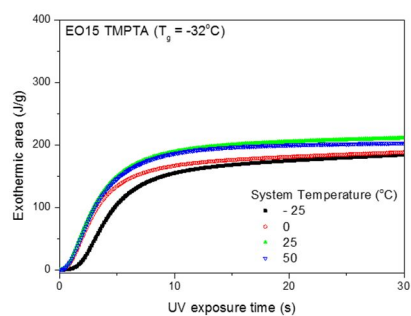
(a)



(b)



(c)



(d)

Fig. 4-53. Exothermic areas of tri-acrylate system (a) TMPTA (b) EO6 TMPTA (c) EO9 TMPTA (d) EO15 TMPTA

Table 4-10. Maximum heat flow and  $\Delta T$  of the tri-acrylate system according to system temperature

Maximum Heat Flow (W/g)	TMPTA	EO6 TMPTA	EO9 TMPTA	EO15 TMPTA
-50°C	0	2.56	2.72	2.05
<b>-25°C</b>	<b>20.82</b>	<b>43.48</b>	<b>35.91</b>	<b>34.83</b>
0°C	43.84	56.74	44.48	42.99
25°C	59.34	69.27	53.8	46.10
<b>50°C</b>	<b>71.94</b>	<b>69.67</b>	<b>48.79</b>	<b>44.53</b>
<b><math>\Delta H (H_{50} - H_{25})</math></b>	<b>51.12</b>	<b>26.19</b>	<b>17.89</b>	<b>9.70</b>

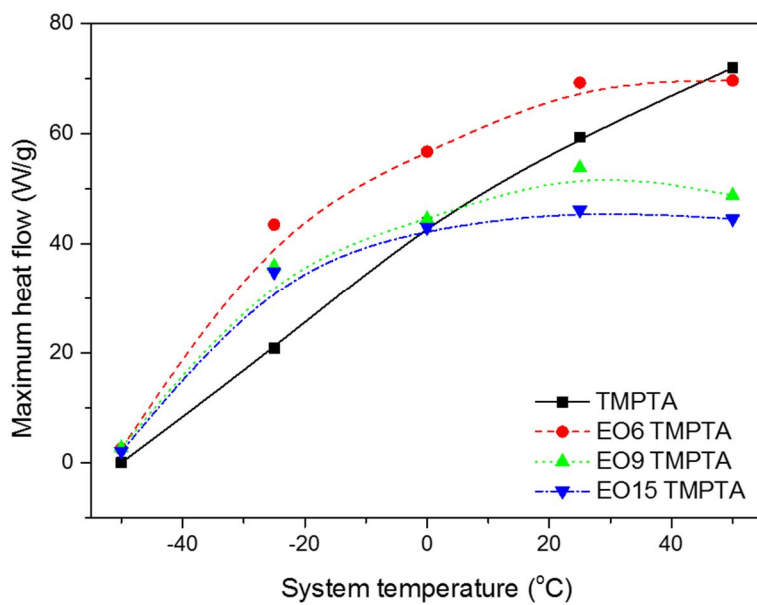


Fig. 4-54. Maximum heat flow of tri-acrylate system

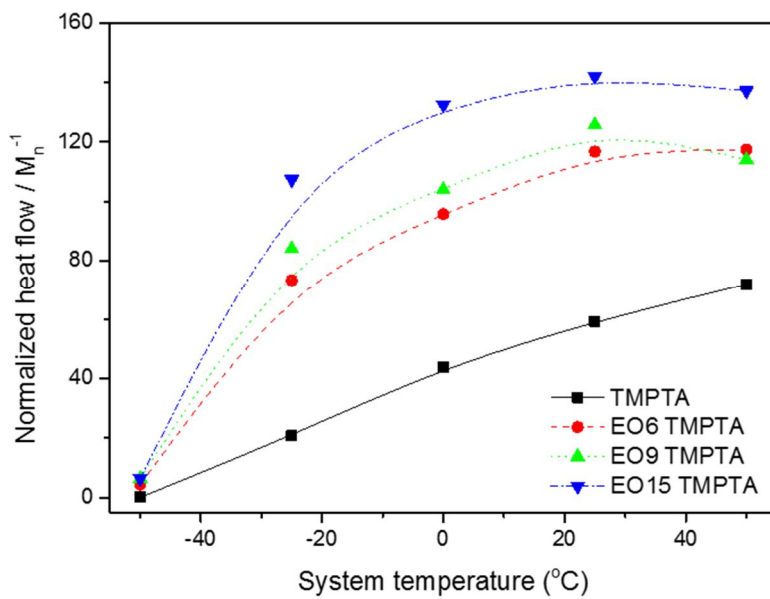


Fig. 4-55. Normalized maximum heat flow of tri-acrylate system

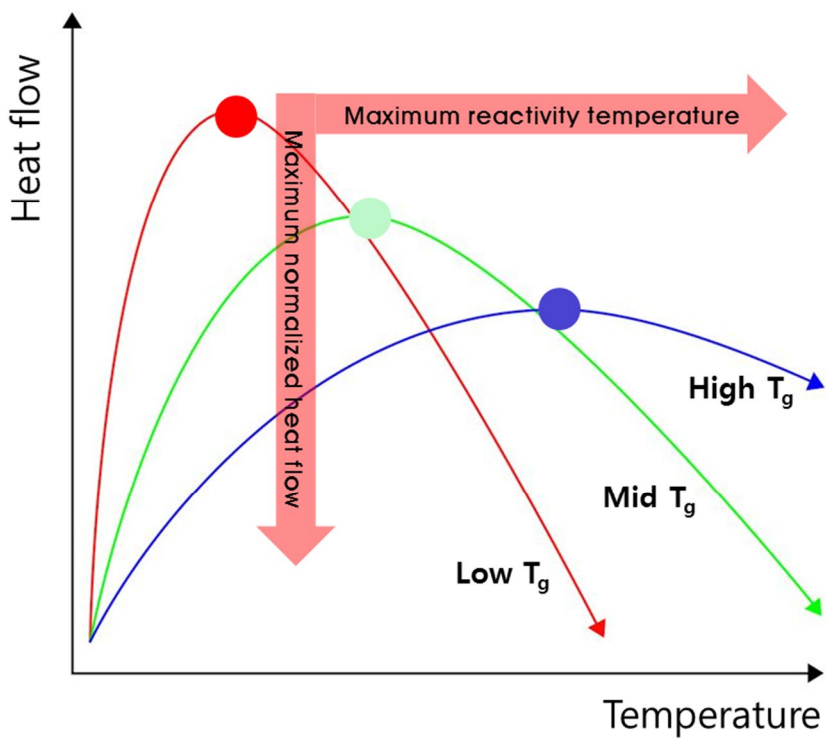


Fig. 4-56. Scheme of maximum heat flow trend by  $T_g$

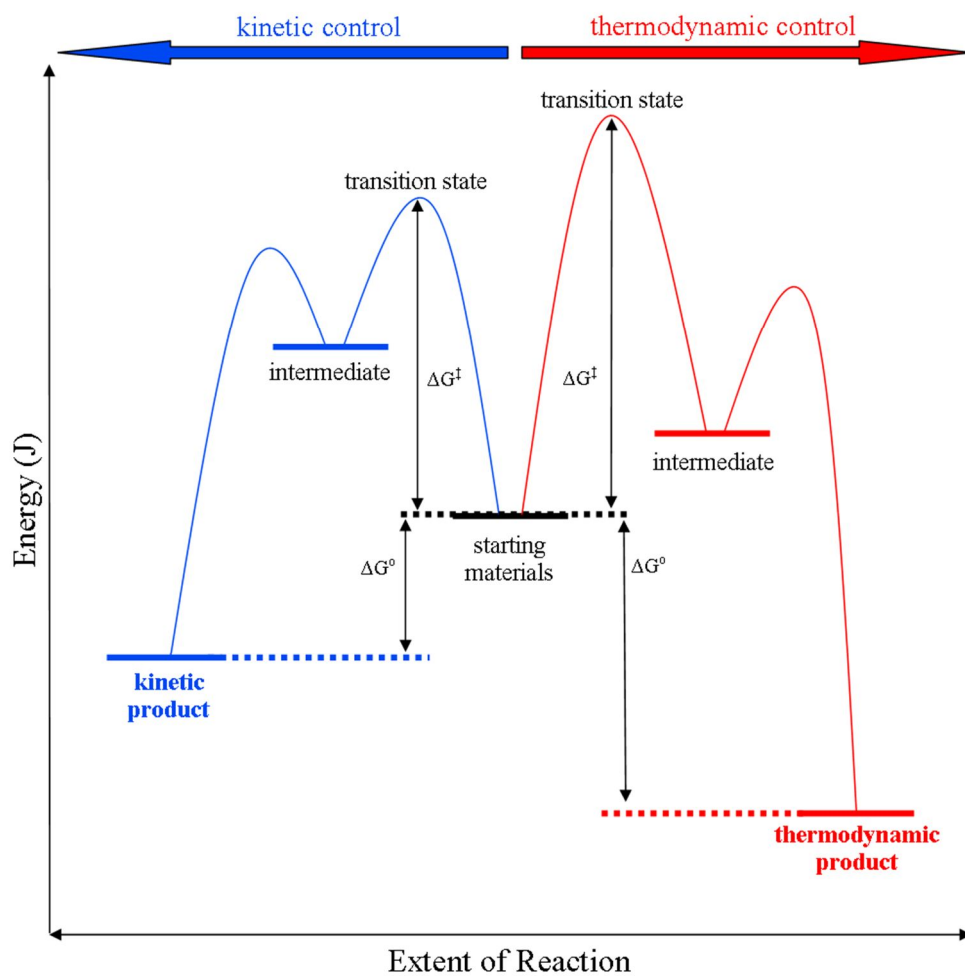


Fig. 4-57. Thermodynamic vs. kinetic control of reaction

# *Chapter 5*

Change of Shrinkage as Function of the  
Change of the Material

## **5. Change of Shrinkage as Function of the Change of the Material**

### 5.1. Change of shrinkage associated with differences in the molecular structure

#### 5.1.1. Shrinkage rate changes in accordance with the number of functional groups

The photo-polymerization kinetics of multi-functional acrylates have been studied extensively since these polymers are used in a wide range of applications from lithography and coatings, to biologically related uses such as dental composites and contact lenses (Bowman, 1992).

The C=C bonds on acrylates react readily in the presence of radicals, and in the case of multi-functional acrylates, which have multiple C=C groups per monomer, reactions between distinct chains are also possible. These types of reactions, known as cross-linking, bind different polymer chains in the reaction volume into an insoluble network (Boddapati, 2010).

It is known that UV curing behavior changes in proportion to the number of functional groups generally. The reason for this change is associated with the

density of acrylate. Because the production of radicals and its chain reaction proceed instantaneously due to the nature of chain reaction, the density of functional groups acts as a very important factor

Four kinds of materials shown in Figure 5-1 were selected to explore the shrinkage characteristics of the multi-functional acrylate. The number of functional groups of each material is two, three, four and six and they do not have an extra intermediate extended structure.

According to the results shown in Figure 5-2, the shrinkage tended to decrease as the number of functional groups increases. In addition, as presented in Figure 5-3, the shrinkage rate tended to decline sharply as the number of functional groups increases. If normalized by functionality number and based on molecular weight of HDDA as the reference, the relative number of reactive site per 1 mol was very similar as 1 in HDDA, 1.15 in TMPTA, 1.28 in PETETA, and 1.17 in DPHA, respectively.

Thus, the reactivity to the proportion of acrylate is not significantly different to the results of the primary shrinkage evaluation. Rather the shrinkage of acrylate with three, four, and six functional groups is relatively smaller than the primary results. The reason why shrinkage decreases depending on the

number of functional groups is evaluated to be the mobility of molecular structure. Since the number of acrylate bound to a single molecule increases as the number of functional groups increases, although the number of acrylate per mol is similar, the mobility of acrylate is relatively lower. The decreasing of mobility considerably influences shrinkage because the UV curing proceeds in the stable environment

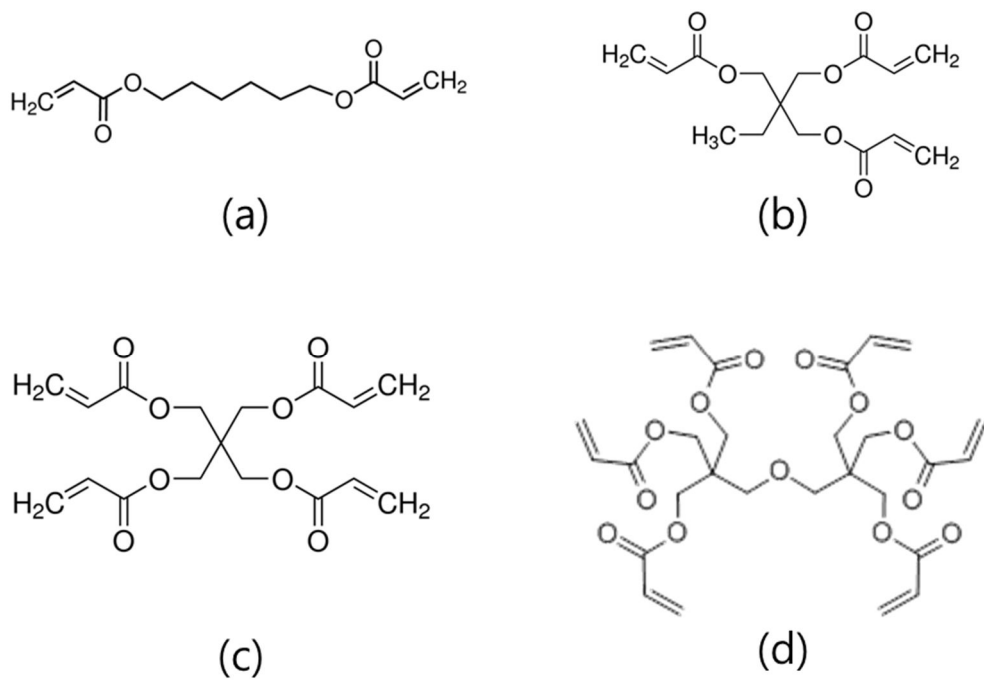


Fig. 5-1. Structure of multi-functional acrylate (a) 1,6-Hexanediol diacrylate  
 (b) Trimethylolpropane triacrylate , (c) Pentaerythritol tetraacrylate  
 (d) Dipentaerythritol hexaacrylate

Table 5-1. Basic information of multi-functional acrylate

Material	Abbreviation	Functionality Number	Molecule weight ( $M_n$ )
1,6-Hexanediol diacrylate	HDDA	2	226.27
Trimethylolpropane triacrylate	TMPTA	3	296.32
Pentaerythritol tetraacrylate	PETETA	4	352.34
Dipentaerythritol hexaacrylate	DPHA	6	578.56

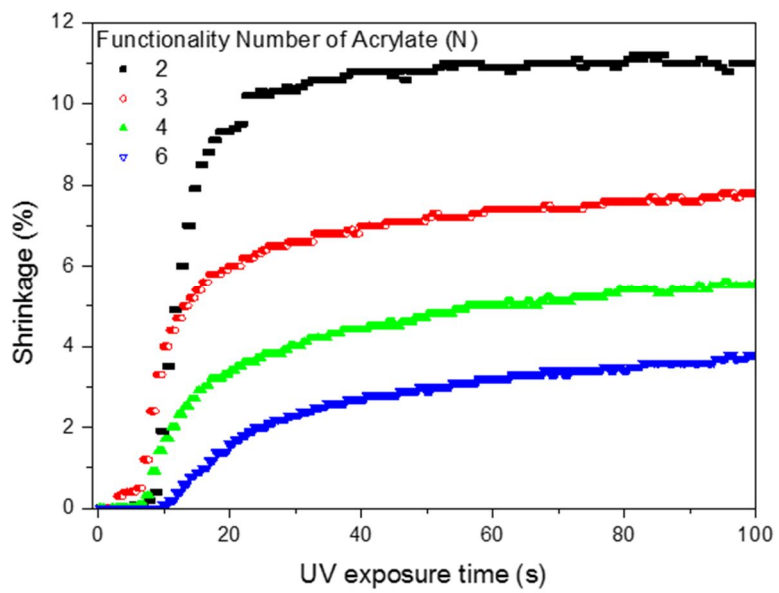


Fig. 5-2. Shrinkage corresponding to the number of functional groups

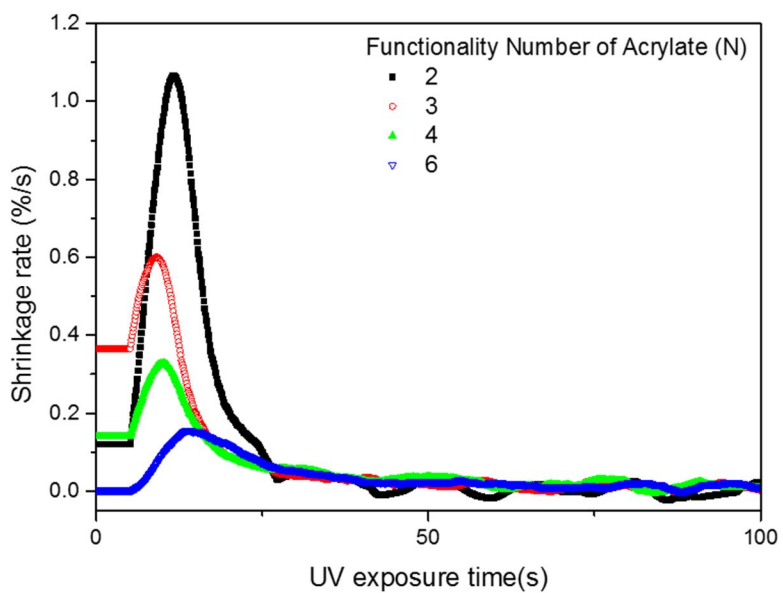


Fig. 5-3. Shrinkage rate corresponding to the number of functional groups

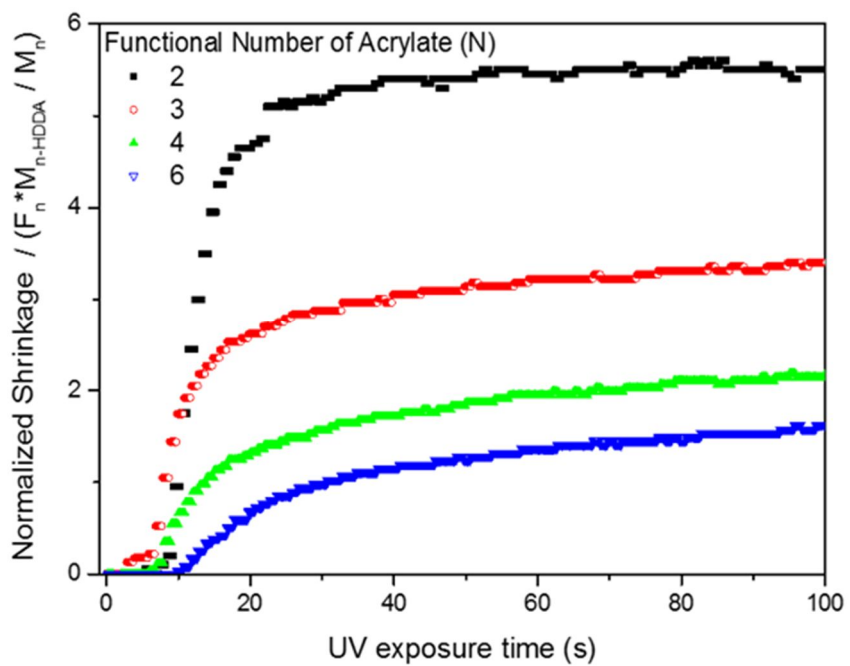


Fig. 5-4. Normalized Shrinkage rate by functionality number/molecular weight

### 5.1.2. Tri-acrylate System based on TMPTA

There are several tri-acrylate systems such as TMPTA ( $M_n=293$ ), EO6 TMPTA ( $M_n=557$ ), EO9 TMPTA ( $M_n=689$ ), and EO15 TMPTA ( $M_n=912$ ). These groups have the same functional group and the same backbone structure. However, they have branches of different length that chain medium are substitutes configured differently. In general, shrinkage of TMPTA must be greater because shrinkage is inversely proportional to molecular weight.

Figure 5-5 shows the shrinkage result of three materials that the order of shrinkage as a TMPTA > EO6 TMPTA > EO9 TMPTA > EO15 TMPTA. As Figure 5-6 through the shrinkage rate has also the order of TMPTA > EO6 TMPTA > EO9 TMPTA > EO15 TMPTA. Through the results of this shrinkage, however, reactivity of TMPTA is cannot confirm to most reactive. Each material has different number of functional groups according to the unit volume; shrinkage only depends on only molecular size because there are no differences in the basic structure. First, shrinkage of three kinds of materials is 9.6%, 7.5%, 6.5% and 4.6%. The number of functionality ratio 1: 0.529: 0.427: 0.324 on the same weight and shrinkage depending on the ratio of

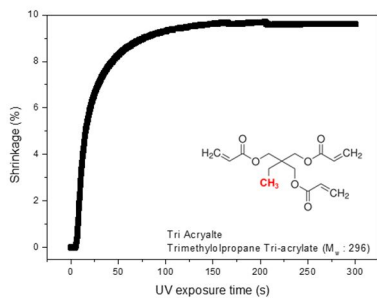
functional groups to calculate are 1: 1.48: 1.58: 1.48 (Measured ratio is 1.00: 0.77: 0.66). This result is the opposite result of shrinkage or shrinkage rate. The degree of conversion ratio is actually the order of the EO9 TMPTA > EO15 TMPTA = TMP (EO) 6TA > TMPTA because shrinkage is directly related to the conversion.

This phenomenon occurs by the different movement of molecules in combination that depending on the size of the actual material. When the shrinkage started, both functional groups of small molecules and large molecules are shown same reactivity at the initial time. The reaction of small molecules is faster than large molecules because the reactors that belong to small molecules are located more and more closely together in the same space. However, materials that have rapidly progressed the reaction may have the following two kinds of problems (Figure 5-7)

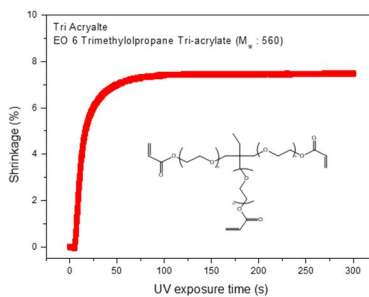
- 1)  $T_g$  of the point at which the reaction started is rapidly increased and partial mobility is reduced. Reduced mobility prevented the movement of the remaining functional groups and movement are sharply reduced and
- 2)
- 3) In addition, because the gap between functional groups in the

combined molecules are too narrow to move and rotate freely, available molecular chain (C-O-C and the like) does not exist. As a result, these problems will cause low conversion.

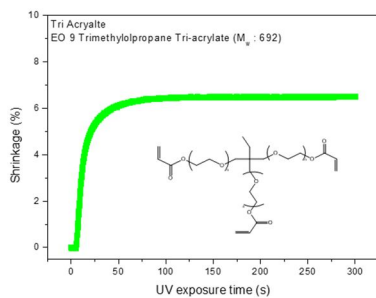
In Figure 5-6 the difference between the respective molecules of theoretical and experimental shrinkage for the respective molecules. Theoretical shrinkage was assumed that the reactions among acrylate existing inside, the material progressed all. Therefore, the experimental shrinkage close to the theoretical one means that the internal functional groups participated in the reaction as much as possible. As above confirmed the change of reactivity according to temperature, it is determined that the difference between theoretical and actual reactivity of materials is depending on these internal and external conditions.



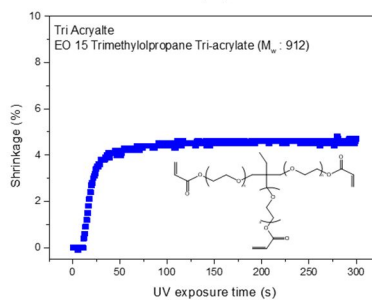
(a)



(b)



(c)



(d)

Fig. 5-5. Shrinkage (a) TMPTA (b) EO6 TMPTA (c) EO9 TMPTA (d) EO15 TMPTA

Table 5-2. Theoretical shrinkage and experimental shrinkage

	TMPTA	EO6 TMPTA	EO9 TMPTA	EO15 TMPTA
Molecule Weight	296	560	692	912
Theoretical maximum Shrinkage	28.83	14.02	10.85	7.61
Shrinkage (%)	9.6	7.5	6.5	4.6

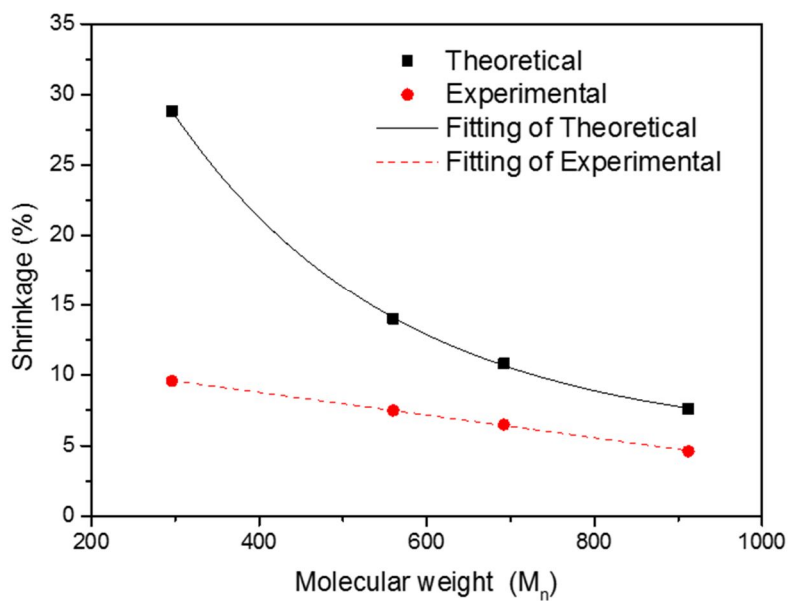


Fig. 5-6. Theoretical shrinkage and experimental shrinkage by molecular weight

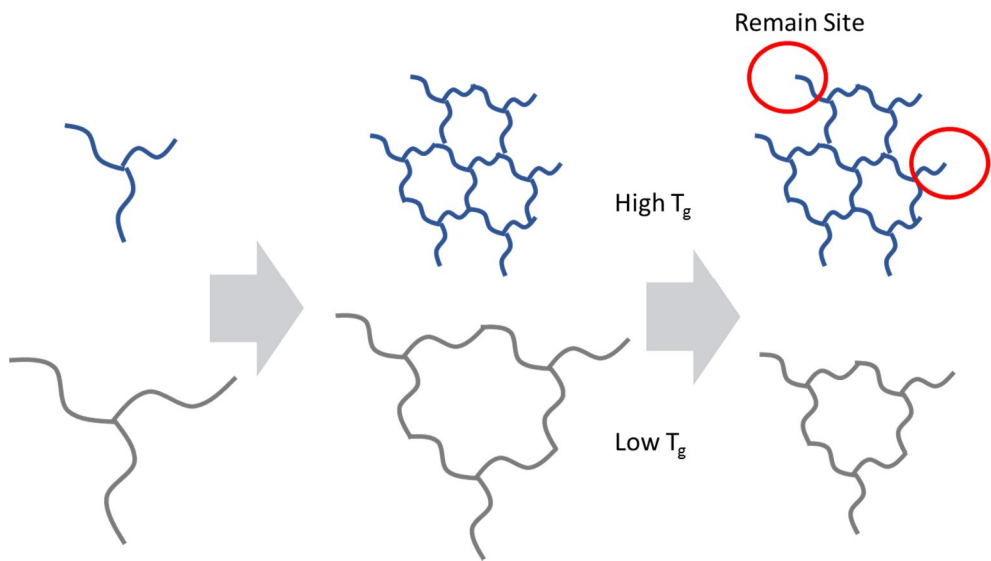


Fig. 5-7. Mobility of molecule depend on molecule's size

## 5.2. Acrylate vs Methacrylate

Though the core structures of molecules composing the UV curable materials are various, the structures of functional groups actually participating in the reaction with UV are mostly acrylate and methacrylate structures. The structure with double bonds such as  $C = C$  can have chain reactions with the radical generated by UV, and the reactivity is different in accordance with the structure. Acrylate and methacrylate differ in structure as one methyl group ( $-CH_3$ ), and this structural difference makes the reactive difference significantly.

With the advent of pulsed laser assisted techniques, propagation rate coefficients are known for many monomers like styrene, methacrylates and acrylates. Termination and transfer coefficients are available, but less precisely known as can be seen by looking at the Polymer Handbook, where even in the same polymerization conditions there is a significant scatter in the data for common monomers such as styrene and methyl methacrylate. Secondary reactions and many copolymerization parameters are even less well known and hence the focus of this report. Table 5-3 shows a summary of experimental  $k_p$  results as measured by Pulsed Laser Polymerization (PLP)

/Size Exclusion Chromatography (SEC) technique. The family behavior observed (eg. All methacrylates have very similar values for activation energies and values) suggest it may be possible to correlate rate coefficients to the structural characteristics of the propagating radicals and monomers (Bebe 2008).

Table 오류! 여기에 표시할 텍스트에 을(를) 적용하려면 [홈] 탭을  
 사용하십시오.-3 Arrhenius  $K_p$  the PLParameters for various  
 monomers determined by PLP-SEC (Bebe, 2008)

Monomer	$E_p$ (kJ/mol)	$\Delta V_p$ (cm <sup>3</sup> /mol)	$A_p$ (L/mol·s)	$k_p$ at 50 °C/1atm (L/mol·s)
Ethylene	34.3	-27.0	$1.88 \times 10^7$	54
Styrene	32.5	-12.1	$4.27 \times 10^7$	238
Methyl methacrylate	22.4	-16.7	$2.67 \times 10^6$	648
Butyl methacrylate	22.9	-16.6	$3.78 \times 10^6$	757
Dodecyl methacrylate	21.0	-16.0	$2.50 \times 10^6$	995
Glycidyl methacrylate	22.9	-15.0	$6.19 \times 10^6$	1230
Cyclohexyl methacrylate	23.0	-16.2	$6.29 \times 10^6$	1204
2-Hydroxypropyl methacrylate	20.8	n.d.	$3.51 \times 10^6$	1504
Vinyl acetate	20.7	-10.7	$1.47 \times 10^7$	6625
Methyl acrylate	17.7	-11.7	$1.66 \times 10^7$	22900
Butyl acrylate	17.4	n.d.	$1.81 \times 10^7$	27900
Dodecyl acrylate	17.0	-11.7	$1.79 \times 10^7$	32000

As listed in Table 5-4, four types of material with the same structure as a whole, but only differ in the structure of functional group were selected to analyze the difference between acrylate and methacrylate in the aspect of reactivity with UV and shrinkage. The materials with large molecular size are used to minimize the effect by methyl groups formed in the methacrylate structure because the molecular size influence on shrinkage.

### 5.2.1. MPEG-A vs MPEG-MA

The evaluation result of the shrinkage was 1.2% of MPEG-A and 1.65% of MPEG-MA, which gave around 30% of differentiation. In predicting the shrinkage through the theoretical calculation of the shrinkage below, the shrinkage of MPEG-A is expected to increase approximately 5% (Table 5-4).

*Theoretical Volume shrinkage (%)*

$$= -2.58 + 3,100 \times \frac{\textit{Functionality}}{\textit{Monomer weight}}$$

(Eq 5-1, Ackem 1995)

However, in the actual evaluation of MPEG-MA shrinkage, it was evaluated more highly. When looking at the index based on the common reactivity, the measure of the MPEG-A shrinkage was required to be higher. In order to determine the reactivity differences compared to the index, the reactivity of photo-DSC was watched.

Looking at the results of the Photo-DSC, the reaction rate of MPEG-A was found to be higher than that of the MPEG-MA, more than three times. However, the activation time of MPEG-MA reaction was relatively long, and the total exothermic energy, calculated based on this showed MPEG-MA is

going beyond MPEG-A in a certain cross-point.

The reason for having this different reaction results are (Figure 5-12):

- 1) Methyl structure, in the initial reaction stage, acts as a disturbance of packing and serves to reduce the density of the acrylate
- 2) But, methacrylate structure continuously supplies free space as the reaction proceeds in order to maintain mobility.

In shrinkage evaluation, it was assessed to have influenced by the low shrinkage of the mono-acrylate, with persistent differences in these responses. Shrinkage is a test that reflects the bulk properties, as mentioned above. Because bulk material reacts as a whole and cross-linking conducts to cause contraction, it was estimated to have the opposite effect from the theoretical shrinkage.

Table 5-4. Basic properties of acrylate/methacrylate monomers

Monomer	Abbreviation	Functionality number	Molecular weight (Mn)	Theoretical shrinkage (%)
Methoxy Polyethylene Glycol (550) Monoacrylate	MPEG-A	1	679	1.99
Methoxy Polyethylene Glycol (550) Monomethacrylate	MPEG-MA	1	693	1.89
Neopentyl Glycol Diacrylate	NEO-DA	2	212	26.66
Neopentyl Glycol Dimethacrylate	NEO-DMA	2	240	23.25
1,6 Hexanediol Diacrylate	HD-DA	2	226	24.85
1,6 Hexanediol Dimethacrylate	HD-DMA	2	254	21.82
Trimethylolpropane Triacrylate	TMP-TA	3	296	28.83
Trimethylolprpane Trimethacrylate	TMP-TMA	3	338	24.93

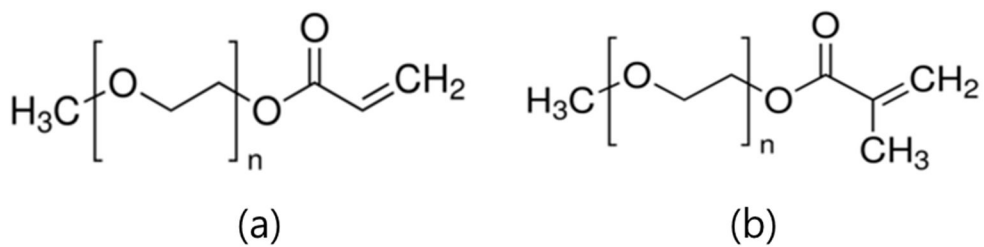


Fig. 5-8. Molecular structure of (a) MPEG-A (b) MPEG-MA

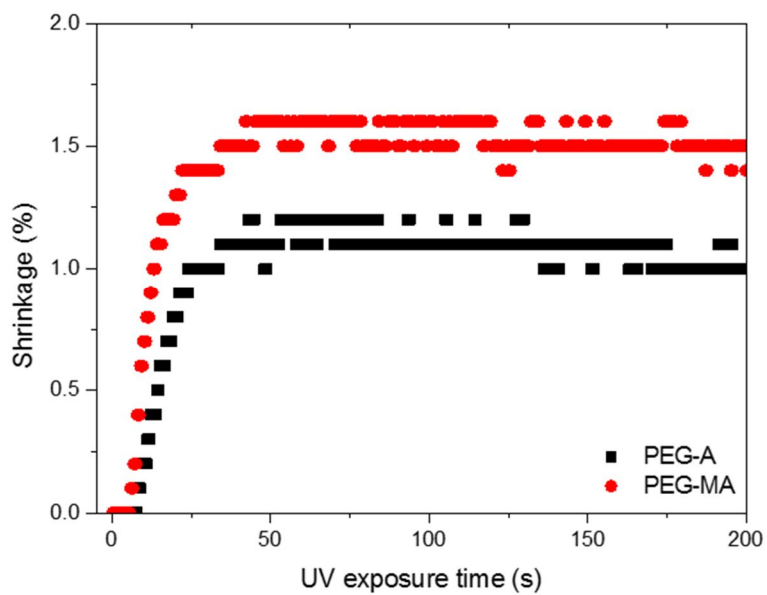


Fig. 5-9. Shrinkage of MPEG-A/MPEG-MA

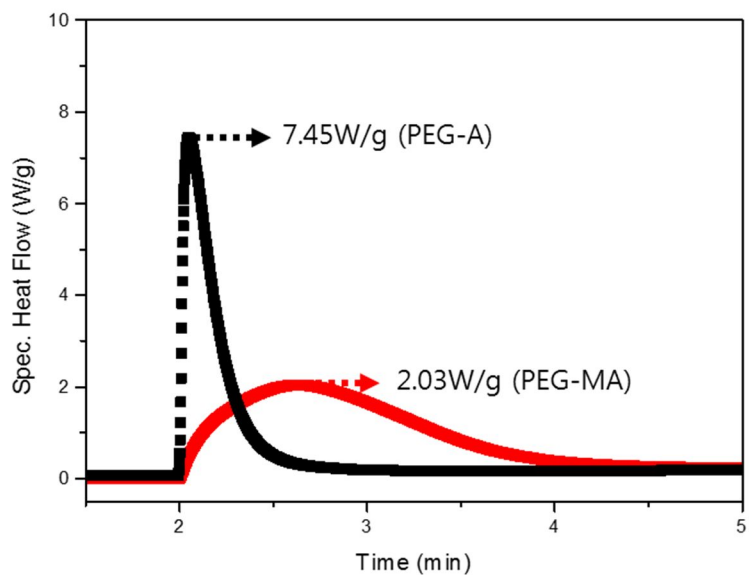


Fig. 5-10. Heat flows of MPEG-A and MPEG-MA

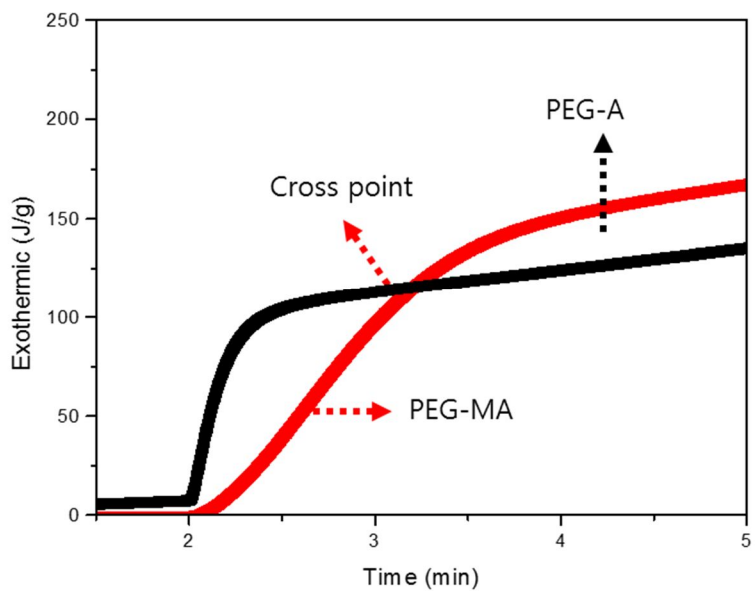


Fig. 5-11. Exothermic areas (total heat dissipation) of MPEG-A and MPEG-MA

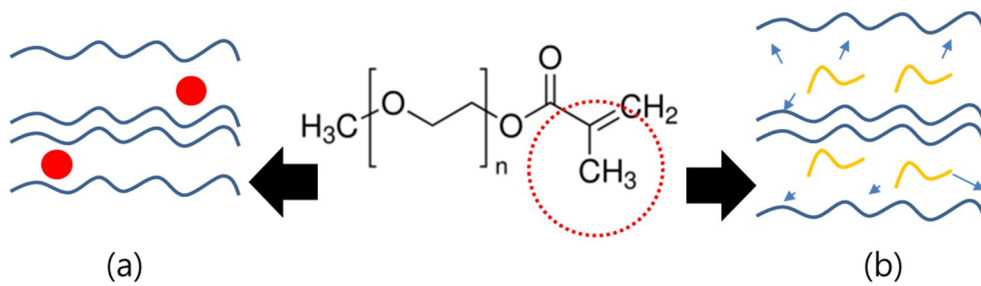


Fig. 5-12. Effect of metha methyl (a) Interfering role of packing, (b) The role of free available space

### 5.2.2. NEO-DA vs NEO-DMA

In the shrinkage evaluation of NEO-DA and NEO-DMA (Figure 5-13), unlike the previous evaluation of PEG series, the shrinkage of the NEO-DA rates more than double. In addition, the reaction speed is slow, delay of analytical shrinkage phenomenon occurred (Figure 5-14). Supplementary looking at the Photo-DSC evaluation, the reaction of the NEO-DMA is lasting longer, however, maximum heat output is showing a 10 times or more difference. It is evaluated as a result of differences in the reactivity of the acrylate and methacrylate. It is predicted that the results were affected by the very large reactivity difference between each reactor, even though the density of functional groups in the material are almost similar.

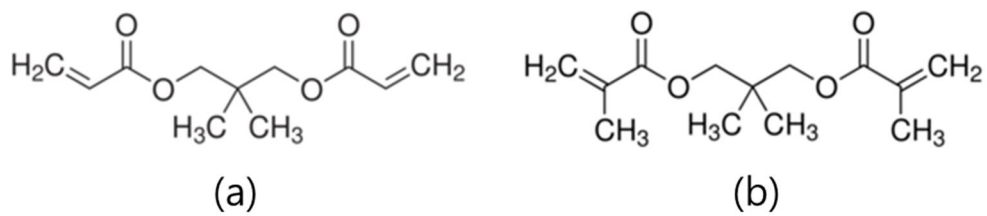


Fig. 5-13. Molecular structure of (a) NEO-DA (b) NEO-DMA

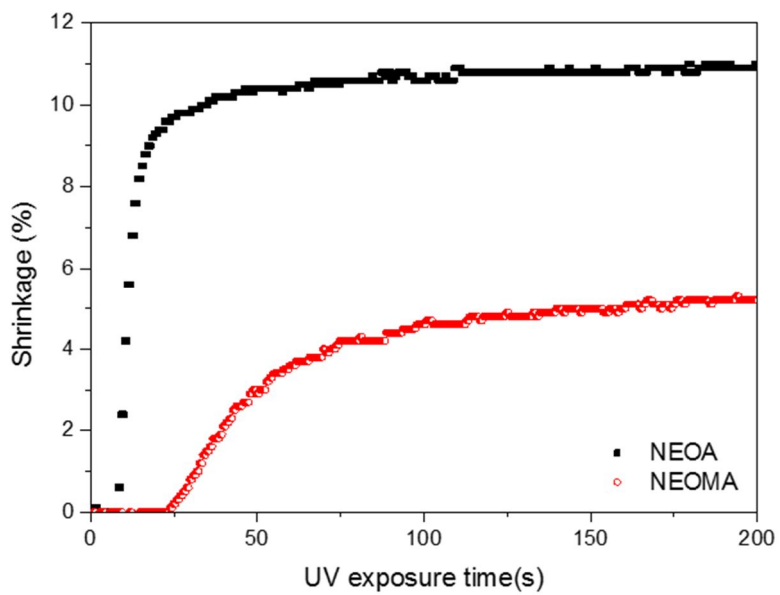


Fig. 5-14. Shrinkage of NEO-DA and NEO-DMA

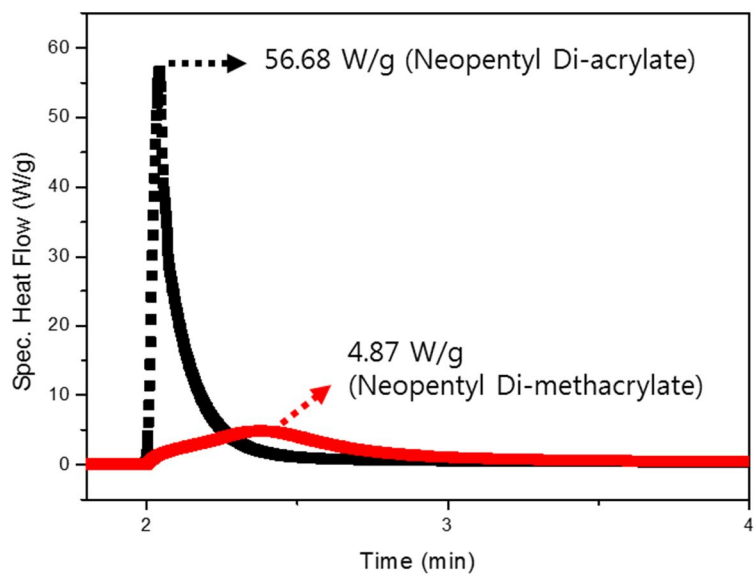


Fig. 5-15. Heat flows of NEO-DA and NEO-DMA

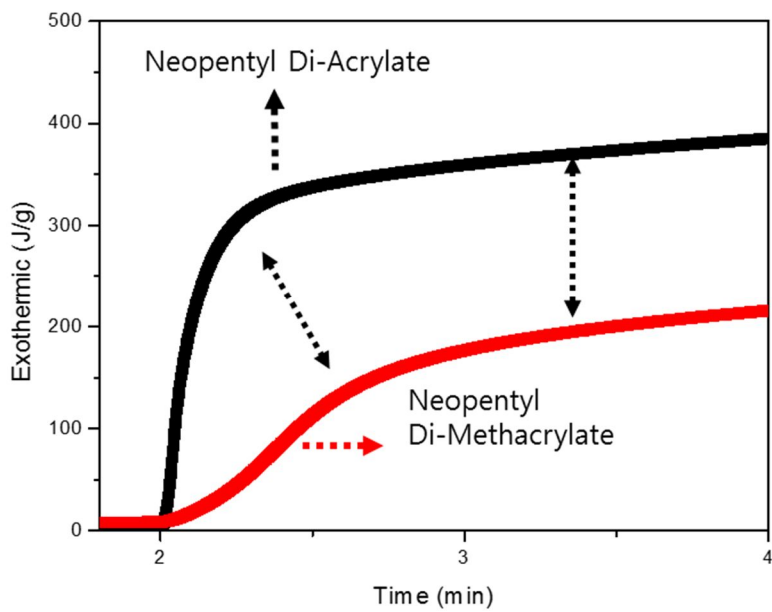


Fig. 5-16. Exothermic areas (total heat dissipation) of NEO-DA and NEO-DMA

### 5.2.3. HD-DA vs HD-DMA

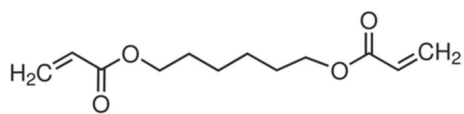
As in the previous evaluation, shrinkage evaluation between HD-DA and HD-DMA was assessed for HD-DA to have higher shrinkage rate by having acrylate structure. However, when compared to the previous series NEO shrinkage, the difference between the HD-DA and the HD-DMA was measured relatively small. In addition, evaluating the shrinkage of HD-DA and NEO-DA / HDDMA and NEO-DMA, the shrinkage of the HD series came out higher, and the shrinkage can also progress faster.

When comparing the two materials with photo-DSC, the reactivity difference between the HD-DA and HD-DMA is not as large as the previous NEO Series, and the overall reaction rate is also fast-paced and rapidly concluded. In the total heat output rating, the difference between the two materials is not as big as the previous NEO Series.

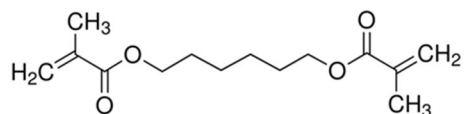
The molecular weight difference between the NEO Series and HD Series is very small. Although the material has the same number of functional groups and structure, the reactivity difference between the two series is significantly bigger. As compared to the Figure 5-21, such reactivity differences are

estimated to be due to the difference between the center structures.

Because the center structure of NEO series is short and rigid, the mobility is reduced sharply when the curing is conducted. Therefore, slow reaction proceeded methacrylate structure has a low shrinkage and the overall rating has very low reactivity. On the other hand, the center structure of HD is relatively long and has a flexible structure; it is evaluated to have high reactivity according to the mobility.



(a)



(b)

Fig. 5-17. Molecular structure of (a) HD-DA (b) HD-DMA

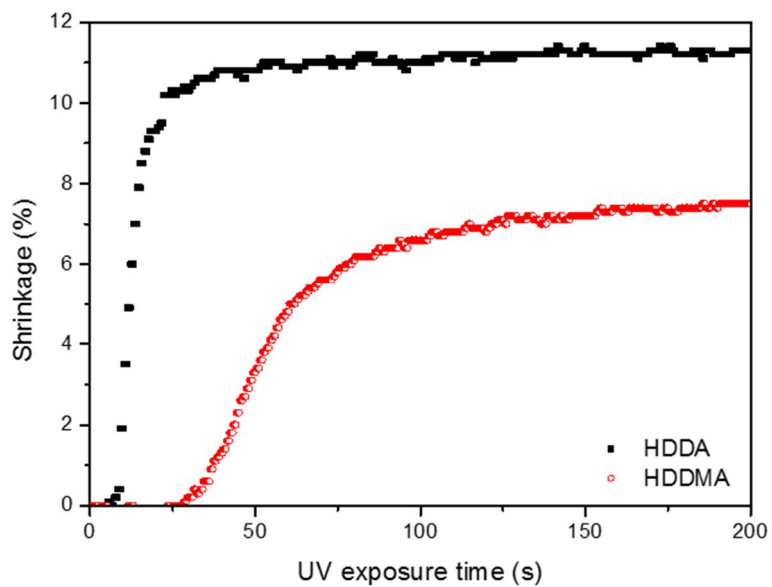


Fig. 5-18. Shrinkage of HD-DA and HD-DMA

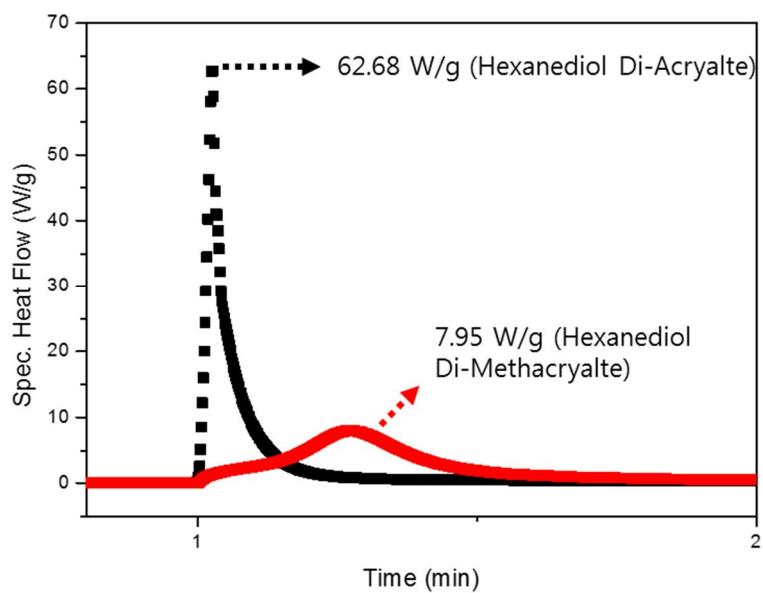


Fig. 5-19. Heat flows of HD-DA and HD-DMA

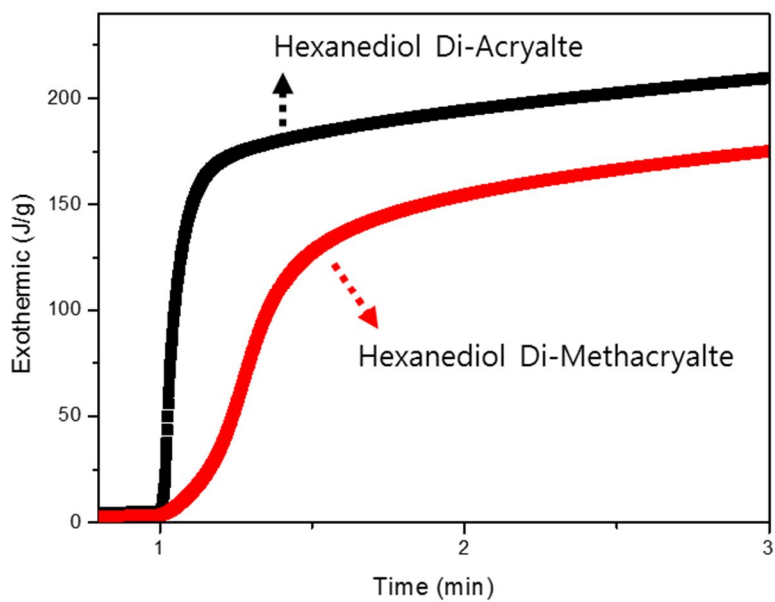
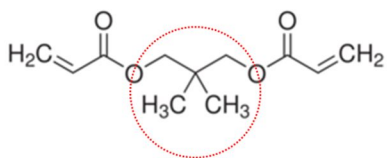
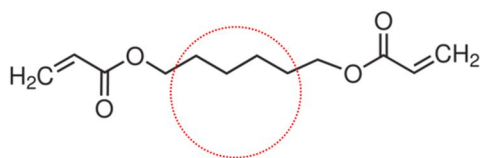


Fig. 5-20. Exothermic areas (total heat dissipation) of HD-DA and HD-DMA



Rigid & Short Back Born

$$T_g = 107 \text{ }^\circ\text{C}$$



Flexible & Long Back Born

$$T_g = 43 \text{ }^\circ\text{C}$$

Fig. 5-21. Core structural differences between NEO-DA and HD-DA

#### 5.2.4. TMP-TA vs TMP-TMA

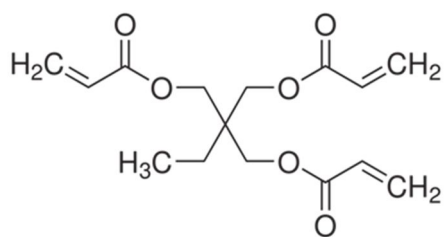
Similarly, the evaluation result of the TMP series with the Tri functional structure shows higher rating on the shrinkage of the TMP-TA. However, unlike the previous di functional system, it was evaluated that the shrinkage rate is slow and the reaction can last longer.

In the photo-DSC Evaluation, the reactivity of TMP-TMA is showing a difference from those leading methacrylate. Completion of the reaction is relatively fast and response speed is high due to high functional density and low mobility of the tri function structure. The difference in reaction rate between TMP-TA, and TMP-TMA is smaller than the previous system, and this difference is evaluated because TMP-TA terminates relatively quickly on continuous reaction by having trap structure.

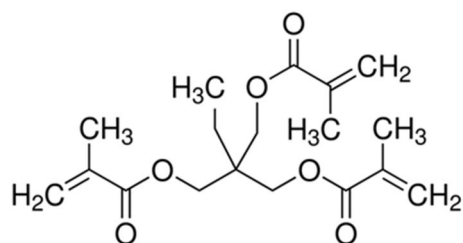
Figure 5-26 shows the results of comparing the graph of four series of shrinkage and total exothermic energy. Results have similar structure in all in four series. By the shrinkage evaluation, the total exothermic energy (= Conversion of the material) of the material can be predicted, and, on the other hand, and the form of the shrinkage was indirectly predicted by the

photo-DSC evaluation.

Depending on the type of material, there are cases when each evaluation is not as credible. Depending on the viscosity and stickiness, each experimental scheme receives a constraint. And, this method is expected to be used as a countermeasure within these situations. Not only it can correspond to a more accurate analysis techniques over the complementary system, but also it is possible to expand to evaluate a variety of materials.



(a)



(b)

Fig. 5-22. Molecular structure of (a) TMP-TA (b) TMP-TMA

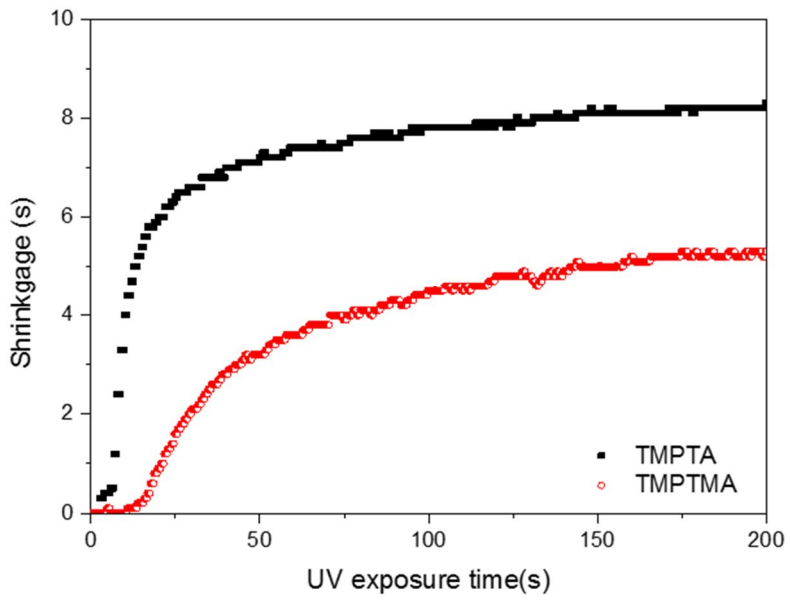


Fig. 5-23. Shrinkage of tri-acrylate TMP-TA and TMP-TMA

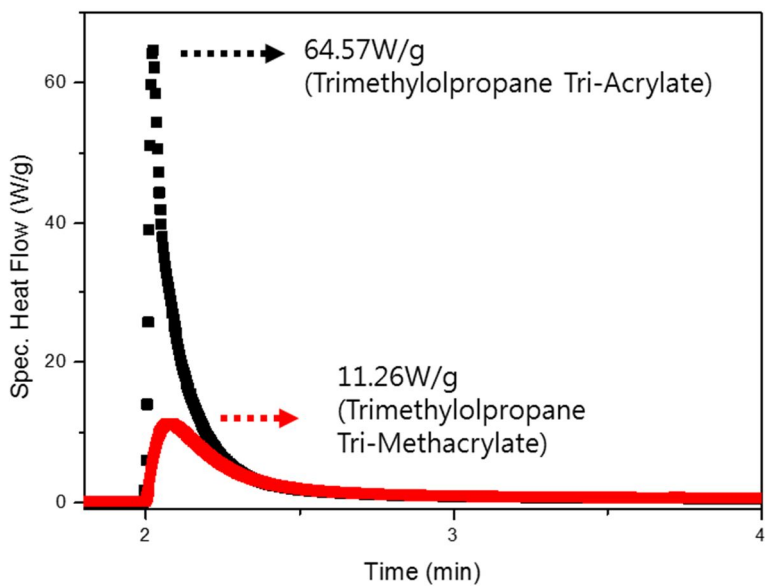


Fig. 5-24. Heat flows of TMP-TA and TMP-TMA

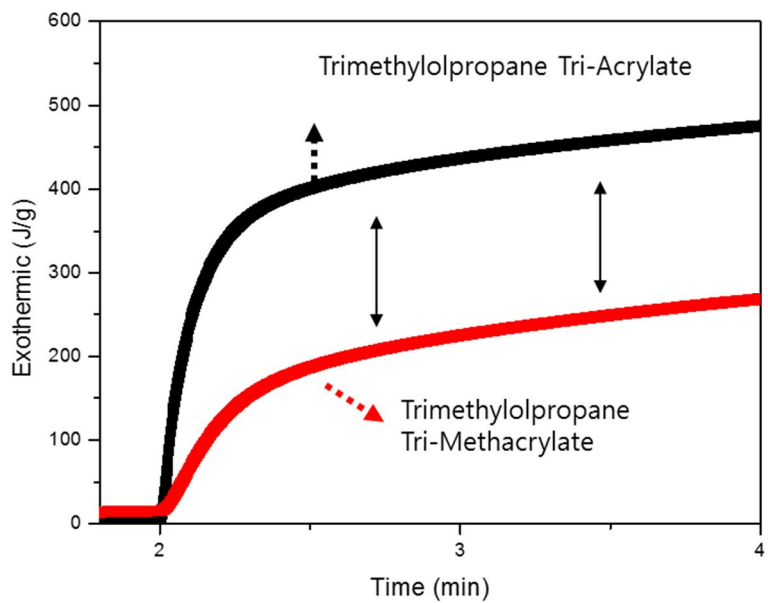


Fig. 5-25. Exothermic areas (total heat dissipation) of TMP-TA and TMP-TMA

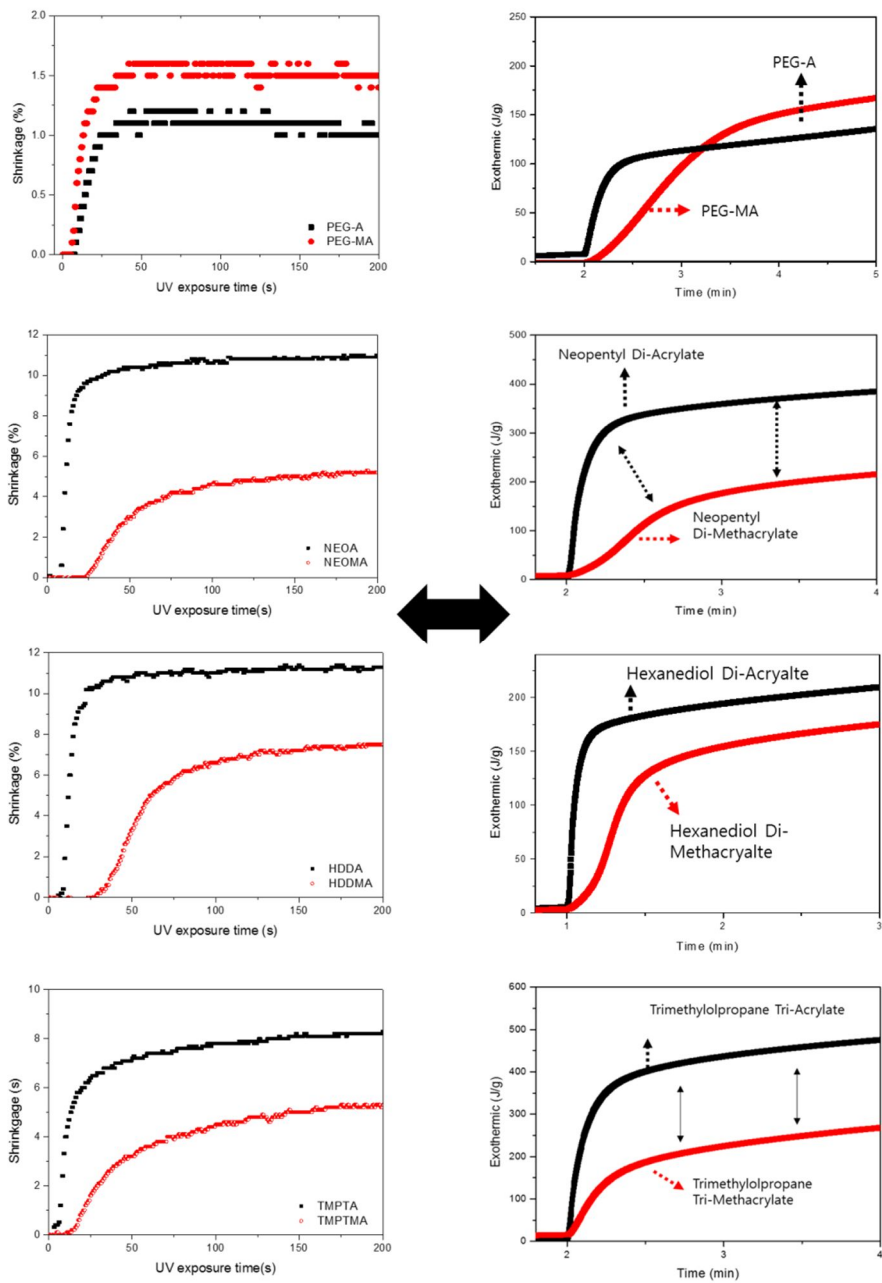


Fig. 5-26. Comparison of the shrinkage evaluation and photo-DSC evaluation results

### 5.3. Shrinkage of the different size in the molecule

We above examined the variation of shrinkage depending on the differences in the number of functional groups and its molecular structure. The number of functional groups and molecular size had no linear effect on shrinkage in certain condition as different from those generally known.

The structural properties of materials affected the mobility of overall materials and density of the functional group structure of the material, and accordingly, the entire reactivity of the material would change.

In order to evaluate the variation of shrinkage according to the structural differences in more detail, the other four kinds of materials were selected with the same molecular weight but partially different structures. These four materials all have a di-functional structure, and each of two molecules between them has the same molecular weight. However, they are isomers, each other due to the differences in core structures

Two series of core structures, 1,3-butanediol and 1,4-butanediol groups, which are isomers in diol groups, are identical in molecular composition but greatly different in physical properties. In particular, their melting point and

boiling point, which are affected by factors such as the packing of materials, is different greatly as  $-50^{\circ}\text{C}/204^{\circ}\text{C}$  and  $20^{\circ}\text{C}/235^{\circ}\text{C}$  respectively. In addition, the differences in core structures affect the structure of di-acrylate.

As confirmed in the results of shrinkage test, acrylate structure had a higher shrinkage and its reaction rate was also faster compared to methacrylate structure in both two series. In addition, delay time generated constantly. These results are consistent with them of the previous test.

In the comparison between 13B-DA and 14B-DA with the same molecular weight, the shrinkage and rate all in the 14B-DA were measured higher and faster relatively than them in 13B-DA. These trends were identical in the comparison between 13B-DMA and 14B-DMA.

However, the trends in the Photo-DSC test differed from them in the above tests. As presented in Figure 5-29, the actual reaction rate was measured to be faster in 13B series. The gap between the reaction rate and shrinkage were assessed due to the levels of packing and the effect on the mobility of molecular structure.

Theoretical molar volume of 13B-DA and 14B-DA are  $191.1\text{cm}^3$  and  $190.8\text{cm}^3$  respectively. This volumetric difference is attributed to molecular conformation change occurs despite the elements are same in the two molecules. Although the difference is not large, it is evaluated to make intermolecular binding force in the structure of 14B-DA higher (Rajasekaran, 1995).

A three-site model is used to represent local monomer structures in which the CH, and CH sites on the backbone, and the CH, and CH, sites on the side chains, are considered as hard spheres. For 200 monomer chains of various architectures. The side-chain sites are found to hinder the inter-chain approaching of backbone sites. These shielding effects are found to be reduced upon adding more backbone sites between the branches. The cohesive energy and isothermal compressibility were calculated for various monomer structures. It is found that the cohesive energy decreases with the increasing linearity of the molecular structure. The symmetry of the branching with respect to the backbone is found to play a crucial role in lowering the cohesive energy (Rajasekaran, 1995).

The difference in the binding force will initially serve to lower the reactivity. However, 14B series shrunk more than 13B series with rigid structure as

shown in figure 5-31. The higher shrinkage in 14B series is evaluated to be because 14B series has the excellent reaction continuity by the mobility in the molecular structure itself can be adopted flexible structures.

Table 5-5. Basic properties of di-acrylate monomers

Monomer	Abbreviation	Functionality number	Molecular weight (Mn)	Theoretical Shrinkage (%)
1,3-Butanediol diacrylate	13B-DA	2	198	28.73
1,3-Butanediol dimethacrylate	13B-DMA	2	226	24.85
1,4-Butanediol diacrylate	14B-DA	2	198	28.73
1,4-Butanediol dimethacrylate	14B-DMA	2	226	24.85

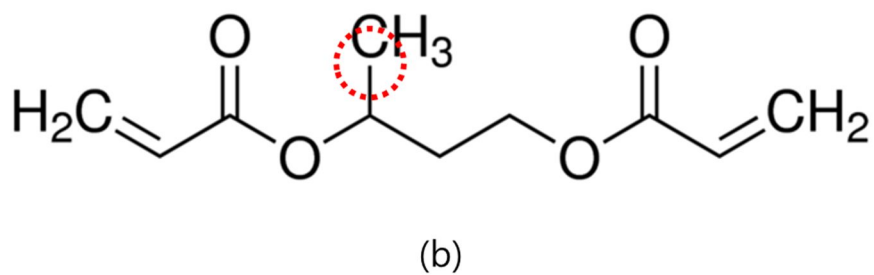
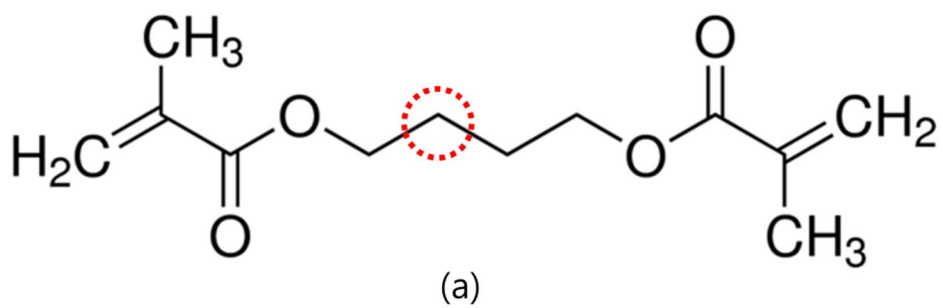


Fig. 5-27. Structural differences between the two materials (a) 1,4 butanediol structure (b) 1,3 butanediol structure

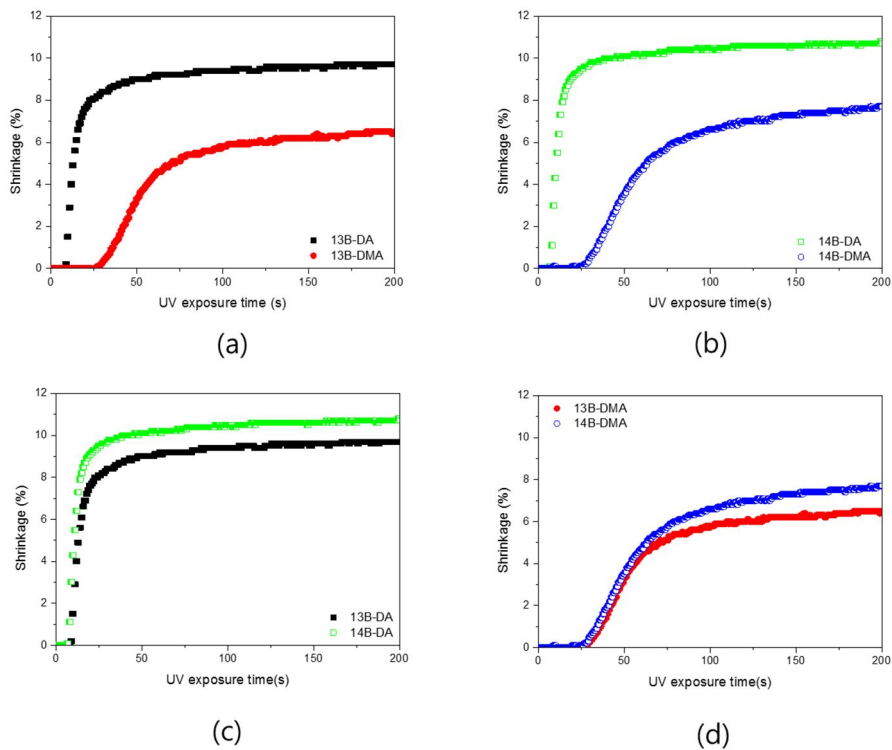


Fig. 5-28. Cross-comparison between four materials (a) 13B-DA and 13B-DMA (b) 14B-DA vs 14B-DMA (c) 13B-DA vs 14B-DA (d) 13B-DMA vs 14B-DMA

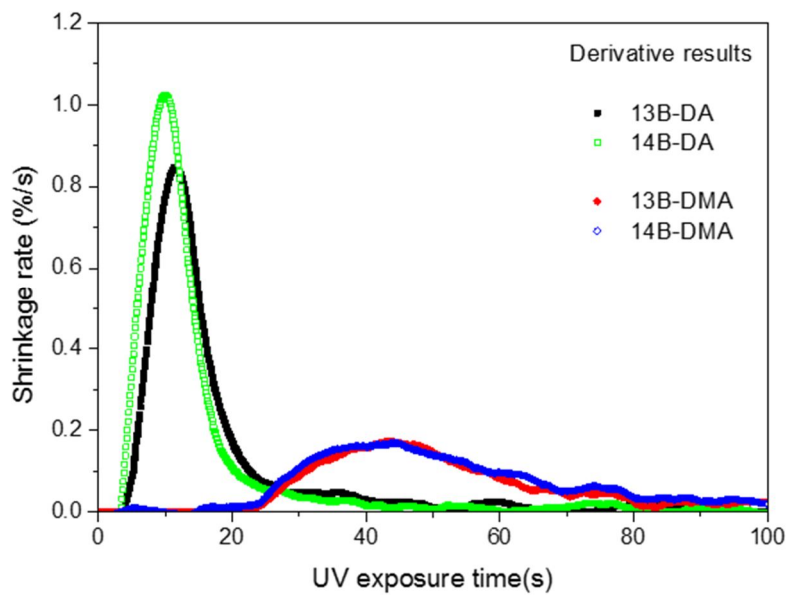


Fig. 5-29. Shrinkage rate of four materials

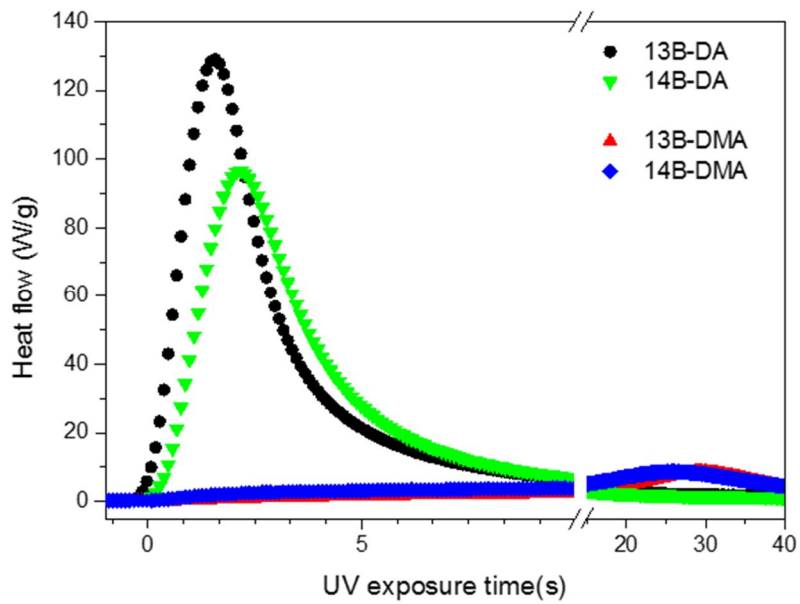


Fig. 5-30. Heat flow of di-functional system

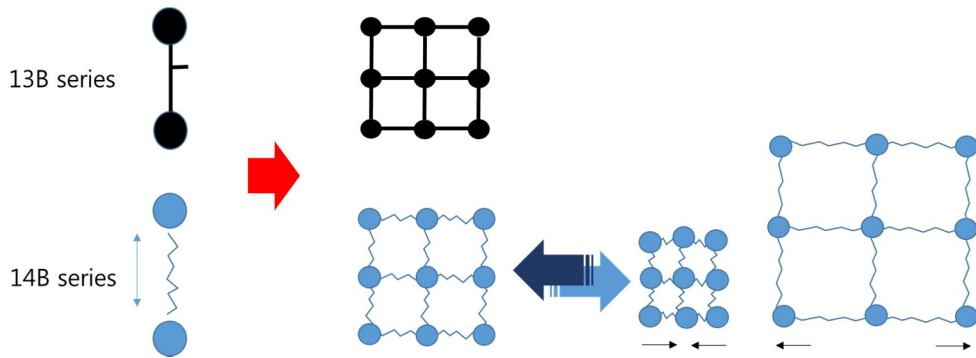


Fig. 5-31. Mobility of the cured polymer which is based on the molecular structure

# *Chapter 6*

## Evaluation of the Actual Materials

## **6. Evaluation of the Actual Material**

The UV curable materials have a variety of composition depending on the application field. As shown in Figure 6-1, UV curing system has a multi-component system structure, which consists of monomer, oligomer, photo-initiator, filler, and a wide range of additive.

The properties in shrinkage presented in the above assessment are limited to the raw material. In multi-component system, it is difficult to directly observe the changing patterns of physical properties due to the many variables. Therefore, it is important to analyze the result depending on the main parameters by simplifying each of the system as much as possible.

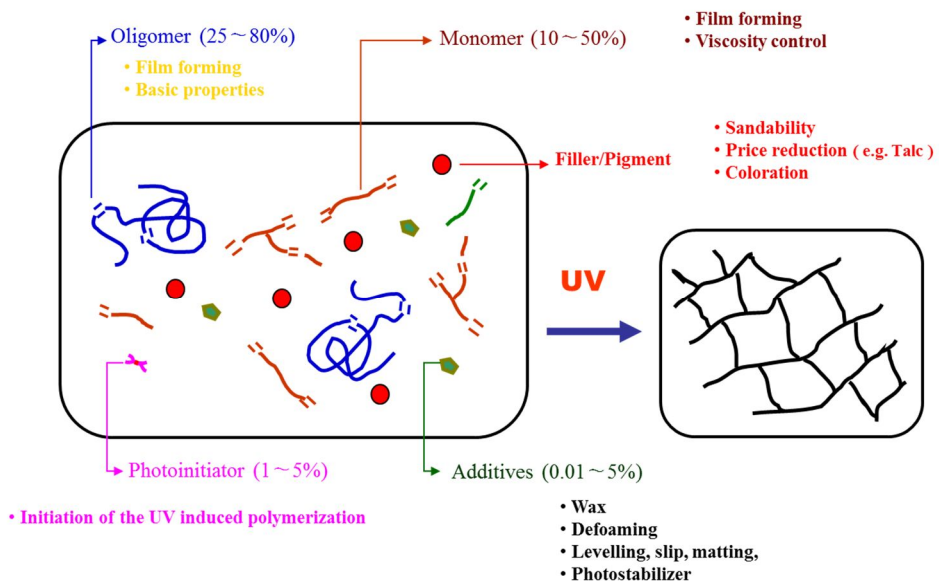


Fig. 6-1. Formulation of UV curing system (Hong, 2002)

## 6.1. Adhesives by Photo Polymerization

### 6.1.1. Preparation of UV Curable Adhesives

UV curing adhesive material prepared by the bulk polymerization has material properties as shown in [Figure 6-2](#). At a primary polymerization process, monomers and photo-initiators are added in the polymerizing bottle, and viscosity to be elevated in certain upper point using a short UV polymerization process. After an additional initiator and reactive diluents are added for the secondary curing, the curing process is progressing after the coating process on the surface of the final product or release film. Monomers used in the primary polymerization can be controlled by the adhesive properties. Reactive diluents entering the secondary curing will be largely influenced on the curing properties (Do, 2006).

2-Ethylhexyl acrylate (2-EHA), isobornyl acrylate (IBA) and N-vinyl caprolactam (VC) were used as monomers without purification. Hydroxydimethyl acetophenone (HP-8) was used as photoinitiator. The content of the entire material, 2-EHA: IBA: NVC = 60: 35: 5 (weight fraction) are applied, the photoinitiator only total monomer ratio 1 part per

one hundred resin (phr) was administered.

The polymerization was performed in a 500 ml four-necked round-bottomed flask equipped with a mechanical stirrer, N<sub>2</sub> inlet, thermometer and LED UV lamp as shown in Figure 6-3. The temperature will be maintained at room temperature with constant stirring with 100 rpm. After N<sub>2</sub> purging for 30 min with constant stirring, Monomer mixtures were subsequently exposed to UV lamp (20 mW/cm<sup>2</sup>) for 70 Sec at room temperature under N<sub>2</sub> purging. The conversion rate of the primary polymerized polymer was measured levels of around 20%. A primary polymerized material called "pre-polymer".

Poly (ethylene glycol) dimethacrylate (PEGDMA) was used as a reactive diluent for the secondary curing process. PEGDMA are distinguished in various grades depending on the size of the intermediate molecule. The grade, according to the size of the molecules, is applied to the experiment by dividing each 100, 200, 400, and 1000. HP-8 was used as a photo initiator; similarly, the content of photo initiator was applied 1 phr.

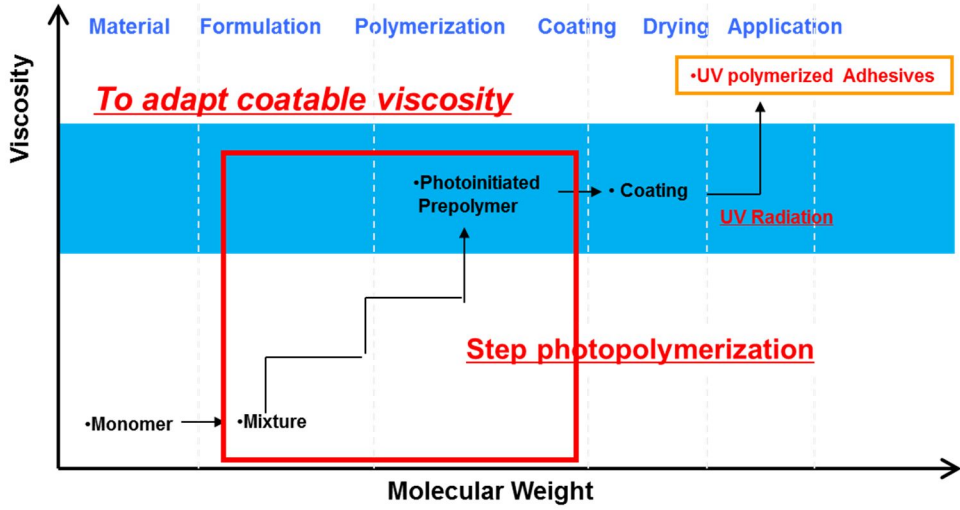


Fig. 6-2. Status of UV polymerized adhesives during the polymerization process

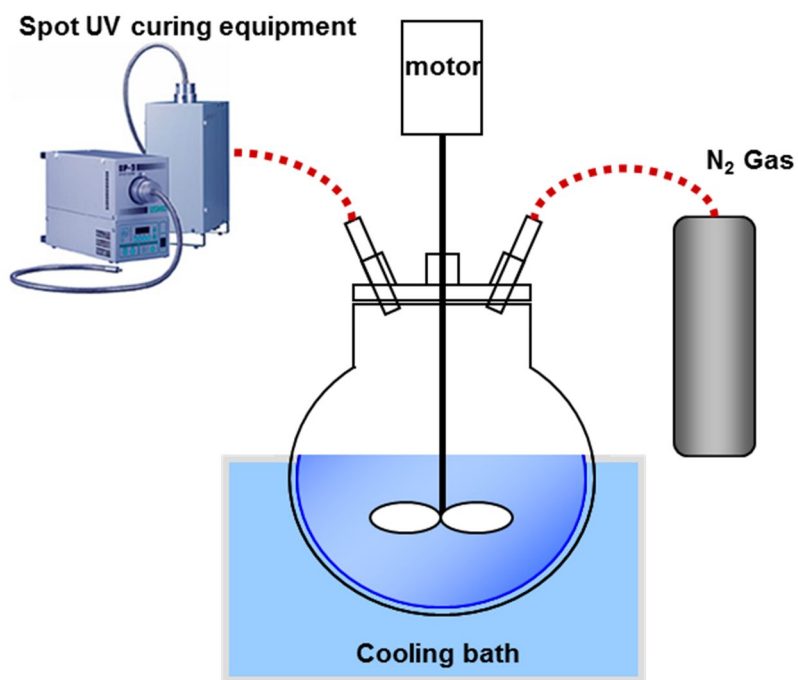


Fig. 6-3. Equipment of UV polymerization process

### 6.1.2. UV Curing Behavior with Photo-DSC

Experimental results of the photo-DSC are as in Figure 6-4. First, looking at the maximum heat, it becomes lower as the content of PEGDMA increases. As the molecular weight of the PEG unit increases its lower width is showing a tendency to decrease. In general, the height of the chart in photo-DSC means the instantaneous reaction rate. When evaluating the materials with the same structure, the lower the molecular weight, the larger the number of functional groups. In addition, methacrylate structure has a less reaction compared to acrylate structure.

Figure 6-5 shows the peak height of UV curable adhesives. Since the content of the diluent is formed by a methacrylate structure than in pre-polymer that has an acrylate structure, methacrylate ratios are increased with concentration of PEGDMA in the UV curable adhesive. Therefore, the changing of the ratios reduces the heat flow. However, the peak is showing some increasing tendency of the content of the diluent to a very low point (0.5 phr). These increase the peak. It can be viewed as if the role of the PEGDMA is cross-linking agent with a small amount of content. The PEGDMA takes a role to accelerate the chain reaction of the mono acrylate-

based pre-polymer as shown in Figure 6-6.

According to Ackem [1996], the actual conversion rate does not reach the theoretical conversion rates when curing is considerably progressed. Park [2013] explained that caging of material causes this phenomenon. It is possible to interpret the results in this system with similar direction. That is, diluent island is aggregated formed by increasing the ratio of diluent. And, the diluent caged zone is formed. In addition, pre-polymer are dispersed and acrylate population is decreased. Especially, cause of caged zone has been described a variety of reasons. According to Park [2012], polymer growth is rather partially proceeding than it is. A part of the grown zone at early stage taken as  $T_g$  increases, it causes a reducing of mobility in the molecules. Since the number of the functional groups decreases with increasing the PEG unit, more reduction of reactions is expected. But the actual reduction rate is not large. The reason is that PEG unit becomes more flexible when the longer molecular structure. Thereby, as described above, the  $T_g$  problem in reaction growth is reduced, as well (Garoushia, 2008).

Time to reach maximum heat flow is shown in Figure 6-7. Reaching time is showing a slow tendency with the content increases and the size of the PEG unit decreases. Peak time means the speed of growth, and can be utilized as

an indicator of how fast the chain reaction in a material reaction that was initiated by UV. Since the structure of the diluent is methacrylate, the reaction rate is slow when compared to the pre-polymer. The reactive gap between acrylate and methacrylate is large at almost cases of UV curing system.

When the PEG unit becomes smaller, the proportion of functional groups of methacrylate structure increases greatly. Therefore, the more methacrylate structure, functional groups, the lower the molecular weight. The molecular weight of each PEGDMA of PEG unit 100, 200, 400 and 1000 corresponds to about 300, 400, 600 and 1200. The methacrylate rate with the material pre-polymer was calculated based on these molecular weights. Most proportion case - PEG unit 100 / 10 phr - state have set the reference point 1, and the opponent for each rate are calculated. And then, a peak time at each relative value are displayed in the figure 6-8.

The results show of linearly increased tendency with the increase in the proportion of methacrylate structure. Correlation between the time and the ratio of methacrylate structure are analyzed by linear regression analysis of the model below, it can be seen that to a very high level of correlation. The  $R^2$  is 0.966. Consequently, the delay effect of methacrylate structure in UV

curing reaction is indicated highly linear in representation. Thus, it is expected that the material can be controlled based on such characteristics by selecting the acrylate and methacrylate because it can control the reaction rate,

$$y = \beta_0 + \beta_1x_1 + \beta_2x_2 \dots + \beta_px_p \quad (\text{Eq 6-1})$$

Based on the results of the photo-DSC, exothermic areas are calculated (figure 6-9). As the size of the PEG unit is small, the width of the change is large. The exothermic area was evaluated to be larger than the neat at all results. At the initial points that have a small amount of PEGDMA, the width of the exothermic area is highest. These increases the exothermic area is evaluated for the role of cross-linking agent of PEGDMA previously described.

The reaction rate of methacrylate structure is slow, however, it contains molecules inducing the overall reaction by performing the bridge in the middle. When the size of the PEG unit is small, it is the same as using a relatively large number of cross-linking agent because it contains a correspondingly relatively more molecules. As the content increases, the

increments have tended to decrease. And, the phenomenon is evaluated as the referred to above case for the internal structure of the molecules when diluent in a higher ratio.

On the other hand, in the case of the larger size of the structure of the PEG unit, the width of increasing is small, and the changing width is small, as well. The reactivity difference in accordance with the size of these molecules can be assessed in a hybrid effect of different sizes of the material that is generated coexist together in the molecular structure. When curing the other of the two materials together that has a different molecular size, shrinkage and reactivity are increased. The presence of small molecules between the large molecules, the structure is able to perform a role to accelerate the overall cure (Park, 2012).

As shown in Figure 6-10, in the use of PEG100, the heat flow structure appeared different from that of the traditional photo-DSC on the initial curing process as the content of PEG100 was up. The initial curing features are drawn in Figure 6-11. If the concentration of PEG was 10 phr, the tendency that the initial peak appears, the flat flow forms, and then the value increases toward the peak is confirmed. Figure 6-12, which analyzed the rate change, shows that plus double peak (the maximum point of the rate change)

appears distinctly as the content of PEG increases

The characteristics in curing process would be because PEG and UV curing resin are gradually separated and express their curing properties independently as the content of PEG increases. Thus, PEG evenly disperses inside other material and generally helps the cross-linking of the resin in the initial state that a small amount of PEG was added. As the content increases, however, the two materials, participate in curing process separately. Therefore, the feature that would affect compatibility between materials should be essentially considered in material designing.

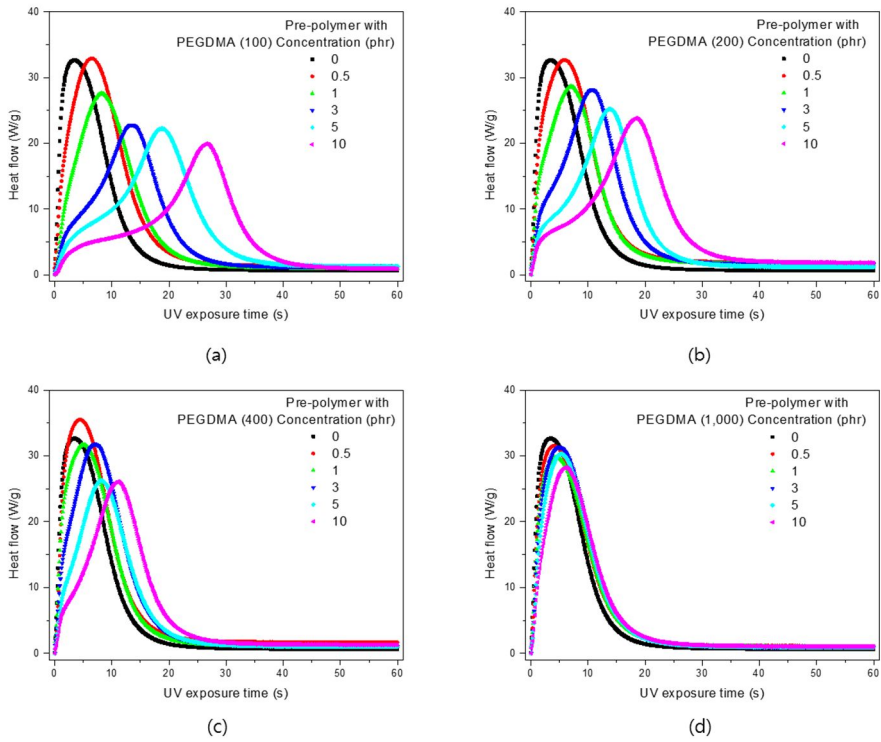


Fig. 6-4. Heat flow profiles of UV curable adhesives with PEG unit (a) 100 (b) 200 (c) 400 (d) 1000

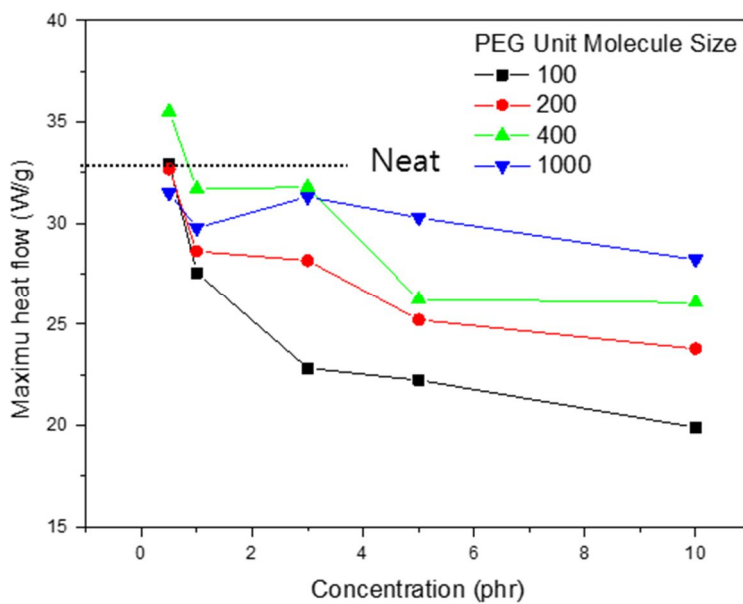


Fig. 6-5. The peak height of UV curable adhesives with PEG

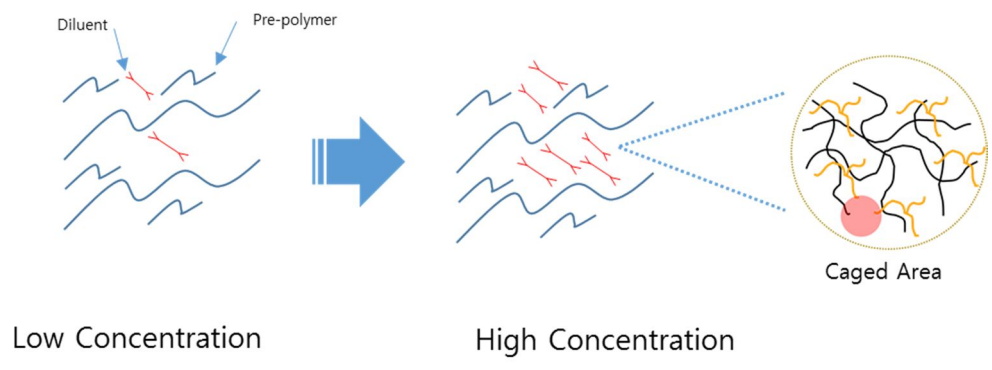


Fig. 6-6. Scheme of diluent role in the pre-polymer

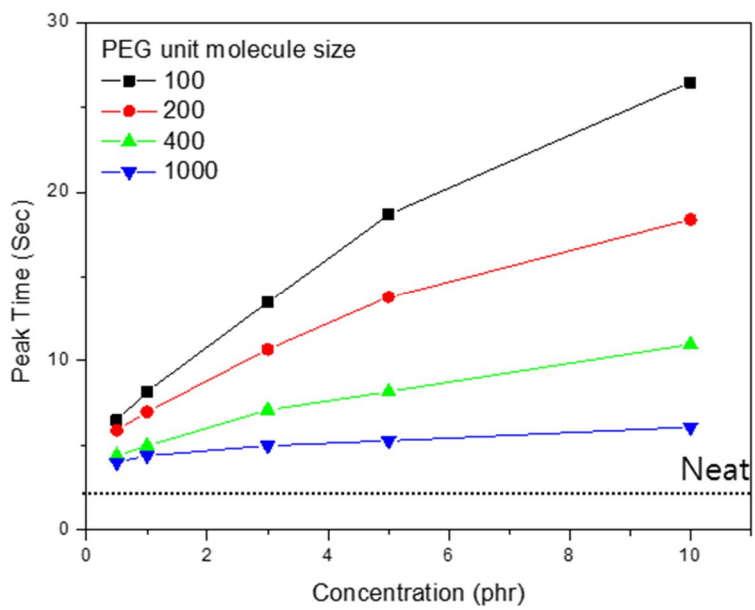


Fig. 6-7. Highest peak time of UV curable adhesives.

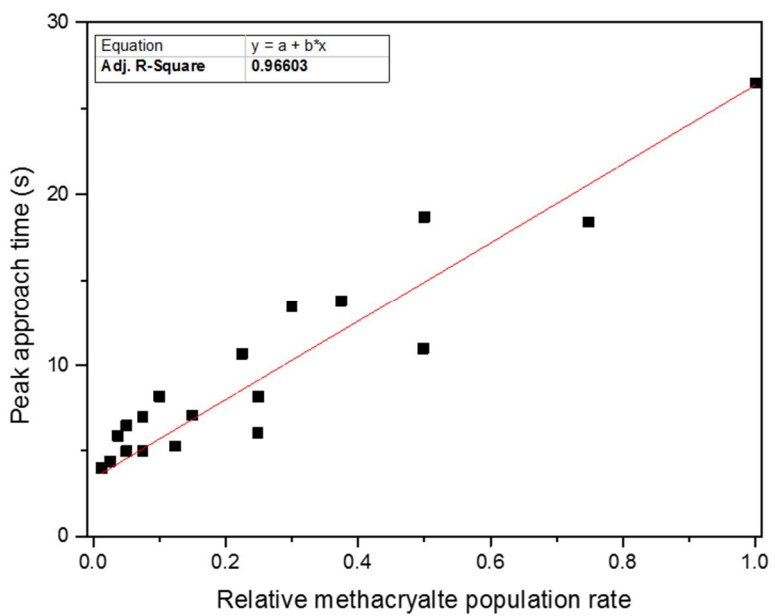


Fig. 6-8. Highest peak time versus methacrylate contents.

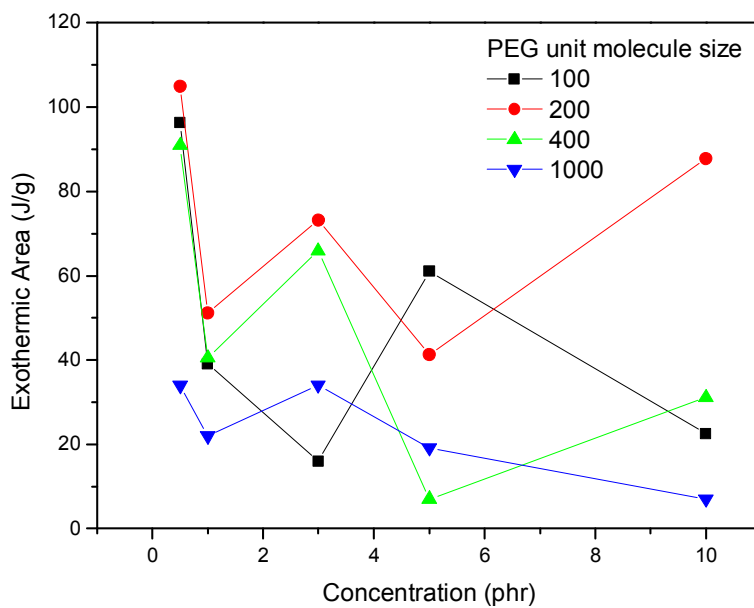


Fig. 6-9. Calculated exothermic area based on neat

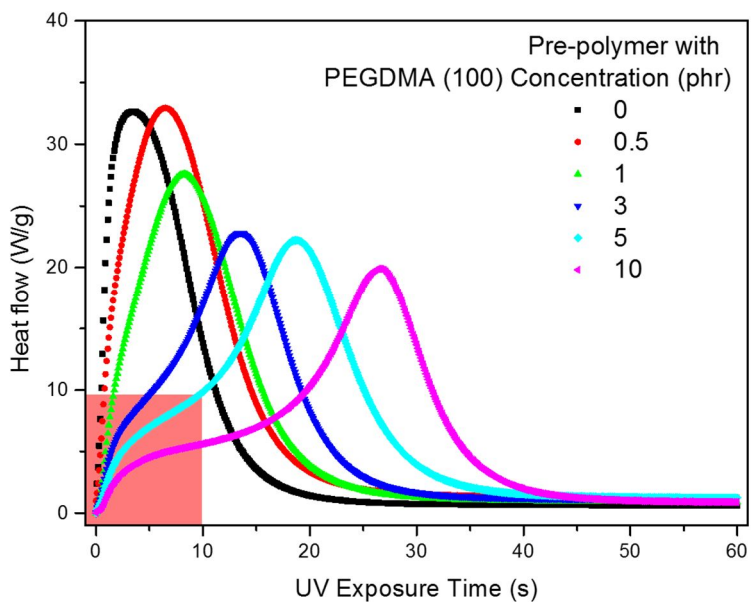


Fig. 6-10. Initial stage of heat flow profiles of UV curable adhesives

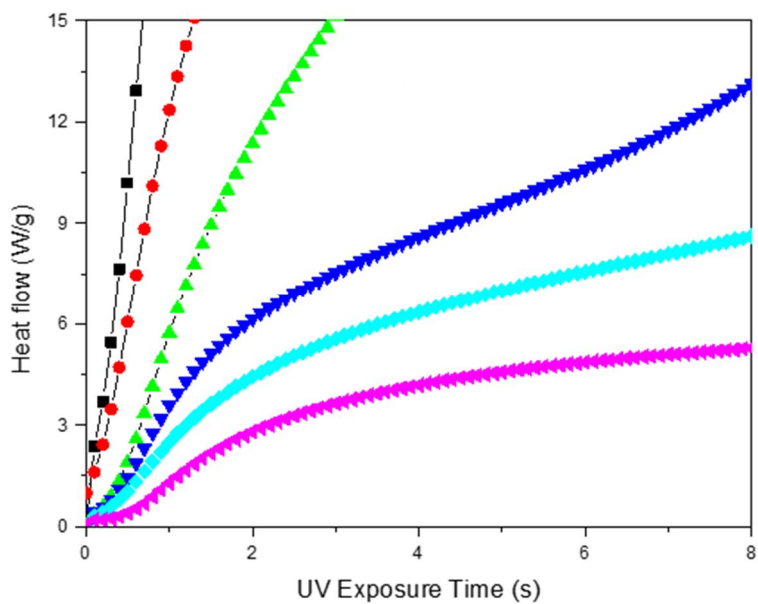


Fig. 6-11. Initial stage of UV curing of UV curable adhesives with PEG 100

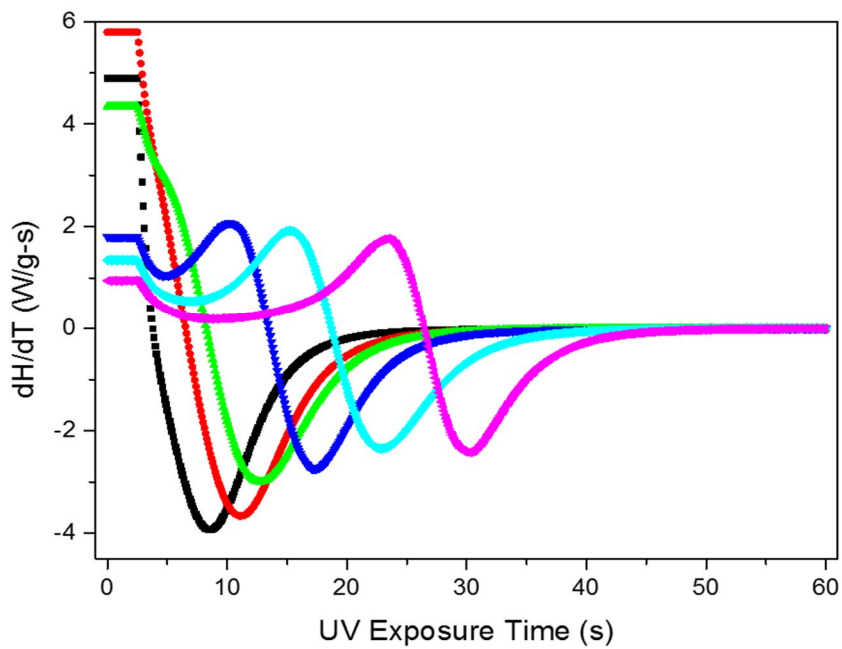


Fig. 6-12. Heat flow value change the rate of UV curable adhesives with PEG 100

### 6.1.3. Shrinkage Test

Measurements of the shrinkage test are shown in Figures 6-13 and 6-14. Shrinkage can be used as an indicator for the curing degree of whole material. Unlike evaluation with photo-DSC, shrinkage did not occur immediately when UV exposure started. This phenomenon is called as shrinkage delay effect. The structure of the entire network is formed. These measurements delay the interpreting evaluated result as well as the evaluation peak time of photo-DSC.

Additionally, the delay effect appears more remarkable because the thickness of the shrinkage specimen is larger than that of photo-DSC. Delay rate of the reaction is evaluated based on the degree to reach a constant shrinkage. The results were evaluated based on the time to reach a level of 2% as shown in Figure 6-15. As approximate content increases, the approaching time also increases. In addition, the delayed rate of the small PEG unit size is larger than smaller one

Shrinkage is increased by structural behavior such as conformation when polymer is formed as larger molecule size. As shown in Figure 6-16,

shrinkage phenomena are generated remarkable even structure of a chain number of reaction proceeds in the same reaction time. By methacrylate structure exists more, the reaction rate is delayed, and shrinkage phenomenon of the entire structure is delayed, as well.

On the other hand, the final shrinkage shows a different tendency compared with the above results. It is possible to evaluate the similar results with the photo-DSC that intended to serve the cross-linking agent when the initial low concentration. However, in certain percentage or more, the shrinkage decreased. This is evaluated to be due to the combined effects. When increased molecules PEG unit size, the conformation effects are increased. But the same time the proportion of the functional group is decreased. These effects are evaluated as being the composite representation. The width of the shrinkage of common UV curable adhesive materials is known in the 2-3% level. More than 1% change from the results is a big difference. Control of these shrinkage, so that a major impact on the change in the results in the final material such as internal stress, rainbow effect and so on.

Evaluation of shrinkage is an indexical numerical value that will show the conversion rates of material. Conversion rate and reaction rate is placed on the relationship of the integration and differentiation. The exothermic area

has been calculated through integrating the developed photo-DSC, Conversely, the shrinkage rate can be calculated by differentiating the shrinkage. Figure 6-17 is a result of the differentiation of the shrinkage (shrinkage rate). Shrinkage rate means the reaction rate. It is similar to the results of the advanced photo-DSC. It can be sure that the delayed shrinkage phenomenon in accordance with the content of PEGDMA. However, the shrinkage rate is a phenomenon that occurs in the bulk structure as compared to photo-DSC, because it can receive various influences, linear relationship results were not displayed.

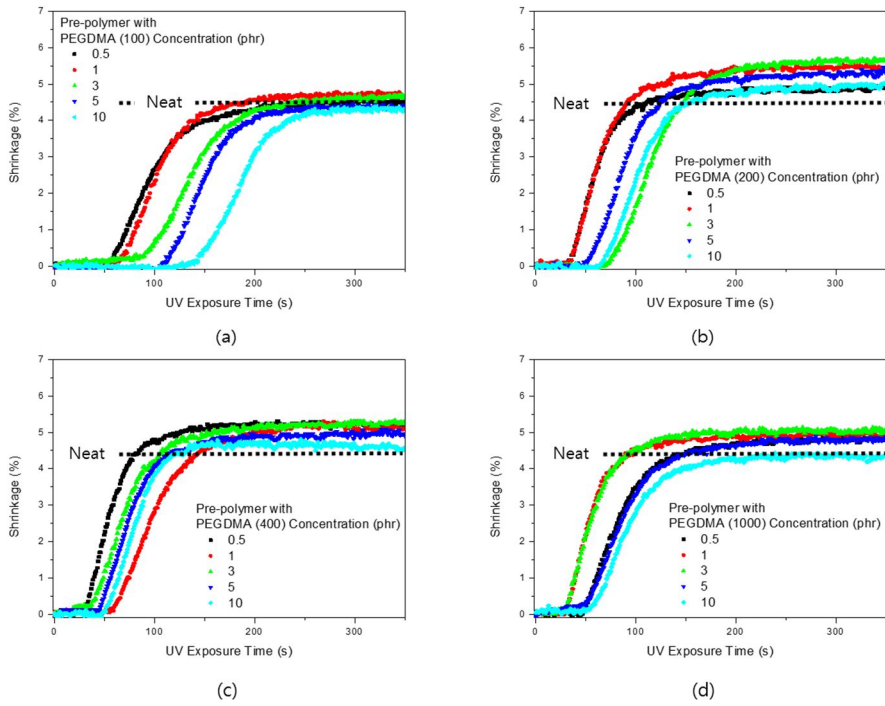


Fig. 6-13. Shrinkage of UV curable adhesives with PEG unit (a) 100 (b) 200 (c) 400 (d) 1000

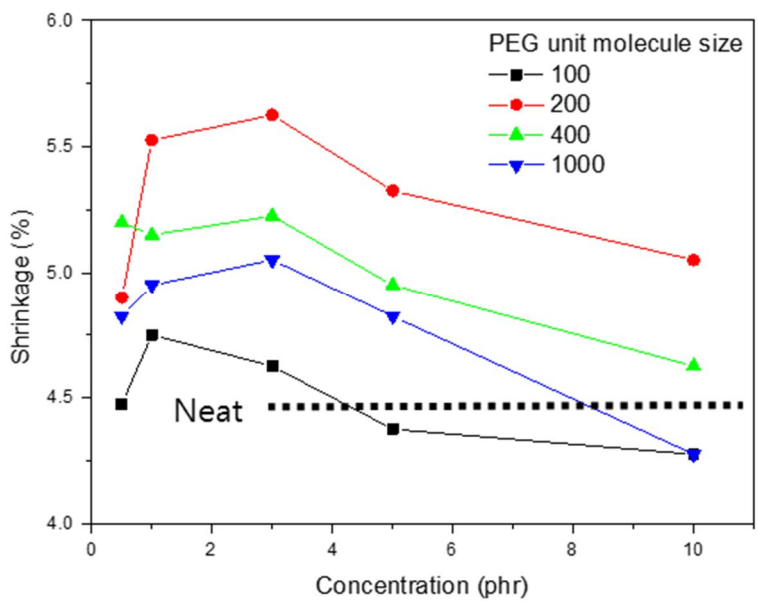


Fig. 6-14. Shrinkage of UV curable adhesives versus PEG concentration

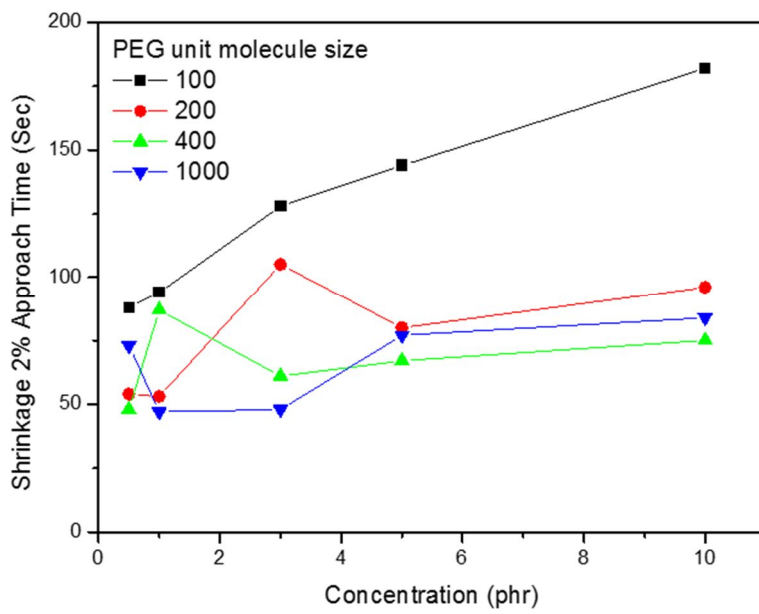


Fig. 6-15. Approach time on specific shrinkage (2%) of UV curable adhesives

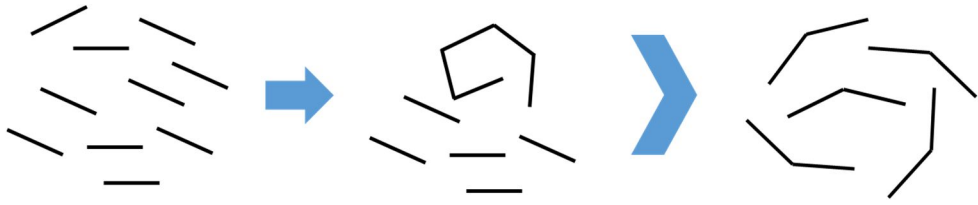


Fig. 6-16. Compare different two cases of structure by curing condition

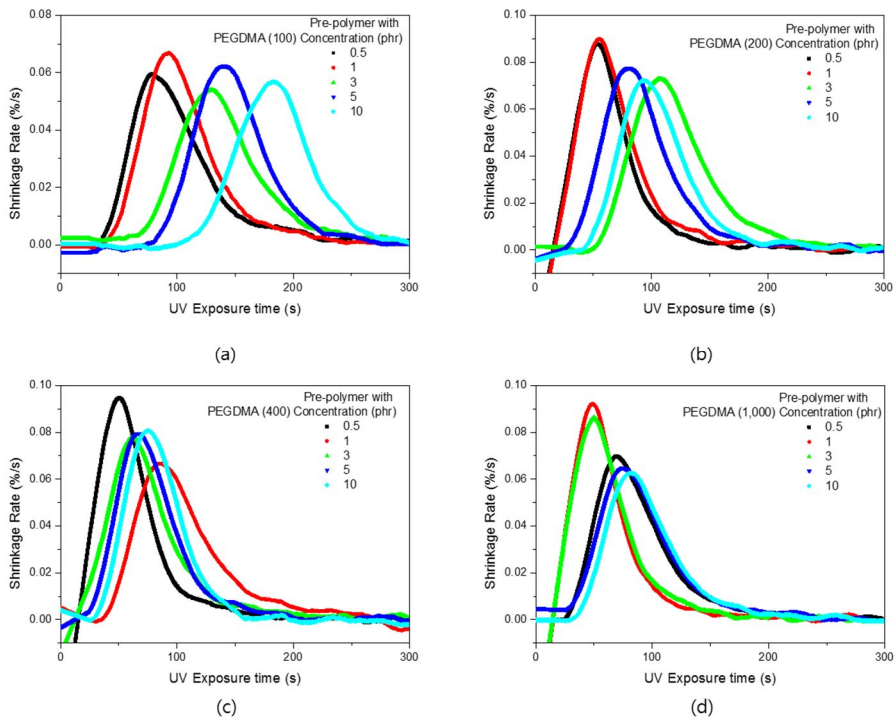


Fig. 6-17. Shrinkage rate of UV curable adhesives with PEG unit (a) 100 (b) 200 (c) 400 (d) 1000

## 6.2. UV curable Adhesives – dental adhesives

Adhesive dentistry is a branch of dentistry which deals with adhesion or bonding with the natural substance of teeth, enamel and dentin. It studies the nature and strength of adhesion of dental hard tissues, properties of adhesive materials, causes and mechanisms of failure of the bonds, clinical techniques for bonding and newer applications for bonding such as bonding to the soft tissue. There's also direct composite bonding which uses tooth-colored direct dental composites to repair various tooth damages such as cracks or gaps.

The denture adhesive is used by applying it to the face of the denture or plate which is particularly adapted to contact and mold itself to the contour of a particular oral surface in the mouth, and placing the denture in the mouth against and in contact with the oral surface.

These denture adhesive formulations provided some improvement over the traditional compositions containing only a natural gum in the powder form or a natural gum in a petrolatum carrier in the case of the cream form. However, these compositions only effectively secure the dentures in the mouth over

short periods of time. Therefore, it has generally been necessary to apply more than one application of the denture adhesive per day in order to obtain and maintain sufficient adhesion throughout the day.

Dental adhesives are intricate mixtures of ingredients. Profound knowledge of these ingredients is one key to better understanding the behavior of adhesives in studies and in clinic (Landuyt, 2007).

Dental adhesives are a visible photo-curable material that has a feature for taking advantage of the existing UV system. These visible photo-curable material consist of a mixture of different materials, the curing degree is variously changed. In the change of the curing system shrinkage forms stable structure and a fine treatment. And, this act as barriers (Lee, 2006). In addition, because a variation of the physical properties is large according to the extent of cure of the material, it is important to control the degree of cure. (Lovell, 2001) Also, fillers are contained for material stability and surface hardness. This filler gives a significant effect on the curing characteristics of the material (Bongiovanni, 2008).

To evaluate the simulation of curing systems of the visible light curable material, 1) a two-component acrylate system was designed, 2) dispersed

silica particle fillers containing system was designed.

#### 6.2.1. Blending System of Multifunctional Acrylate

This study uses TMPTA and EO6 TMPTA, which are representatively used as a multi-functional acrylate, to evaluate the blending systems. They were adopted in this study for having a characteristic of linearly changing by the shrinkage size of ethoxylated TMPTA and the photo-curing properties of molecular size.

Each of TMPTA and EO6 TMPTA prepared five kinds of composition 100:0, 75:25, 50:50, 25:75, 0:100. And, photo-DSC evaluation and shrinkage evaluation were conducted.

In the shrinkage evaluation of TMPTA and EO6 TMPTA, as with the previous results, the shrinkage of TMPTA was 9.8% and EO6TMPTA was 6.7%. The shrinkage of TMPTA was 40% higher than EO6TMPTA

However, the linear results show some results in the blending system (Figure 6-19). Assuming that the percent shrinkage is determined by the mixing ratio of the two materials

$$\begin{aligned} \text{Shrinkage ratio of binary system} & \quad (\text{Eq 6-2}) \\ & = 6.7 + 3.1 \times R_{TMPTA} \end{aligned}$$

It shows upper equation. Here  $R_{TMPTA}$  refers to the weight fraction of TMPTA. Based on the above formula, calculate the shrinkage of when 25%, 50%, and 75% gives 7.48, 8.25 and 9.03%. However, the actual shrinkage evaluation results were 7.7, 9.53 and 9.98%. Not only it is out of the linear proportional relationship, but also shows the result that goes over the maximum shrinkage at system of TMPTA 75%

The results of photo-DSC were investigated to determine whether the actual curing rate give affects. Referring to Figure 6-20, curing rate also does not change in linear. When comparable only to the results of maximum heat flow in Figure 6-21, it shows the fastest curing rate at 50% of mixing conditions.

It is correct that EO6 TMPTA has relatively high shrinkage while the absolute reaction rate is never higher. The difference in the shrinkage and the reaction rate can be evaluated as an effect of the nano-porous. As represented in Figure 6-22, it can maximize the reactivity while small molecules are located between the large molecules. In particular, the input of energy is extremely important to ensure liquidity and the density of acrylate in a small structure; it was evaluated that these effects should be maximized. The low mobility TMPTA carries can be overcome by high energy.

To investigate these effects, the UV curing behavior was investigated by varying the UV intensity. Referring to Figure 6-23, the form of the graph is changing as UV intensity is increasing. Specifically, confirmation can be made for the reactivity of the TMPTA to increase sharply. In particular, as a final result, the shrinkage and responsiveness can be confirmed a significant importance to search on the condition that the material cures.

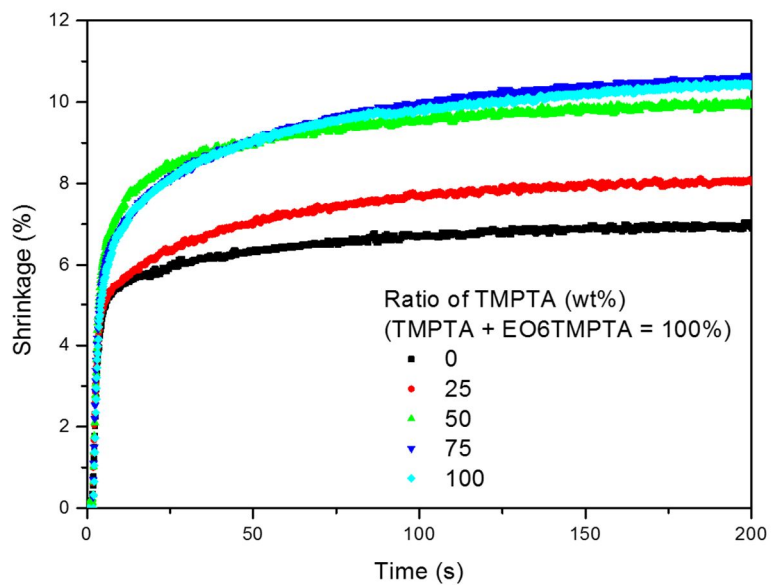


Fig. 6-18. Shrinkage of binary monomer system

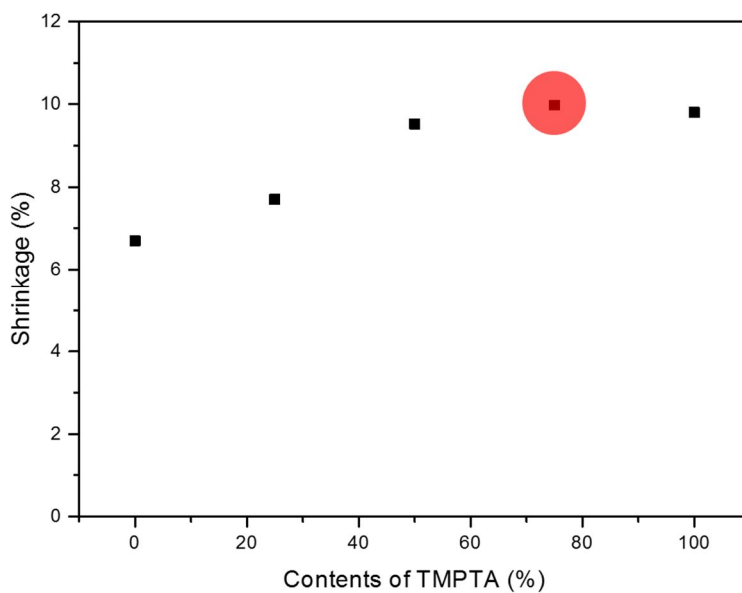


Fig. 6-19. Maximum shrinkage of binary monomer system

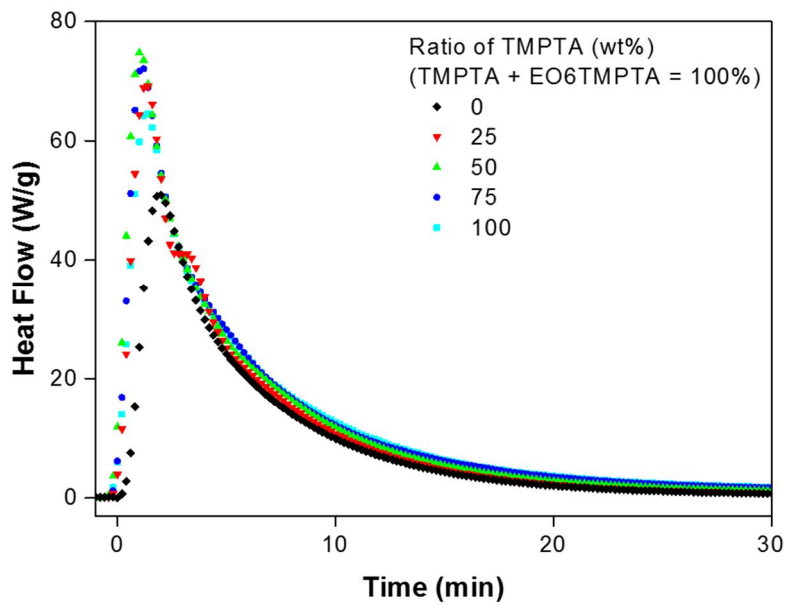


Fig. 6-20. Heat flow of binary monomer system

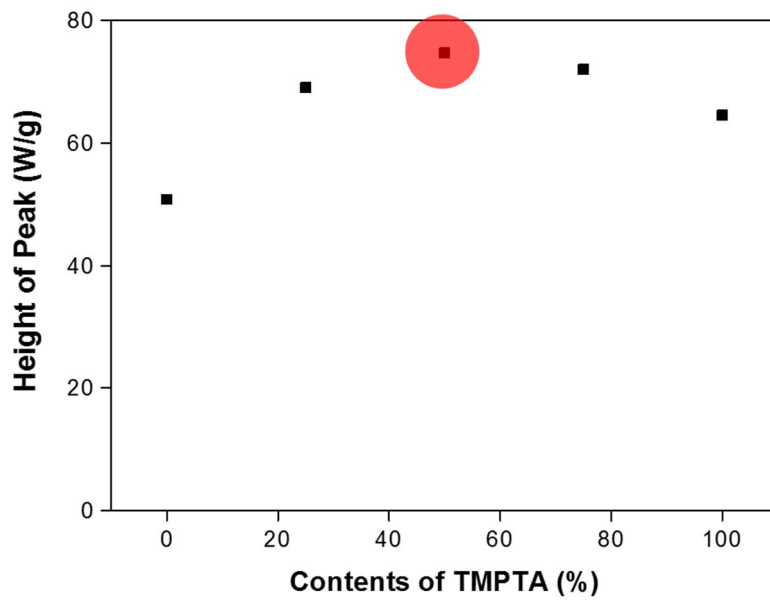


Fig. 6-21. Maximum heat flow of binary monomer system.

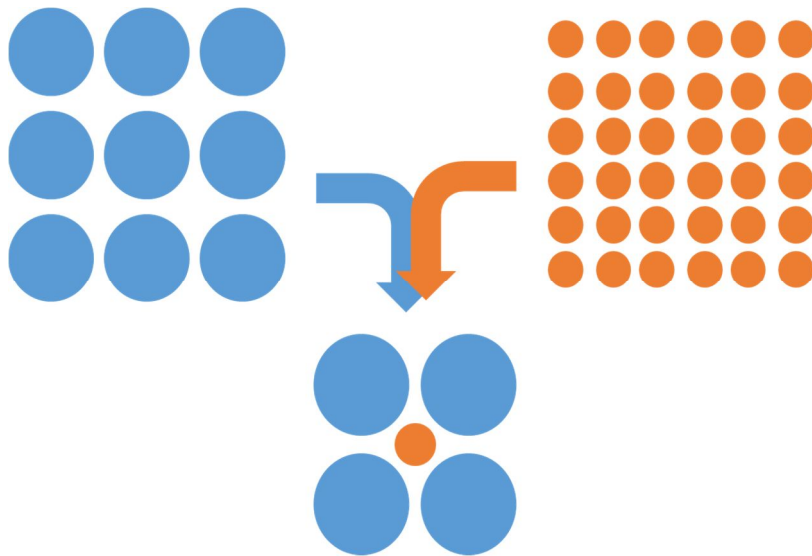


Fig. 6-22. Scheme of nano-porous effect of binary monomer system.

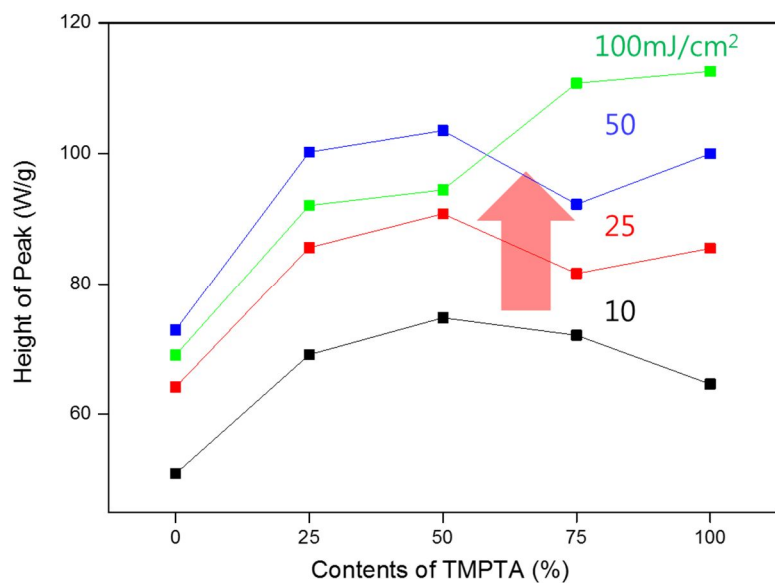


Fig. 6-23 Heat flow of binary monomer system are accordance with UV intensity

### 6.2.2. Filler Contained Acrylate System

Fillers exist in a variety of systems such as organic, biological, biomimetic, and polymeric materials (Ahmad, 1998). In the latter instance, the fillers are intentionally added. In polymer systems, fillers not only reduce the cost of the material, but also improve the mechanical and dynamic properties of the compounds. Silica and other types of fillers have a weaker polymer-filler interaction and are extensively used where a high degree of reinforcement is not essential (Zhang, 2001).

Composite materials that contain metal oxides and silica nanoparticles in polymeric matrices are commonly used for dental fillings as a replacement for amalgam. Strong adhesion accompanied by minimal shrinkage is essential in dental applications. Dental matrices are composed of acrylate or methacrylate-based monomers that can be photo-polymerized, chemically polymerized, or dual-cured (Dodiuk-Kenig, 2006)

Utilizing silica filler has advantages such that the curing stability of material rises and the mechanical properties enhance after curing. If the filler is contained, however, it would affect the curing properties, but also a problem

of the uncured may occur depending on the types of filler.

A method for producing nano-silica from TEOS has been introduced variously, and manufacturing nano-silica from sol-gel method and a variety of coating materials using it is expanding their application recently. However, nano-silica filler needs to be improved because nano-silica with the untreated surface it's difficult to be dispersed and its physical properties change severely.

In this study, a nano-silica core multi-functional acrylate (NSC-MF acrylate) was made by replacing the surface of nano-silica with acrylate directly, a composite resin was prepared by using it, and measured the shrinkage of the prepared resin was measured the characteristics of shrinkage variation was also investigated.

The method shown in Figure 6-24 was adopted to make pure silica particles. Thus, the sol-gel method based on the TEOS was used, and the size of silica produced was fixed at 20-30 nm. Since the size of the filler has an optical effect on the resin, the nanoscale particles were prepared to minimize this problem.

Utilizing the condensation reaction, we directly attached the acrylate on the surface of the prepared pure silica. Two acrylates, 2-hydroxyethyl acrylate (2HEA) and pentaerythritol triacrylate (PETA) were used in this experiment.

The final NSC-MF acrylate was composed of 50% of nano-silica, 35% of PETA, and 15% of 2HEA by weight.

Three other acrylates of PETA, TMPTA, and BIS-GMA were selected to blend the prepared materials in a variety of environments. As NSC-MF acrylate and each of the materials were mixed by the ratio of 100:0, 80:20, 60:40, 40:60, 20:80, and 0:100, the proportion of nano-silica was designed to be 50, 40, 30, 20, 10, and 0 %, respectively.

Figure 6-26 presents the results of the evaluation for the system with PETA. Because PETA was mainly used to treat the surface of nano-silica, blending between the two materials was excellent. As mentioned above, the nanoporous effect occurs if two materials are mixed. Since NSC-MF acrylate is a very large molecular mass itself, the PETA is able to fill the space between them.

Figure 6-28 shows the variation is even greater in system with TMPTA. It

was found that the more the curing condition improved, the higher the shrinkage of TMPTA was in the previous test. The shrinkage could increase in the mixed conditions because NSC-MF acrylate enhance the mobility of TMPTA.

Whereas, the effect was very large in the system with BIS-GMA. It is because an island-bridge effect occurred, according to the structural difference between BIS-GMA and NSC-MF acrylate. NSC-MF acrylate is a very large structure and its overall mobility is very low while

BIS-GMA as the di-functional monomer with lower viscosity could improve flexibility and consistently induce the reaction between functional groups. In addition, as shown in Figure 6-30, 31, the molecular chains themselves act a role as a spring to boost the overall shrinkage as the reaction continues. The change of curing properties was assessed to be great depending on the structural characteristics of the material blended, if the filler is directly designed for the core structure and materialized.

Figures 6-32, 6-33 present the results of evaluation for the photo-DSC. First, system with PETA revealed a linear result as the same as one of shrinkage tests. There would be no significant differences in blending characteristics

because its structure is similar to the surface substitute-structure of NSC-MF acrylate. Finally, there is no phase separation between PETA and NSC MF acryalte.

Meanwhile, Figures 6-34 and 6-35 shows the result in the system with TMPTA that the curing rate became faster in the blending condition. It is considered that the nano-porous effect, according to molecular size was maximized. Since TMPTA has a high  $T_g$  and the self-inhibiting effect appears in the course of reaction, it is important to secure the molecular mobility or molecular reaction sufficiently. Thus, the application of macromolecule, NSC-MF acrylate would form the structure in which the mobility is constantly ensured and their reactivity can be maximized.

On the other hand, the reaction rate did not increase significantly in the system with BIS-GMA. As presented in Figures 6-36 and 6-37, most of the reaction rate appeared to be constant and there was no difference depending on the blending condition. Whereas, the previous assessments for shrinkage revealed the system had a great synergistic effect. Thus, it could be evaluated that the effect of the increased shrinkage of the flexible structure of BIS-GMA is greater rather than one of the increased reactivity of the nano-porous feature.

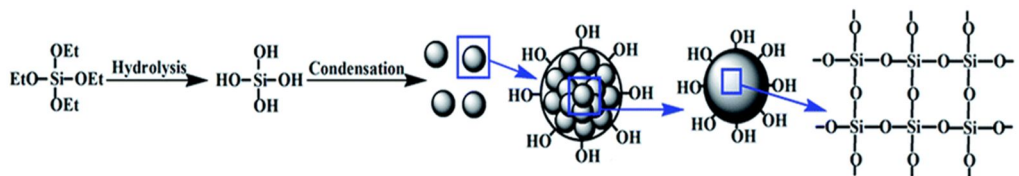


Fig. 6-24. Preparation of nano-silica with sol-gel reaction (Zhang, 2014)



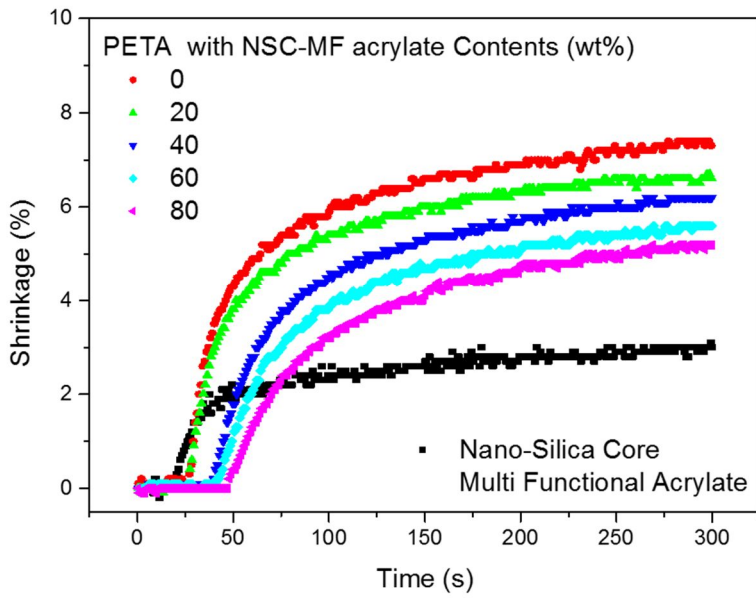


Fig. 6-26. Shrinkage of NSC-MF acrylate and PETA blending system

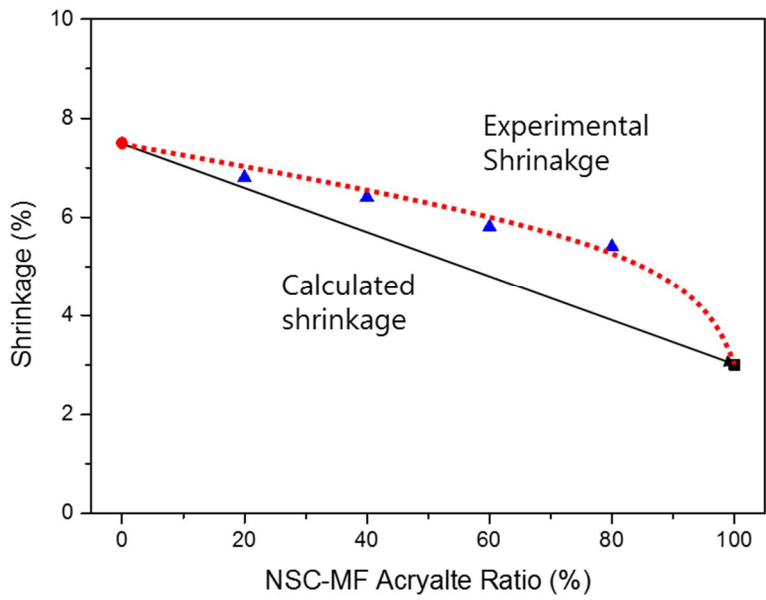


Fig. 6-27. Shrinkage of NSC-MF acrylate and PETA blending system – black straight line is calculated shrinkage, red dot line is experimental shrinkage-

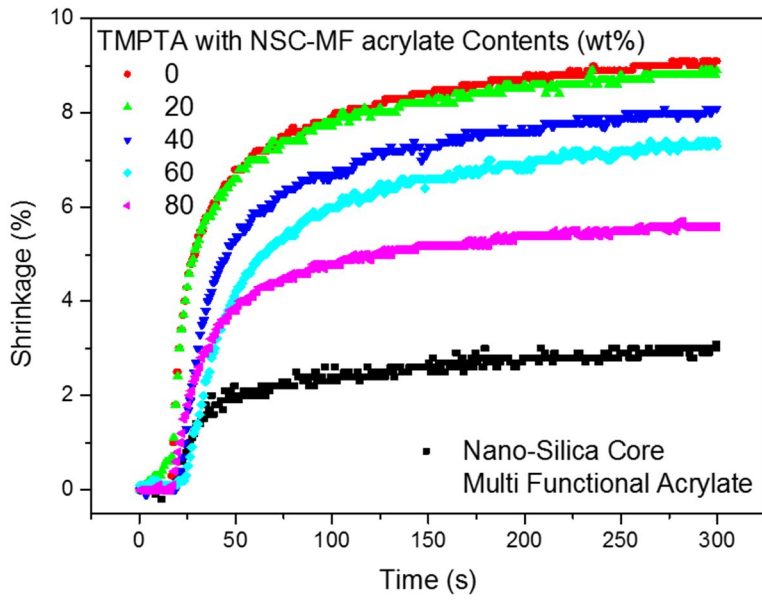


Fig. 6-28. Shrinkage of NSC-MF acrylate and TMPTA blending system

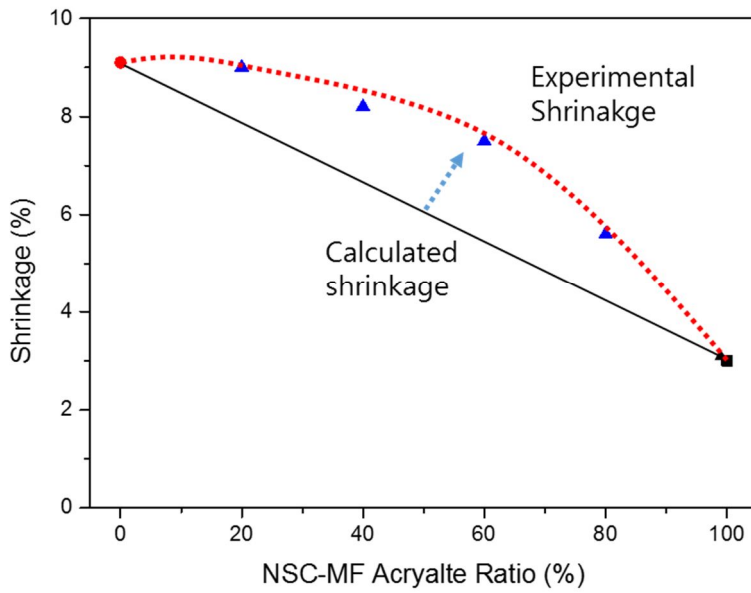


Fig. 6-29. Shrinkage of NSC-MF acrylate and TMPTA blending system – black straight line is calculated shrinkage, red dot line is experimental shrinkage-

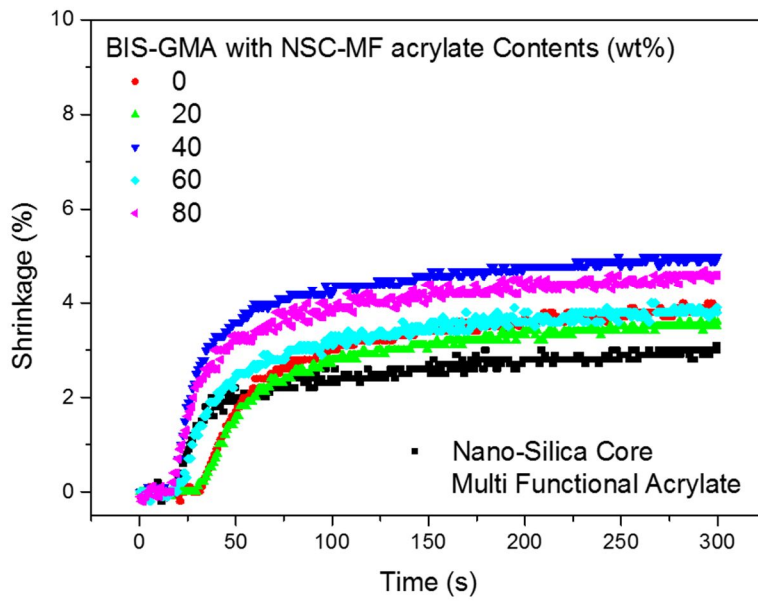


Fig. 6-30. Shrinkage of NSC-MF acrylate and BIS-GMA blending system

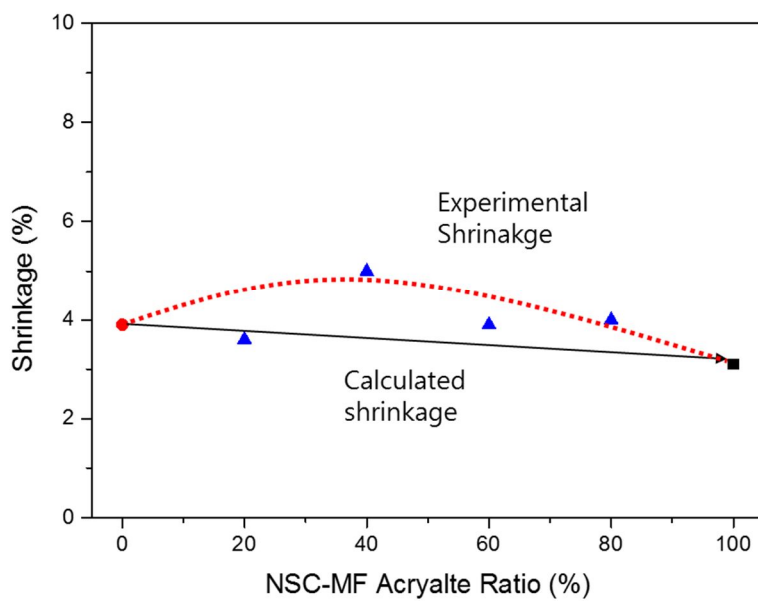


Fig. 6-31. Shrinkage of NSC-MF acrylate and BIS-GMA blending system – black straight line is calculated shrinkage, red dot line is experimental shrinkage-

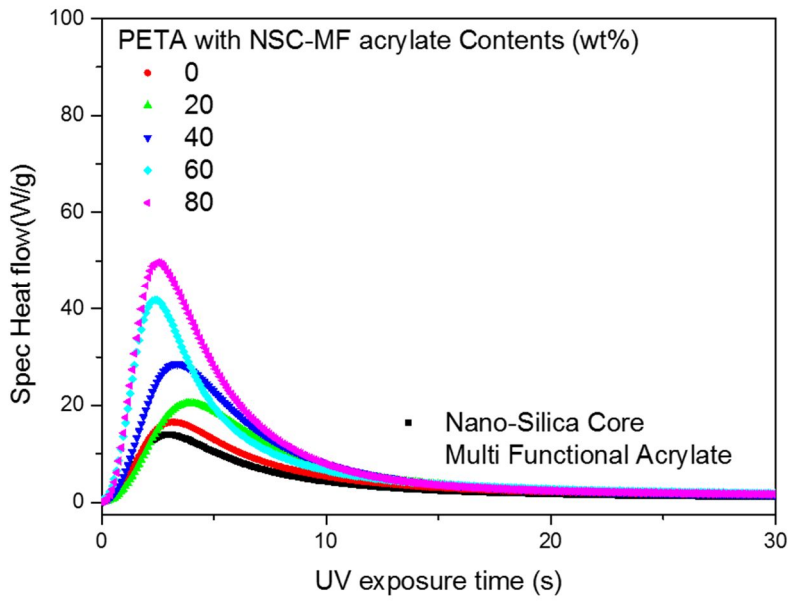


Fig. 6-32. Heat flow of NSC-MF acrylate and PETA blending system

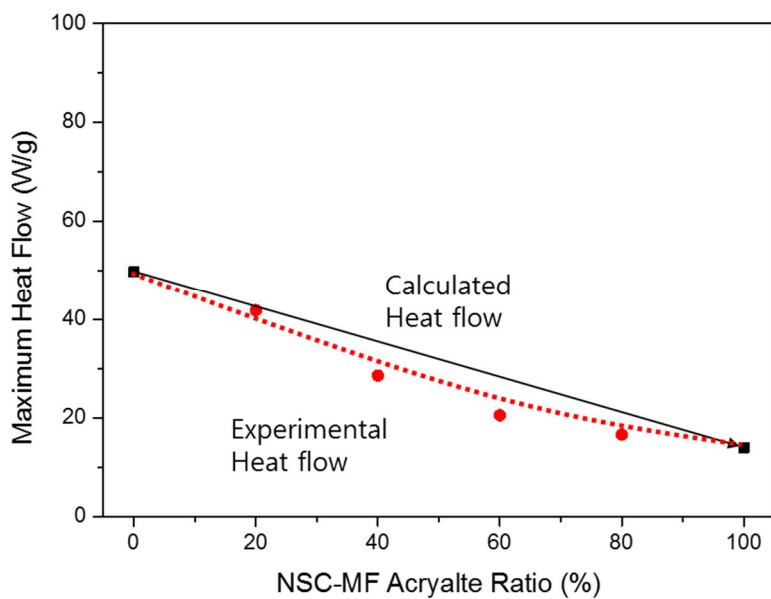


Fig. 6-33. The maximum heat flow of NSC-MF acrylate and PETA blending system – black straight line is calculated heat flow, red dot line is experimental heat flow-

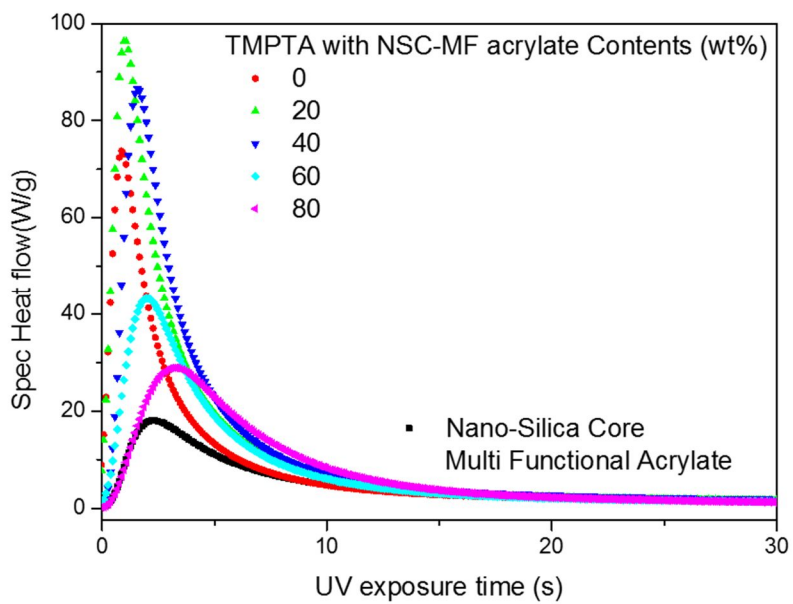


Fig. 6-34. Heat flow of NSC-MF acrylate and TMPTA blending system

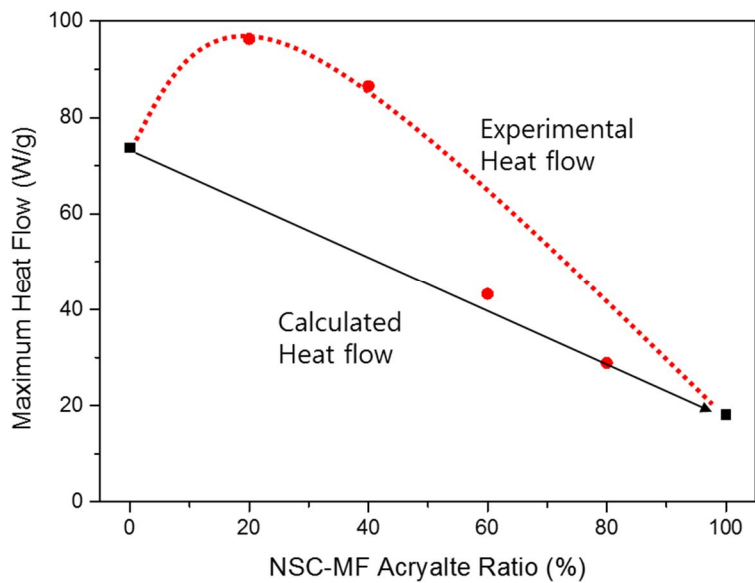


Fig. 6-35. The maximum heat flow of NSC-MF acrylate and TMPTA blending system – black straight line is calculated heat flow, red dot line is experimental heat flow-

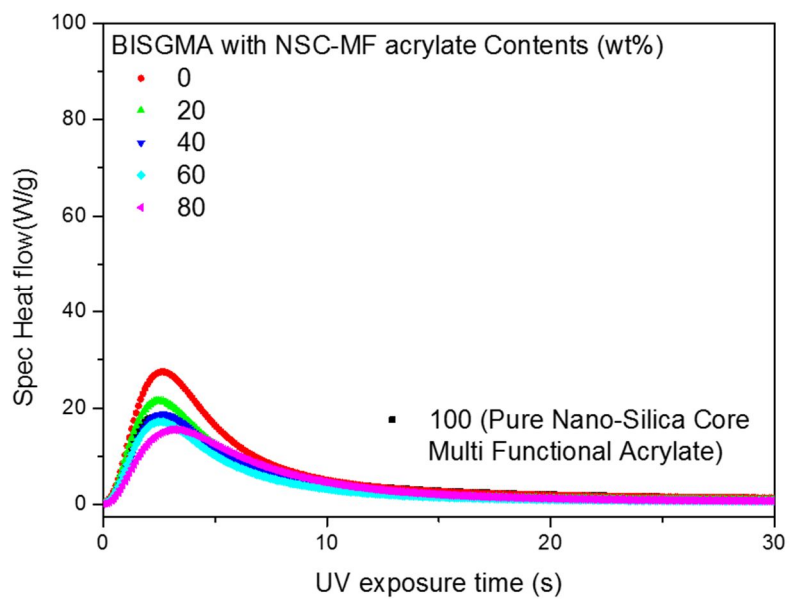


Fig. 6-36. Heat flow of NSC-MF acrylate and BIS-GMA blending system

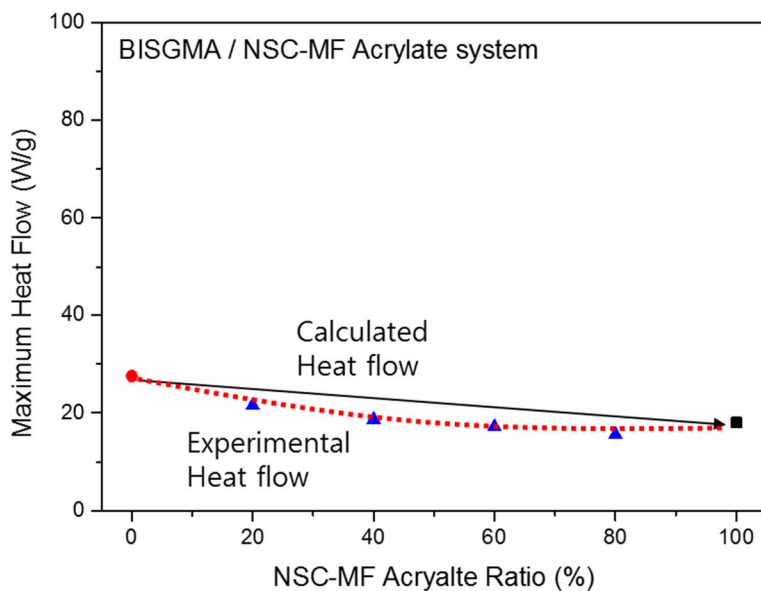


Fig. 6-37. The maximum heat flow of NSC-MF acrylate and BIS-GMA blending system – black straight line is calculated heat flow, red dot line is experimental heat flow-

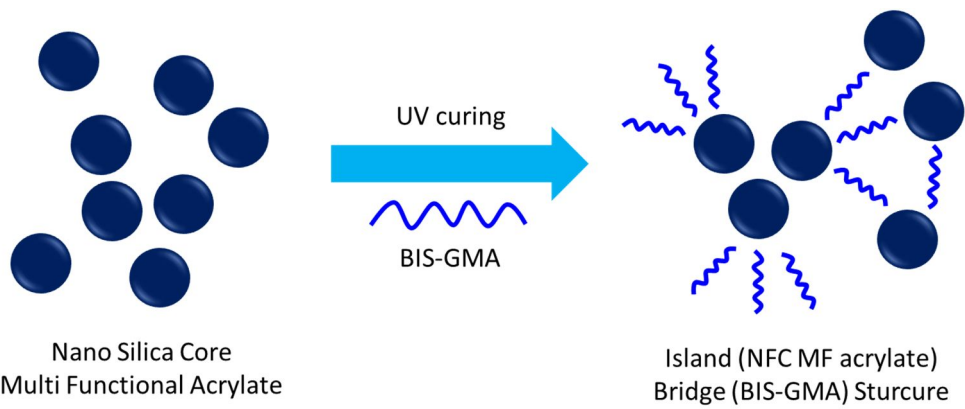


Fig. 6-38. Island/bridge structure of mixture system with NFC MF acryalte and BIS-GMA

# *Chapter 7*

## Concluding Remarks

## 7. Conclusion

There are many kinds of analysis technique for photo curing behavior. Photo-DSC is representative methods to the analysis Thermochemistry mechanism of materials. Otherwise, test methods of shrinkage are distinguishing characteristic that is analyzing the bulk properties of materials. The two systems are complementary to each other

1. In order to evaluate the shrinkage of the same material, various variables apply to the change in shrinkage.
  - A. The influence factor of sampling condition such as side curls and thickness of the specimen is changed by complexes with the unique physical properties of the material. In particular, in order to obtain a constant shrinkage, aspect ratio is must set larger to the maximum. In this study, it was set to 40 or more
  - B. Variables such as photo-initiator, UV intensity and environmental temperature of the system may be one of the experimental variables. However, to a comparison of the shrinkage of materials, the variables should be controlled.
  - C. UV intensity acts as a major factor in changing the depth profile, depending on the content of the photoinitiator. At this time, the

control of  $E_{\max}$  role as an important factor in the shrinkage evaluation. Therefore, in order shrinkage phenomenon occurs, there is a need for a long time about light intensity is weak.

D. Partial cross-linking is to proceed while the material of the curing. As a result, the partial mobility reduction phenomenon occurs. These trends are depending on the specific  $T_g$  of each material. The higher materials have  $T_g$ , the more sensitive materials are reacted. The reaction is increased to a specific temperature, thereafter, the reaction is decreased by effect of thermodynamics

2. Acrylate material has a variety of structures. The difference between these structures is a significant effect on the reactivity and shrinkage.

A. In general, the photoactive increases as the functionality number increases. However, reactivity and shrinkage of low functional materials are higher than high functional materials because higher functional materials have low mobility and trap formation occurred more.

B. Acrylate and methacrylate is known as a typical photo-curable material. Reactivity of acrylate is faster than methacrylate. Despite there is little difference of the molecular weight and the

functional group, it is found that reactivity and shrinkage differ materially.

- C. Reactivity between isomer are vary depending on the mobility difference by the core structure.
3. Adhesive with photo curable systems has the feature as a multi-component system, however, the properties of the adhesives are inferred by the simplifying materials system.
- A. An adhesive system in which the base is Photo-polymerization, it was not able to accurately investigate the characteristics of the pre-polymer. It was possible to analyze the relationship between the reactive diluents and pre-polymer and the characteristics of shrinkage that associated with the reactive diluent.
  - B. The multi-component system, without changing the curing behavior linear, showed a tendency to further increase. These trends were assessed to be due to nano-porous effect.
  - C. The photo curable systems with filler can be expected a synergistic effect due to mixing of the material. In the absence of the miscibility of materials, the photo-curing properties were evaluated that do not affect each other.

# *Reference*

**A. J. Desmarais. (1991). U.S. Patent No. 5,024,701.**

Washington, DC: U.S. Patent and Trademark Office.

**A. Nebioglu, M.D. Soucek. (2007).** Reaction kinetics and network characterization of UV-curing polyester acrylate inorganic/organic hybrids.

*European Polymer Journal*, 43(8), 3325–3336.

**A. Moeck, R. Bianchi, V. Petry, R. Weder, D. Helsby. (2014).** *Shrinkage of UV Oligomers and Monomers*. Proceeding presented at the global conference & expo for UV and EB curing technology (RADTECH) 2014, Rosemont, IL.

**A. Palanisamy, B.S. Rao. (2007).** Photo-DSC and dynamic mechanical studies on UV-curable compositions containing diacrylate of ricinoleic acid amide derived from castor oil.

*Progress in Organic Coatings*, 60(3), 161-169.

**A. Boddapati. (2010).** Modeling cure depth during photopolymerization of multifunctional acrylates (Master's degree thesis, Georgia Institute of Technology).

**B. Golaz, V. Michaud, Y. Leterrier, J. -A. E. Månson. (2012).** UV intensity, temperature and dark-curing effects in cationic photopolymerization of a

cycloaliphatic epoxy resin.

*Polymer*, 53(10), 2038-2048.

**B. Nearingburg, A.L. Elias.** (2011). Characterization of surface plasmon energy transduction in gold nanoparticle/polymer composites by photo-DSC.

*Thermochimica Acta*, 512(1-2), 247-253.

**B. S. Rao, Aruna Palanisamy.** (2008). Synthesis, photo curing and viscoelastic properties of triacrylate compositions based on ricinoleic acid amide derived from castor oil.

*Progress in Organic Coatings*, 63(4), 416-423.

**B. S. Rao, Aruna Palanisamy.** (2010). Photocuring and thermomechanical properties of multifunctional amide acrylate compositions derived from castor oil.

*Progress in Organic Coatings*, 67(1), 6-11.

**C. Alvarez-Gayosso, F. Barcelo'-Santana, J. Guerrero-Ibarra, G. Sa'ez-Esp'ınola, M.A. Canseco-Mart'ınnez.** (2004). Calculation of contraction rates due to shrinkage in light-cured composites.

*Dental Materials*, 20, 228-235.

**C. Esposito Corcione, M. Frigione, A. Maffezzoli, G. Malucelli.** (2008). Photo-DSC and real time-FT-IR kinetic study of a UV-curable epoxy resin containing o-Boehmites.  
*European Polymer Journal*, 40(7), 2010-2023.

**C. Schmidt, T. Scherzer.** (2015). Monitoring of the Shrinkage during the Photopolymerization of Acrylates Using Hyphenated Photorheometry/Near-Infrared Spectroscopy.  
*Journal of Polymer Science, Part B: Polymer Physics*, 53, 729–739.

**D. Foix, X. Ramis, A. Serra, M. Sangermano.** (2011). UV generation of a multifunctional hyperbranched thermal crosslinker to cure epoxy resins.  
*Polymer*, 52(15), 3269-3276.

**C. S. B. Ruiz, L. D. B. Machado, E. S. Pino, M. H. O Sampa.** (2002). Characterization of a clear coating cured by UV /EB radiation.  
*Radiation Physics and Chemistry*, 63(3-6), 481-483.

**C. Decker, K. Moussa.** (1990). Kinetic investigation of photopolymerizations induced by laser beams.  
*Die Makromolekulare Chemie (Makromol. Chem.)*, 191, 963-979.

**A. T. Di-Benedetto.** (1987). Prediction of the glass transition temperature of polymers: A model based on the principle of corresponding states.

*Journal of Polymer Science Part B: Polymer Physics*, 25(9), 1949–1969.

**D. S. Esen, F. Karasu, N. Arsu.** (2011). The investigation of photoinitiated polymerization of multifunctional acrylates with TX-BT by Photo-DSC and RT-FTIR.

*Progress in Organic Coatings*, 70(2-3), 102-107.

**G. Lachenal, A. Pierre, N. Poisson.** (1996). FT-NIR spectroscopy: Trends and application to the kinetic study of epoxy/triamine system.

*Micron*, 27(5), 329-334.

**G. Litwinienko, T. Kasprzycka-Guttman, M. Studzinski.** (1997). Effects of selected phenol derivatives on the autoxidation of linolenic acid investigated by DSC non-isothermal methods. *Thermochimica Acta*, 307(1), 97-106.

**H. Xu, F. Qiu, Y. Wang, W. Wu, D. Yang, Q. Guo.** (2012). UV-curable waterborne polyurethane-acrylate: preparation, characterization and properties.

*Progress in Organic Coatings*, 73(1), 47-53.

**H. Wang, S. Xu, W. Shi.** (2009). Photopolymerization behaviors of hyperbranched polyphosphonate acrylate and properties of the UV cured film.

*Progress in Organic Coatings*, 65(4), 417-424.

**H.-D. Hwang, H.-J. Kim.** (2011). UV-curable low surface energy fluorinated polycarbonate-based polyurethane dispersion.

*Journal of Colloid and Interface Science*, 362(2), 274-284.

**H.-D. Hwang, C.-H. Park, J.-I. Moon, H.-J. Kim, T. Masubuchi.** (2011). UV-curing behavior and physical properties of waterborne UV-curable polycarbonate-based polyurethane dispersion.

*Progress in Organic Coatings*, 72(4), 663-675.

**H.-D. Hwang, H.-J. Kim.** (2011). Enhanced thermal and surface properties of waterborne UV-curable polycarbonate-based polyurethane (meth)acrylate dispersion by incorporation of polydimethylsiloxane.

*Reactive and Functional Polymers*, 71(6), 655-665.

**H.-S. Do, J.-H. Park, H.-J. Kim.** (2008). UV-curing behavior and adhesion

performance of polymeric photoinitiators blended with hydrogenated rosin epoxy methacrylate for UV-crosslinkable acrylic pressure sensitive adhesives. *European Polymer Journal*, 44(11), 3871-3882.

**I.-B. Lee, B.-H. Cho, H.-H. Son, C.-M. Um, B.-S. Lim.** (2006). The effect of consistency, specimen geometry and adhesion on the axial polymerization shrinkage measurement of light cured composites. *Dental Materials*, 22, 1071–1079.

**I. Benedek.** (2004). *Pressure-Sensitive Adhesives and Applications, second edition.*  
New York, NY: Marcel Dekker, Inc.

**J. Z. Y. Wang, R. H. Bogner.** (1995). Techniques to monitor the UV curing of potential solvent-free film-coating polymers. *International Journal of Pharmaceutics*, 113(1), 113-122.

**J. R. Nair, C. Gerbaldi, M. Destro, R. Bongiovanni, N. Penazzi.** (2011). Methacrylic-based solid polymer electrolyte membranes for lithium-based batteries by a rapid UV-curing process *Reactive and Functional Polymers*, 71(4), 409-416.

**J. Kong, X. Fan, G. Zhang, X. Xie, Q. Si, S. Wang.** (2006). Synthesis and UV-curing behaviors of novel rapid UV-curable polyorganosilazanes.

*Polymer*, 47(5), 1519-1525.

**J. Jin, S. Chen, J. Zhang.** (2010). UV aging behaviour of ethylene-vinyl acetate copolymers (EVA) with different vinyl acetate contents.

*Polymer Degradation and Stability*, 95(5), 725-732.

**J. Bai, Z. Shi, J. Yin.** (2013). A novel main chain benzoxazine polymer with the ability of UV-induced selfsurface modification

*Polymer*, 54(10), 2498-2505.

**J. Johnston.** (2003). *Pressure Sensitive Adhesive Tapes, second edition.*

Northbrook, IL: Pressure Sensitive Tape Council.

**J.-D. Cho, S.-T. Han, J.-W. Hong.** (2007). A novel in situ relative-conductivity-based technique for monitoring the cure process of UV-curable polymers.

*Polymer Testing*, 26(1), 71-76.

**J.-D. Cho, J.-W. Hong.** (2005). Photo-curing kinetics for the UV-initiated

cationic polymerization of a cycloaliphatic diepoxide system photosensitized by thioxanthone.

*European Polymer Journal*, 41(2), 367-374.

**J.-D. Cho, H.-K. Kim, Y.-S. Kim, J.-W. Hong.** (2003). Dual curing of cationic UV-curable clear and pigmented coating systems photosensitized by thioxanthone and anthracene.

*Polymer Testing*, 22(6), 633-645.

**K. Resch, G. M. Wallner, R. Hausner.** (2009). Phase separated thermotropic layers based on UV cured acrylate resins – Effect of material formulation on overheating protection properties and application in a solar collector.

*Solar Energy*, 83(9), 1689-1697.

**L. Hu, W. Shi.** (2011). UV-cured organic-inorganic hybrid nanocomposite initiated by trimethoxysilane modified fragmental photoinitiator.

*Composites Part A: Applied Science and Manufacturing*, 42(6), 631-638.

**L. G. Lovell, H. Lu, J. E. Elliott, J. W. Stansbury, C. N. Bowman.** (2001). The effect of cure rate on the mechanical properties of dental resins.

*Dental Materials*, 17(6), 504-511.

**M. Urbaniak.** (2011). A relationship between the glass transition temperature and the conversion degree in the curing reaction of the EPY® epoxy system.

*Polimery*, 56(3), 240.

**M. Sangermano, R. A. Ortiz, B. A. Puente Urbina, L. Berlanga, Duarte, A. E. Garcia Valdez, R. G. Santos.** (2008). Synthesis of an epoxy functionalized spiroorthocarbonate used as low shrinkage additive in cationic UV curing of an epoxy resin.

*European Polymer Journal*, 44(4), 1046-1052.

**M. Rosentritt, A. C. Shortall, W. M. Palin.** (2010). Dynamic monitoring of curing photoactive resins: A methods comparison.

*Dental Materials*, 26(6), 565-570.

**R. Bongiovanni, E. A. Turcato, A. D. Gianni, Ronchetti.** (2008). Epoxy coatings containing clays and organoclays: Effect of the filler and its water content on the UV-curing process.

*Progress in Organic Coatings*, 62(3), 336-343.

**J. J. Rajasekaran, J. G. Curro.** (1995). Intermolecular packing of freely jointed branched polyalkene melts: a microscopic approach.

*Journal of the Chemical Society, Faraday Transactions*, 91(16), 2427-2433.

**S.-W. Lee, J.-W. Park, C.-H. Park, D.-H. Lim, H.-J. Kim, J.-Y. Song, J.-H. Lee.** (2013). UV-curing and thermal stability of dual curable urethane epoxy adhesives for temporary bonding in 3D multi-chip package process.

*International Journal of Adhesion and Adhesives*, 44, 138-143.

**S.-W. Lee, J.-W. Park, C.-H. Park, Y.-E. Kwon, H.-J. Kim, E.-A. Kim, H.-S. Woo, S. Schwartz, M. Rafailovich, J. Sokolov.** (2013). Optical properties and UV-curing behaviors of optically clear PSA-TiO<sub>2</sub> nanocomposites.

*International Journal of Adhesion and Adhesives*, 44, 200-208.

**S.-W. Lee, J.-W. Park, Y.-E. Kwon, S. Kim, H.-J. Kim, E.-A. Kim, H.-S. Woo, J. Swiderska.** (2012). Optical properties and UV-curing behaviors of optically clear semi-interpenetrated structured acrylic pressure sensitive adhesives.

*International Journal of Adhesion and Adhesives*, 38, 5-10.

**S.-Y. Lin, S.-L. Wang.** (2012). Advances in simultaneous DSC–FTIR microspectroscopy for rapid solid-state chemical stability studies: Some dipeptide drugs as examples.

*Advanced Drug Delivery Reviews*, 64(5), 461-478.

**S. Tasic, B. Bozic, B. Dunjic.** (2004). Synthesis of new hyperbranched urethane-acrylates and their evaluation in UV-curable coatings.

*Progress in Organic Coatings*, 51(4), 320-327.

**S. Simić, B. Dunjić, S. Tasić, B. Božić, D. Jovanović, I. Popović.** (2008). Synthesis and characterization of interpenetrating polymer networks with hyperbranched polymers through thermal-UV dual curing.

*Progress in Organic Coatings*, 63(1), 43-48.

**S.-J. Wang, X.-D. Fan, J. Kong, J.-R. Lu.** (2009). Synthesis, characterization and UV curing kinetics of hyperbranched polysiloxysilanes from A2 and CB2 type monomers.

*Polymer*, 50(15), 3587-3594.

**S. Garoushia, P. K. Vallittu, D. C. Watts, L. V. J. Lassila.** (2008). Polymerization shrinkage of experimental short glass fiber-reinforced

composite with semi-inter penetrating polymer network matrix.

*Dental Materials*, 24, 211–215.

**T. F. Scott, W. D. Cook, J. S. Forsythe.** (2002). Photo-DSC cure kinetics of vinyl ester resins. I. Influence of Temperature.

*Polymer*, 43(33), 5839-5845.

**T. F. Scotta, W. D. Cook, J. S. Forsythe.** (2003). Photo-DSC cure kinetics of vinyl ester resins II: influence of diluent concentration.

*Polymer*, 44(3), 671-680.

**T. Kijchavengkul, R. Auras, M. Rubino.** (2008). Measuring gel content of aromatic polyesters using FTIR spectrophotometry and DSC.

*Polymer Testing*, 27(1), 55-60.

**K. L. Van Landuyt, J. Snauwaert, J. De Munck, M. Peumans, Y. Yoshida, A. Poitevin, B. Van Meerbeek.** (2007). Systematic review of the chemical composition of contemporary dental adhesives.

*Biomaterials*, 28(26), 3757-3785.

**S. Velankar, J. Pazos, S. L. Cooper.** (1996). High-performance UV-curable

urethane acrylates via deblocking chemistry.

*Journal of Applied Polymer Science*, 62(9), 1361-1376.

**X. Wang, M.D. Soucek.** (2013). Investigation of non-isocyanate urethane dimethacrylate reactive diluents for UV-curable polyurethane coatings.

*Progress in Organic Coatings*, 76(7-8), 1057-1067.

**X.-E. Cheng, W. Shi.** (2010). UV-curing behavior and properties of tri/di(acryloyloxyethoxy) phenyl silane used for flame-retardant coatings.

*Progress in Organic Coatings*, 69(3), 252-259.

**X. Xiao, C. Hao.** (2010). Preparation of waterborne epoxy acrylate/silica sol hybrid materials and study of their UV curing behavior.

*Colloids and Surfaces A: Physicochemical and Engineering Aspects*, 359(1-3), 82-87.

**Y. Zhao, Y. Dan.** (2007). Synthesis and characterization of a polymerizable benzophenone derivative and its application in styrenic polymers as UV-stabilizer.

*European Polymer Journal*, 43(10), 4541-4551.

**Y. Zhang, H. Miao, W. Shi.** (2011). Photopolymerization behavior and properties of highly branched polyester acrylate containing thioether linkage used for UV curing coatings.

*Progress in Organic Coatings*, 71(1), 48-55.

**Y. Zhang, F. Zhan, W. Shi.** (2011). Photopolymerization behavior and properties of highly branched poly (thioetherurethane) acrylates used for UV-curing coatings

*Progress in Organic Coatings*, 71(4), 399-405.

**Y.-J. Park, D.-H. Lim, H.-J. Kim, D.-S. Park, I.-K. Sung.** (2009). UV- and thermal-curing behaviors of dual-curable adhesives based on epoxy acrylate oligomers.

*International Journal of Adhesion and Adhesives*, 29(7), 710-717.

**Z. Doğruiyol, N. Arsu, S. Keskin Doğruiyol, Ö. Pekcan.** (2011). Critical phenomenon during photoinitiated gelation at different temperatures: A Photo-DSC study.

*Progress in Organic Coatings*, 72(4), 763-768.

**Z. Huang, W. Shi.** (2007). UV curing behavior of hyperbranched

polyphosphate acrylate/di(hydroxylpropyl methacrylate) piperazine and properties of the cured film.

*Progress in Organic Coatings*, 59(4), 312-317.

**Z. Yang, D. A. Wicks, J. Yuan, H. Pu, Y. Liu.** (2010). Newly UV-curable polyurethane coatings prepared by multifunctional thiol- and ene-terminated polyurethane aqueous dispersions: Photopolymerization properties.

*Polymer*, 51(7), 1572-1577.

**Z. Chen, D. C. Webster.** (2006). Study of cationic UV curing and UV laser ablation behavior of coatings sensitized by novel sensitizers

*Polymer*, 47(11), 3715-3726.

# 광경화 수축현상의 분석기법 개발 및

## 광경화 접착소재에 대한 응용 연구

박 지 원

서울대학교 대학원

산림과학부

환경재료과학전공

본 연구에서는 광경화형 소재의 경화 수축률 평가 시스템을 설계하고, 설계한 시스템의 신뢰성을 높이기 위해 실험환경적 변수를 분석하고자 하였다. 이 시스템에 따라 구조가 다른 단량체들의 경화 수축률을 측정하였다. 단량체 평가 결과를 바탕으로 실제 제품의 특징을 모사한 복합재료의 경화 수축률을 평가하고 수축률에 영향을 미치는 요인을 평가하였다.

내부적인 변수로는 시편의 형태와 두께가 수축률에 상당한 영향을 주었다. 특히, 시편의 종횡비가 작으면 축방향 수축률이 크게 감소하는 현상이 발생하였다. 모델링을 통해 재료의 측면에서의 수축현상이 축방향 수축에 큰 영향을 줄 수 있으며 이 영향을 최소화 하

기 위해 종횡비는 40 이상이 되어야 함을 확인하였다.

중합개시제의 함량 및 광의 세기는 중합반응의 속도에 영향을 주어 전체적인 경화 수축률의 차이를 유도하였다. 특히, 중합개시제의 함량과 광의 세기는 두께방향 경화에 복합적으로 작용하여 수축 지연 효과를 유도하였다.

광시차주사열량측정법(photo-differential scanning calorimetry)을 통한 경화특성평가에서는, 평가환경온도에 따른 UV경화는 소재의 유리전이온도에 따라 변하며, 이 변화는 경화과정에서 발생하는 부분적 가교와 이에 따른 유동성 저하에 의한 것으로 평가되었다. 특히, 반응성은 일정 온도까지 증가한 후 다시 감소하는 경향을 보이는데, 이는 온도 상승에 따라 역학적 반응보다 열역학적 반응이 우세해지기 때문이다.

일반적으로 작용기의 개수가 증가하면 UV경화반응속도가 빨라진다고 알려져 있으나, 본 연구에서는 반대의 결과가 도출되었다. 2개의 작용기를 가진 단량체가 6개의 작용기를 가진 단량체에 비해

높은 경화 수축률과 반응속도를 보였다. 작용기가 2개인 단량체로 구성된 소재의 분자구조가 더 유연하고, 경화과정에서도 소재의 유동성을 지속적으로 유지 할 수 있기 때문이다.

아크릴레이트와 메타아크릴레이트 구조는 광경화 시스템에서 가장 많이 활용하는 구조이다. 두 구조 모두 반응성은 뛰어나지만 아크릴레이트의 반응성이 메타아크릴레이트에 비해서 높은 것으로 알려져 있다. 모노아크릴레이트 시스템에서는 메타아크릴레이트의 반응성이 우수하였는데, 이는 메틸구조에 따른 중합물의 유동성 유지 때문으로 평가되었다. 다관능 시스템에서는 아크릴레이트의 수축률과 반응속도가 모두 빨랐다. 특히, Photo-DSC로 부터 얻은 결과와 수축률 평가로부터 얻은 결과의 그래프 모양이 동일함을 확인할 수 있었으며, 이러한 photo-DSC평가가 수축률 평가를 예측해 볼 수 있는 방식임을 확인 할 수 있었다.

Isomer 시스템을 이용한 수축률 평가에서는 core의 구조에 따라 그 반응성이 달라진다는 것을 확인 하였다. core에 선형적인 구조를 가진 경우와 곁사슬 구조를 가진 분자는 각각 유동성과 분자

밀집도가 달라 경화특성이 다르게 발현되었다. 선형적인 구조를 가진 경우 경화 후에도 분자 구조가 유동적이기 때문에 지속적인 반응이 가능했다.

UV 중합형 접착시스템은 미리 중합된 pre-polymer와 반응형 희석제를 블렌딩하는 방식을 통해 모사 구현하였다. 이때 반응형 희석제의 크기가 작고, 그 함량이 많을 수록 반응이 지연되는 현상을 확인 할 수 있었다.

치과용 접착소재는 경화 과정에서의 수치안정성이 중요하고, 경화 후의 경도가 우수해야 하기 때문에 필러를 활용한 시스템으로 설계된다. 나노실리카 입자를 코어구조로 가지고 있는 아크릴레이트를 제조하여, 이를 기반으로 한 필러함유형 UV경화 접착소재 시스템을 모사 구현하였다. 블렌딩되는 소재에 따라 수축률이 변화하였으며, 이때 분자 크기가 다른 분자들이 섞이게 되면 nano-porous 효과가 발현되어 그 반응성이 더욱 증가하게 되는 것을 확인 할 수 있었다.

본 연구에서는 축방향 수축률 측정 장비를 설계하여 축방향 수축률을 평가하고 그 결과를 바탕으로 부피 수축을 추정하는 시스템을 제안하였다. 수축률 평가에 영향을 줄 수 있는 내외부적인 인자들을 분석하였으며, 이를 통제함으로써 보다 정확한 수축률을 예상할 수 있었다. 다양한 소재가 가지는 구조적인 특성이 수축률에 영향을 미치고 있으며, 이는 소재의 반응속도와 소재의 유동성에 따른 결과로 평가되었다. 제품 모사 평가에서는 단순화된 시스템을 통해 수축률 및 광경화 변화인자를 살펴볼 수 있었으며, 각 시스템에서의 주된 영향인자를 분석할 수 있었다.

키워드 : 부피 수축률, 축방향 수축률, 모델링, 광개시제, 광의 세기, 아크릴레이트, 환경 온도, 광경화형 접착제, 다관능 단량체

학 번 : 2008-21297